8-2003

Strategies for Enhancing the Performance of Chemical Sensors Based on Microcantilever Sensors

Christopher Tipple
University of Tennessee - Knoxville

To the Graduate Council:

I am submitting herewith a dissertation written by Christopher Tipple entitled "Strategies for Enhancing the Performance of Chemical Sensors Based on Microcantilever Sensors." I have examined the final electronic copy of this dissertation for form and content and recommend that it be accepted in partial fulfillment of the requirements for the degree of Doctor of Philosophy, with a major in Chemistry.

Michael J. Sepaniak, Major Professor

We have read this dissertation and recommend its acceptance:

Kelsey Cook, Robert Hinde, Panos Datskos

Accepted for the Council:

Carolyn R. Hodges

Vice Provost and Dean of the Graduate School

(Original signatures are on file with official student records.)

To the Graduate Council:

I am submitting herewith a dissertation written by Christopher A. Tipple entitled "Strategies for Enhancing the Performance of Chemical Sensors Based on Microcantilever Sensors." I have examined the final electronic copy of this dissertation for form and content and recommend that it be accepted in partial fulfillment of the requirements for the degree of Doctor of Philosophy, with a major in Chemistry.

Michael J. Sepaniak
Major Professor

We have read this dissertation
And recommend its acceptance:

Kelsey Cook

Robert Hinde

Panos Datskos

Accepted for the Council:

Anne Mayhew
Vice Provost and Dean
of Graduate Students

(Original signatures are on file with official student records)

STRATEGIES FOR ENHANCING THE PERFORMANCE OF CHEMICAL SENSORS BASED ON MICROCANTILEVER SENSORS

A Dissertation
Presented for the
Doctor of Philosophy Degree
The University of Tennessee, Knoxville

Christopher Alan Tipple
August 2003

DEDICATION

This dissertation is dedicated to my mother Sharon and my brother Bobby, without whose support and love this work would not have been possible.

This dissertation is also dedicated to my wife Jessica for her countless sacrifices, unconditional love and support that allowed this work to be completed.

ACKNOWLEDGMENTS

I would like to take this opportunity to thank all of the people who helped to make this work possible. I must first and foremost thank God, through whom all things are possible. I would not be the person I am today without His abounding grace and amazing love which He has freely given to me.

I would also like to thank my family. The incredible love and support I have received from both my mother and brother have made this work worth all the effort. We did it! I also wish to thank my amazing wife Jessica for her total support of everything I have set out to do during our time here. Her guidance and encouragement sustained me in all of the difficult times that I faced during the course of this work.

I also wish to thank the many friends who took this long journey with me. To Phil Stimac, the first friend I made in Knoxville. Thanks for all the good times we had, both in and out of school. I wish you the best of luck and great success in all of your endeavors. Thanks to Charles O' Brien, Nathan Crawford, and Jaime Blanton for the many memorable moments we shared over the past 5 years. Many thanks to past group members Tim Gibson, Will Nirode, Gerald Devault, Shannon Fox, Jim Schaeper, Mustafa Culha and Jeremy Headrick for all your advice and the great times we enjoyed. You each taught me some valuable lessons. A special thanks to Jeremy Headrick for helping to keep me sane over the past 5 years, as one of the few people who can truly understand how difficult this work was at times. I also wish to thank current group members Lance Riddle, Maggie Connatser, Kathleen Giesfeldt, Marco De Jesus, and Jenny Oran for helping to make this experience more enjoyable. Good luck to you all in

the future! I also wish to thank Dr. Panos Datskos for his invaluable time and interest in this work. Thanks for the many lively conversations and all of your guidance. I have to thank Dr. Nickolay Lavrik for all of his help with many facets of this work. His expertise in this field, as well as in the lab, was greatly appreciated.

I would also like to thank Tim Free, whose assistance and guidance in the machine shop helped make some of this work much easier than it would have been otherwise. Great job Tim! Thanks also to all of the staff in the chemistry department. You are the people who truly make this place run. Keep up the great work!

I wish to thank the chemistry department and the Science Alliance for providing me with the financial support necessary to complete this work.

I would also like to thank my committee members: Dr. Cook, Dr. Hinde, and Dr. Datskos. Thank you all for your timely insights and willingness to share in this research.

Finally, I would like to thank Dr. Sepaniak for his time, effort, and dedication. This has been one experience I will never forget.

ABSTRACT

Microcantilever (*MC*) based chemical sensors have become more widely used during the past 10 years due to the advantages they possess over other chemical sensors. One of the most significant characteristics is their extremely high surface to volume ratio. This key facet allows surface forces that can be ignored on a macroscale to become a significant sensing transduction mechanism. *MC* based sensors also exhibit a higher mass sensitivity to adsorbates than do many other chemical sensor platforms. Under many conditions, *MC* based sensors directly translate changes in Gibbs free energies due to analyte-surface interactions into mechanical responses. However, the widespread application of *MC*s in the field of sensors has yet to be fully realized. This is primarily due to the lack of a unifying methodology and instrumentation that would allow various research groups to benefit from a combined wealth of knowledge on the subject.

The underlying goal of this research is to broaden the depth and scope of knowledge of *MC* based chemical sensors. By working on several areas in a coherent order, the limitations of *MC* based sensors have been determined and largely overcome. The information gathered in all aspects of this project will be useful to present and future researchers in this field. The initial research was focused on the application of various chemical films to *MC* sensors to be able to measure a wide range of chemical species. In one case, thin films of polymeric gas chromatography (GC) phases were deposited onto V-shaped *MC*s. A main strength to using GC phases was that the responses of the analytes could be predicted before hand by using the McReynolds constants of the phases used. This allowed for the detection and quantification of various chemical species using these moderately selective phases.

During this phase of research it was discovered that methods for enhancing *MC* response were needed to overcome some of the traditional problems facing *MC* based sensors. By employing a new type of underlying nanostructured metallic film, *MC* response was greatly enhanced. This resulted in a better limit of detection and wider dynamic range relative to previous results with smooth surface *MC*s.

In addition to advances resulting from nanostructuring, important advances were made in *MC* coating strategies. The widely used and well-characterized process of physical vapor deposition was used to deposit both organic and polymeric materials onto the *MC* surface. This process allowed for uniform films to be deposited with tailored thicknesses and for individual *MC*s on a single chip to be coated selectively. Another approach involving the immersion of *MC*s into fused silica capillaries containing solutions of thiolated materials was also developed. This method also allowed for individual *MC*s in an array to be selectively coated.

Finally, out of these results and a developing trend of using sensor arrays came the need to increase the robustness and selectivity of *MC* based systems. Two different systems for achieving these goals were developed. First, a simple differential system based upon dual diode lasers was constructed in order to eliminate common sources of noise and non-specific interactions that decrease the dynamic range of these sensors. This system was also applied to the quantification of individual components in a binary mixture. While this system has met only limited success, it has been a beneficial first step towards *MC* systems of higher order. Towards that goal, a system designed to measure multiple *MC*s simultaneously using an array of vertical cavity surface emitting lasers was also used. This system measures the responses of multiple *MC*s exposed to an

analyte in a single run and provides unique response patterns for that analyte. This allowed for the qualitative analysis of a simple mixture to be performed.

ORGANIZATION

Chapter 1 is intended to introduce the reader to the fundamentals of chemical sensors. The various types of chemical sensors are discussed. Particular attention is paid to *MC* based chemical sensors, which encompasses all of the work presented in this dissertation. Comparisons are made to the other types of chemical sensors, with both strengths and limitations explored. Different modes of cantilever deflection and detection are also presented.

Chapter 2 discusses certain types of chemically selective films that have been applied to *MC* sensors. The major focus of the chapter is the ability to impart selectivity to *MC* based sensors by employing different chemical films. Conventional GC phases were applied to *MC*s that were used for gas phase sensing. An important advantage to the work is that there is a wealth of information available concerning these phases, specifically McReynolds constants. This information can be used to predict responses and choose relevant films depending on the analyte to be studied. In the study presented in this chapter, *MC* responses to analytes correlated well based on the McReynolds constants of the films used. Methods of applying these films to the *MC* surface are discussed. Changes in *MC* response to particular analytes are shown to be based upon film differences and analyte concentration.

Chapter 3 bridges the gap between gas and liquid phase sensing. In an attempt to enhance *MC* response, a new type of underlying metallic film with nanosized features was developed using chemical dealloying of codeposited metallic films. Utilizing this surface structuring approach first developed and tested using gas phase analytes, the

approach was then tested in the liquid phase. The chapter presents advances in *MC* sensor response through the combination of thicker receptor phases and nanostructured surfaces. Nanostructured (dealloyed) surfaces that show enhanced *MC* response are compared to nonstructured (smooth) metallic surfaces. The effect of film thickness on *MC* response was also investigated.

Chapter 4 details the design and implementation of a dual diode laser (DDL) differential based *MC* system and a second system based upon an array of vertical cavity surface emitting lasers (VCSELs) used to measure multiple *MC*s simultaneously. Through the use of the differential system, the most common sources of ambient noise in *MC* measurements can be alleviated. The DDL system has also proven useful for increasing the selectivity that can be attained when using only one *MC*. This is primarily due to the subtraction of any non-specific interactions that occur during *MC* response. This can be particularly important in biological based systems, where non-specific interactions can be quite large. The second system was used to measure unique response patterns of individual analytes to an array of *MC*s treated with different chemically selective coatings. Individual *MC*s were coated using nebulized solutions of polymers deposited through a mask. After the unique response patterns were measured for individual analytes, a mixture of these analytes was then qualitatively analyzed.

Chapter 5 presents a summary of the work presented in Chapters 2-4 and outlines some of the future directions and applications in which *MC* based sensors might head.

TABLE OF CONTENTS

CHAPTER PAGE

LIST OF TABLES

LIST OF FIGURES

ABBREVIATIONS AND SYMBOLS

A	absorbance
Å	Angstrom
AC	Alternating current
AFM	Atomic force microscopy
APM	Acoustic plate mode
A_r	area
A_{cr}	cross-sectional area
A_s	surface area
a_i	activity of ion i
a_j	activity of ion j
atm	atmosphere
BioFET	biologically selective field effect transistor
CCD	Charge couple device
CD	cyclodextrin
CHEMFET	chemically selective field effect transistor
cm	centimeter
c_m	mass sensitivity factor
C_O^o	concentration of oxidized species at the electrode
c_o	concentration of the oxidized species
C_{ox}	oxide capacity per unit area
C_R^o	concentration of reduced species at the electrode

C_θ	sum of the thermal capacities of the calorimeter components
C4A	4-tertybutylcalix[4]arene
C6A	4-tertbutylcalix[6]arene
C8A	4-tertbutylcalix[8]arene
D	diffusion coefficient
DC	direct current
DDL	dual diode laser
DHN	dihydroxynaphthalene
DMSO	dimethylsulfoxide
DNA	deoxyribonucleic acid
D_o	diffusion coefficient of oxidized species
dc	change in concentration
dp	penetration depth
dx	change in distance
E	applied potential
E_{cell}	cell potential
E^o	standard redox potential
ENFET	enzyme based field effect transistor
F	Faraday's constant
FIB	Focused ion beam
FTIR	Fourier transform infrared spectroscopy
f	frequency
f_1	mass loaded resonance frequency

f_o	resonance frequency or frequency before mass loading
FET	field effect transistor
FPW	flexural plate wave
g	grams
HDATB-β-CD	heptakis-(2,3-O-diacetyl-6-O-tertbutyl-dimethylsilyl)-β-CD
HM-β-CD	heptakis-6-mercapto-β-CD
Hz	hertz or s^{-1}
I	current
I_{ave}	average McReynold's constant
I_d	drain current
IDT	interdigital transducers
IMFET	immunological field effect transistor
ISE	ion-selective electrode
ISFET	ion-selective field effect transistor
K	constant of the electrochemical system
k	Spring constant
k_f	frequency constant of the crystal
kHz	Kilohertz
K_{ij}	selectivity coefficient for ions i and j
$k_{1,2}$	material constants
LOD	Limit of detection
l	length
m	meter

m_a	mass
M	Molar
mM	millimolar
MC	microcantilever
MHz	Megahertz
m_s	areal mass loading on the sensor surface
m^*	effective mass
ml	milliliter
mm	millimeter
Δm_s^{min}	minimum detectable surface mass density
N	Newton or kg m^2/s^2
n	geometrical factor
n_g	another geometric factor
N_m	number of moles
NA	numerical aperture
NMR	Nuclear magnetic resonance
n_1	refractive index of the core
n_2	refractive index of the cladding
η	liquid viscosity
ne^-	number of electrons
n_e	moles of electrons used
nm	nanometer
n_o	index of refraction of the surrounding medium

η_q	viscosity of quartz
OV-25	poly(phenyl-methyl dimethylsiloxane)
O_x	oxidized species
PDPP	polydiphenoxyphosphazene
PECH	polyepichlorohydrin
PIB	polyisobutylene
PSD	position sensitive detector
ρ	liquid density
ppb	parts per billion
ρ_m	density of the applied chemical film
ppm	parts per million
ρ_q	density of quartz
PVD	Physical vapor deposition
Q	number of coulombs
q	heat
QCM	quartz crystal microbalance
R	universal gas constant
R_c	Radius of curvature
R_{ed}	reduced species
RF	response factor
RMS	Root mean square
rpm	revolutions per minute

SAM	self-assembled monolayer
SAW	surface acoustic wave
SFM	Scanning force microscopy
S/N	signal to noise ratio
S_m	mass sensitivity
SP-2340	poly(bis-cyanopropylsiloxane)
SPR	surface plasmon resonance
T	temperature
t	thickness
TCE	trichloroethylene
t_f	film thickness
TrCE	tetrachloroethylene
μ	electron mobility
μL	microliter
μm	micrometer
VCSEL	vertical cavity surface emitting laser
V_{ds}	drain-source voltage
V_{gs}	input gate voltage
V_t	threshold voltage
ν_p	Poisson's Ratio
ν_o	acoustic wave phase velocity
$\Delta\nu$	change in acoustic wave phase velocity

w	width
XPS	X-ray photoelectron spectroscopy
x	distance
Y	Young's modulus
Y*	effective Young's modulus
z	deflection or bending
z_{max}	maximum deflection
z_i	charge of ion i
z_j	charge of ion j
β	maximum half acceptance angle
$\Delta\sigma$	differential surface stress
ε_e	elastic surface strain
γ	surface free energy
λ_o	incident wavelength
Φ	flux
σ	surface stress
σ_c	stress on the coated surface
σ_{si}	stress on the silicon surface
θ_1	angle of incidence
θ_2	angle of refracted light
8-HQ	8-hydroxyquinoline

CHAPTER 1

INTRODUCTION TO CHEMICAL SENSORS, MICROCANTILEVERS, AND DETECTION METHODS

1.1 INTRODUCTION TO CHEMICAL SENSORS

With the recent terrorist attacks that have been occurring all over the world, there is a greater need for the development of chemical sensors. Chemical sensors have been at the forefront of analytical chemistry since its inception. Some examples of early chemical sensors are the pH electrode and calorimeters used to measure heats of reactions. One would find it very difficult to think of some aspect of everyday life that does not involve or directly depend on some type of chemical sensor. The human body itself is composed of many different chemical sensors, each of which has a specialized function to perform. As such, the past 20 years have seen a dramatic increase in the research, funding, and development of chemical sensors.[1] A quick perusal of the analytical literature demonstrates the popularity of chemical sensor research. As of 1995, roughly 8% of all analytical abstracts in the *Analytical Abstracts* database contain the term sensor or electrode.[1] This corresponds to approximately a 6% increase since 1980. In addition to the literature, the commercialization of sensor devices, including portable devices, during the last several years indicates the upswing in sensor research and development. One of the biggest driving forces behind this trend is the need for sensors in biomedical, industrial, environmental and homeland defense applications. These factors have all combined to produce growth rates in the commercialization of chemical

sensors of up to 40% per year.[1] These rates are expected to continue as the need for chemical sensors continues to increase.

1.2 PROPERTIES OF CHEMICAL SENSORS

There are several fundamental properties that an ideal chemical sensor should possess. The first property of an ideal chemical sensor is that its signal output should have a functional relationship to the amount or concentration of analyte present in the sample. Ideally, this relationship will be linear over a wide dynamic range. This provides a means of quantitatively comparing samples and providing meaningful data about the sample. The second property of an ideal sensor is that there should be minimal hysteresis effects. In order to be truly applicable, the sensor must return to its initial state after being exposed to the analyte. The third property of an ideal sensor is that it exhibits fast response times. This is especially significant in certain applications, such as chemical warfare agent detection, in-line process detection, and monitoring chemical reactions. An ideal chemical sensor also has high sensitivity and low intrinsic noise levels that afford low limits of detection and the ability to distinguish between small differences in analyte concentration. This property is critical to being able to measure low amounts of analyte in a sample. This property can be greatly enhanced by using techniques designed to minimize the effects of noise on chemical measurements. An ideal sensor should also be characterized as selective. While it is true that there are relatively few sensors that are capable of demonstrating infinite selectivity (i.e. it will respond to only one analyte), a moderate degree of selectivity is necessary to ensure that the sensor is responding to the analyte. While few chemical sensors excel in all of the

properties mentioned above, it is important that a chemical sensor does excel in one of them and performs at a moderate level in the others.

1.3 TYPES OF CHEMICAL SENSORS

At this point, it would be wise to formulate a working definition of the term chemical sensor. One of the most accepted definitions has been provided by Janata and Bezegh. These researchers define a chemical sensor as *a transducer which provides direct information about the chemical composition of its environment; it is composed of a physical transducer and a chemically selective layer* [2], as seen in Figure 1.1. This clearly differentiates a chemical sensor from simple physical transducers such as thermocouples, flowmeters, humidity sensors, photodiodes, etc by the addition of a chemically selective layer. The importance of the chemically selective layer will be discussed in greater detail later in this dissertation. In addition to these two basic components of a chemical sensor, signal processing and data collection devices are typically employed in sensor systems.

Chemical sensors are most often differentiated by the type or class in which they are placed. The most common classes of chemical sensors are thermal, electrochemical, optical, and mass.[2] Each of these classes will be described in further detail below.

1.3.1 Thermal Sensors

Thermal sensors have been employed in a wide range of applications. As the name implies, thermal sensors measure changes in temperature. These changes in temperature or heat flow can be due to heats of reaction, mechanical work, formation or

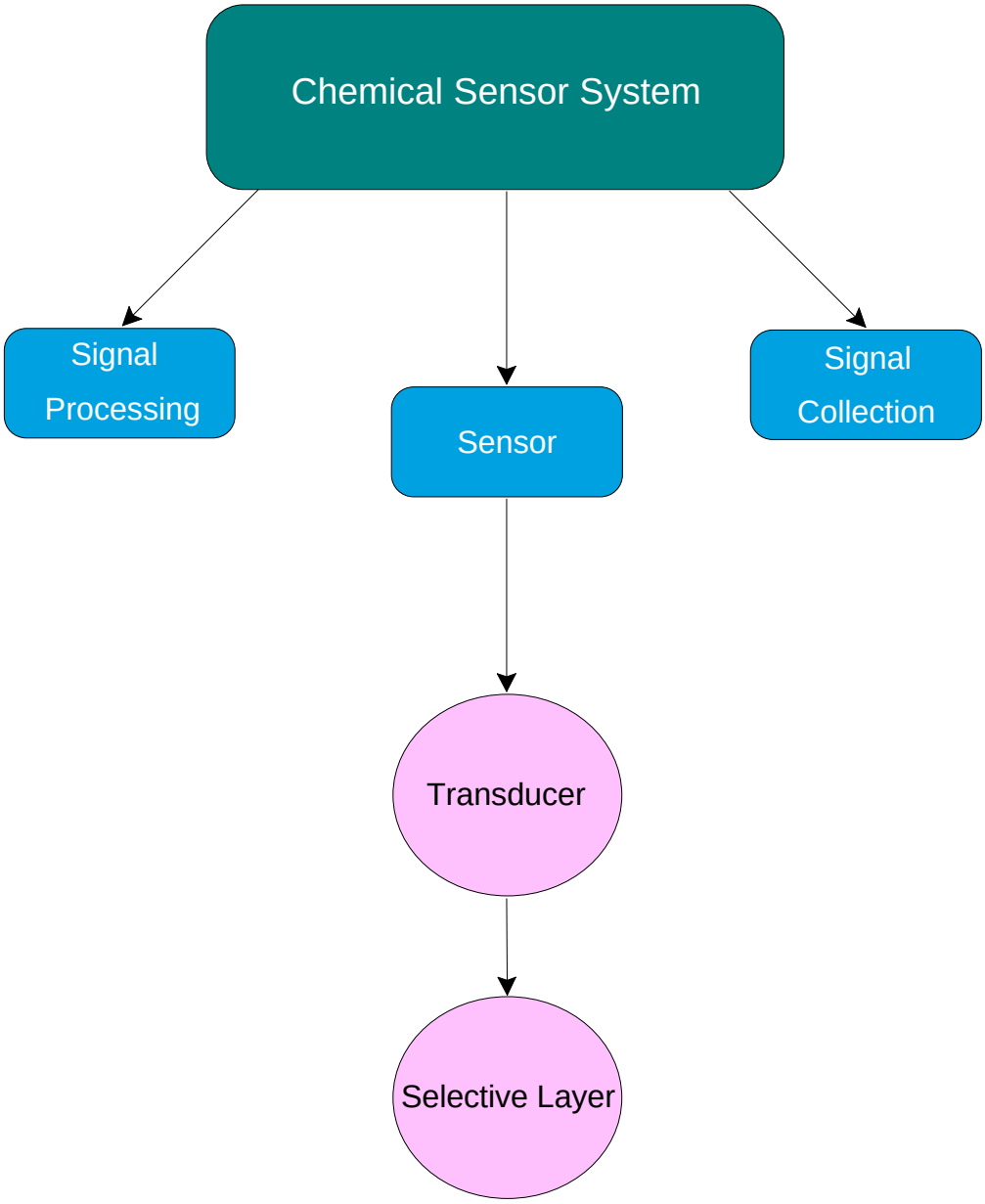

Figure 1.1. Typical components of a chemical sensor system.

dissociation of compounds, and phase changes, just to name a few.[3] There are several different types of devices for measuring changes in temperature or heat flow. These include calorimeters, thermometric sensors, pyroelectric gas sensors, and piezoelectric thermal sensors.[3] It should be pointed out that not all thermal sensors have a chemically selective phase. Despite their lack of this film, they are still generally regarded as chemical sensors.

Calorimeter based sensors measure the temperature change in a mass according to Equation 1.1,

$$\Delta \mathbf{T} = \Delta \mathbf{q} / \mathbf{m_a} \mathbf{C}_q \qquad (1.1)$$

where Δq is the energy released as heat, m_a is the total mass of the calorimeter, and C_θ is the sum of the thermal capacities of all the components in the calorimeter. This type of measurement is made by placing a known mass into a vacuum chamber that acts to thermally isolate it from the surroundings. The temperature change is then monitored and the heat released by the reaction can then be calculated. This type of device is particularly well suited for measuring heats of chemical reactions of gas phase compounds.

Thermometric sensors are based upon silicon technologies and *p-n* junctions. These junctions are aligned so as to form a thermocouple. With many different junctions in the arrangement, individual junctions combine to form a thermopile that enhances the response of the system.[3] A pellistor, seen in Figure 1.2, is also a type of thermometric sensor, but it operates on the principle of detecting a change in the temperature of a heated catalytic element when it is exposed to a mixture of combustible gases.[4]

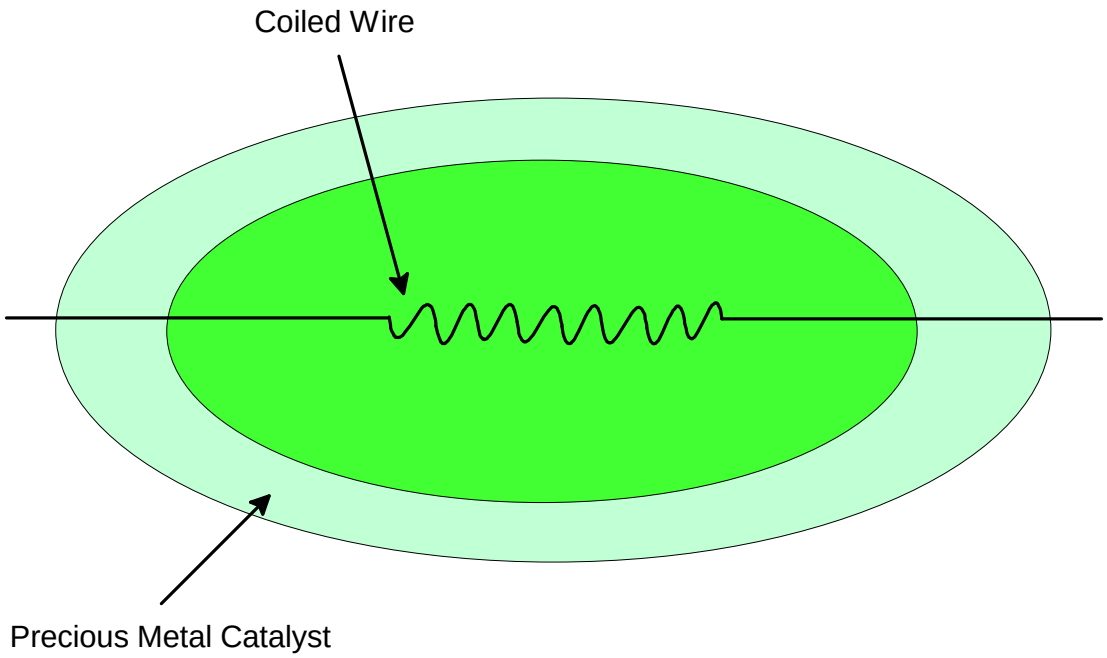

Figure 1.2. Schematic diagram of a pellistor.

Typically, a coil of fine wire is embedded in a material impregnated with a precious metal catalyst. The coil of wire is used to heat the surrounding material to its operating temperature. Once a combustible gas interacts with the catalyst, the temperature in the surrounding material increases and is detected by the central coil. These devices are very sensitive to small temperature changes.[3]

Pyroelectric gas sensors are insensitive to temperature and instead measure heat flow. In order to be used as a pyroelectric material, the material must lack a center of inversion in its primitive cell.[3] When this type of crystal is subjected to a thermal stress, it generates a surface charge and becomes pyroelectric. As these ions move across the surface, a current is generated and detected. This current directly relates to the heat flow in the sensor.[3] It is a relatively sensitive method, with detectable hydrogen limits of approximately 1 ppb in air [3] having been reported. However, these sensors cannot be used in liquids, which limits their usefulness.

Piezoelectric thermal sensors function based upon the fact that their piezoelectric constants are temperature dependent. This being the case, the resonance frequency will change as a function of temperature. This change in frequency with temperature can be calibrated for the desired working range of the sensor before measurements are initiated. Because there exists a large difference between the mechanical resonance frequency and the pyroelectric frequency, these two phenomena can be employed using the same sensor.[3] This large difference allows for these two effects to be electrically separated and monitored. These sensors are therefore generally used to monitor desorption processes. These measurements are quite sensitive and can be used together to measure the enthalpy

of desorption. The desorption of monolayers of organic solvents has been measured using these sensors. These sensors also have potential liquid phase applications.

1.3.2 Electrochemical Sensors

Sensors that measure changes in the electrical properties of a sample are abounding. These sensors can be potentiometric or voltammetric in nature. They usually involve measuring samples with electroactive species present in the liquid phase. In many cases, a thin film is employed to attract the analyte to the surface so that some type of electrochemistry can take place. This can range from redox type reactions to something as complex as a catalysis reaction. These sensors have also been employed for gas phase measurements.

Potentiometric sensors consist of mainly ion-selective electrodes (ISEs). A typical ISE is shown in Figure 1.3. These electrodes measure the potential in an electrochemical cell. In addition, ISEs do not relate an analytical signal to the concentration of the analyte, but rather to its activity. However, at low total analyte concentrations the activity and concentration are assumed to be essentially equal. This technique allows free ions to be distinguished from bound ions and the activities of different oxidation states of an ion to be determined. In its simplest form, potentiometry measures the cell potential at different analyte activities using two electrodes. A reference electrode is employed to eliminate any drifts or changes in solution composition with time. In general, this value remains constant. A working electrode is then used to monitor the potential change as a function of analyte activity. Comparing these two values allows for the determination of the analyte to be made.

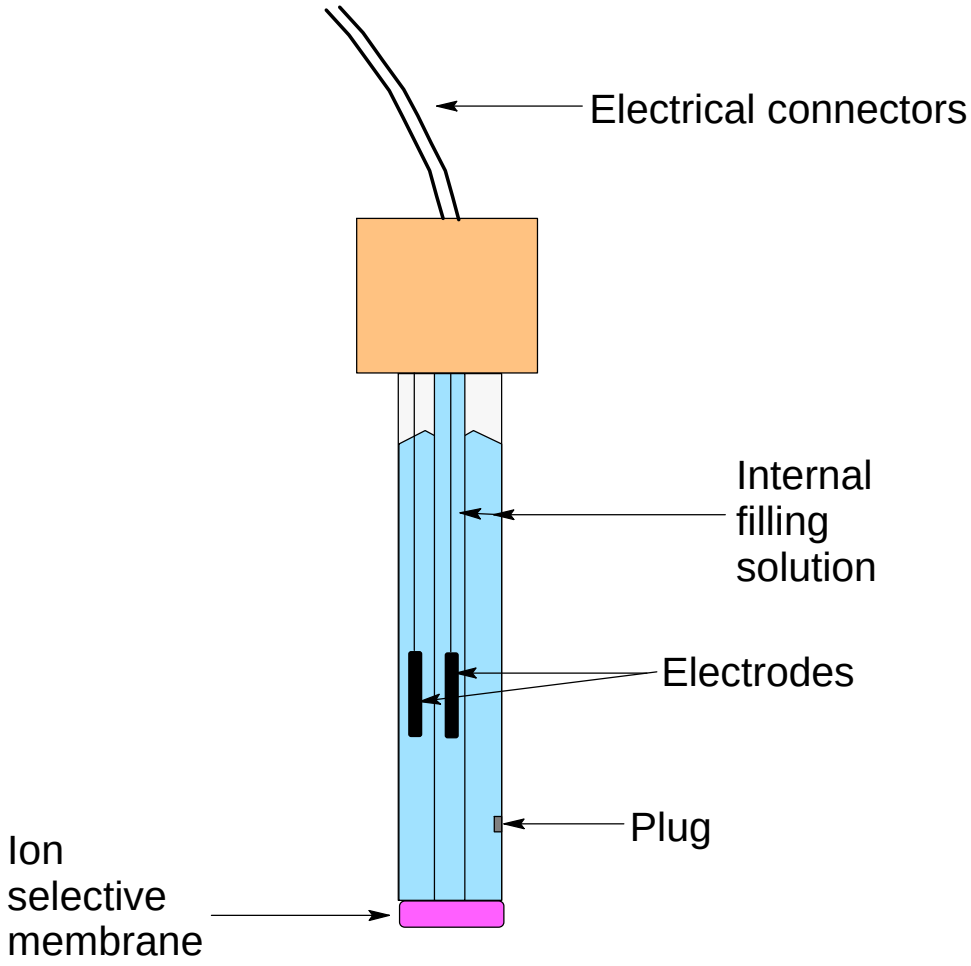

Figure 1.3. Schematic diagram of an ion selective electrode (ISE).

One of the most well known equations in analytical chemistry is the Nernst Equation. Equation 1.2 is a specific form of the Nernst Equation that assumes only one species influences the overall cell potential. This form of the Nernst Equation states that

$$\mathbf{E_{cell} = K + \frac{RT}{z_i F} ln(a_i)} \qquad (1.2)$$

where R is the gas constant, K is a constant of the system, T is the temperature, z_i is the charge on the analyte i, F is Faraday's constant, and a_i is the activity of ion i. This is the fundamental equation that is used in all potentiometric systems. However, because the above equation assumes that only one species influences the potential of the cell, a more complete form of the equation has been derived because most sensors are also susceptible to interferants, or species that create a potential due to their migration to the working electrode. After Equation 1.2 has been modified to include the effects of various interfering species, Equation 1.3 states that

$$\mathbf{E_{cell} = K + \frac{RT}{z_i F} ln\left(a_i + \sum_j K_{ij} a_j^{z_i/z_j} \right)} \qquad (1.3)$$

The constants here are the same as in Equation 1.2, with the addition of a_j being the activity of the interfering ion, z_j being the charge on the interfering ion, and K_{ij} being the selectivity coefficient. The lower the selectivity coefficient, the less impact the interferant has on the potential of the system.

While there is not a traditional selective "film" used in this type of chemical sensor, it can employ a selective membrane through which the analyte passes to reach the working electrode and cause a change in potential. These membrane-based electrodes are the most common type of electrodes used in chemical sensing. Of these, glass is the most

common type employed. This electrode is selective for hydrogen ions, which is the basis for pH measurements. Other films also exist for measuring pH.[5, 6] Electrodes also exist for environmental contaminants.[7, 8] Solid-state electrodes that employ crystals or pellets of the salts of the analyte are also quite common. Most fluoride ISEs, for example, are based upon this type of membrane.[9, 10] Liquid membranes that contain an ionophore in a polymeric matrix have also been used.[11, 12] Ionophores selectively complex ions and aid in the transport of ions through a membrane. As such, ionophores can be tailored to form complexes with various ions selectively. Gas permeable membranes that allow gaseous analytes to diffuse through and then dissolve into the reference electrode solution are also common membrane based electrodes. Ammonia ISEs are the best examples of this type of electrode.[13, 14]

Metal working electrodes that measure the activity of metal ions in solution that are the same as the electrode material can also be used. These electrodes can be used to measure many different metal ions in solution.[15] These electrodes are classified by four different types: electrodes of the first, second, and third kind, and redox electrodes. Electrodes of the first type are simply composed of a piece of metal that is then immersed in a solution containing cations of that same type of metal. An example of this is a silver wire in a solution of silver ions. An electrode of the second kind consists of a piece of metal coated with an insoluble metal salt. The most common example of this is the silver/silver chloride electrode. An electrode of the third kind responds to a cation other than that of the metal used as the electrode material. These electrodes are much less commonly used due to problems with interferants that plague the measurements. Redox

electrodes are composed of inert metals and measure the ratio of various oxidation states of a given analyte in solution.

Another type of potentiometric sensor that is commonly used is the field effect transistor (FET). The FET is typically composed of two n-type silicon layers separated by a p-type silicon layer, as seen in Figure 1.4. The two n-type regions act as a source and a drain for electrons, respectively. The source is electrically biased as compared to the drain region by a small applied potential, V_{ds}. The gate and silicon layers form a capacitor by placing a silicon dioxide layer between them. Applying a potential, V_{gs}, then charges the gate. There is also an intrinsic threshold potential of the system, V_t. This is the voltage across the gate at which inversion occurs. The initial value of V_{gs} is made to be less than V_t so that when V_{gs} exceeds V_t, a surface inversion occurs.[16] This is caused by the electron-dominated surface becoming a hole-dominated region.[17] This surface inversion causes the p-type region to become an n-type region and allows the flow of electrons from the source to the drain. This current, I_d, is then measured and is given by Equation 1.4,

$$\mathbf{I_d = C_{ox}\,\mu\frac{w}{l}\left[\left(V_{gs}-V_t\right)V_{ds}-\frac{1}{2}V^2_{ds}\right]}, \qquad (1.4)$$

where C_{ox} is the oxide capacity per unit area, μ is the electron mobility in the channel , w and *l* are the width and length of the channel, V_{gs} is the input voltage on the gate, V_t is the threshold voltage, and V_{ds} is the applied drain-source voltage.[18] Any analyte interactions with the gate region influence V_{gs} and can cause this surface inversion to occur. There is also a change in I_d that is measured and used to quantify the amount of analyte present.

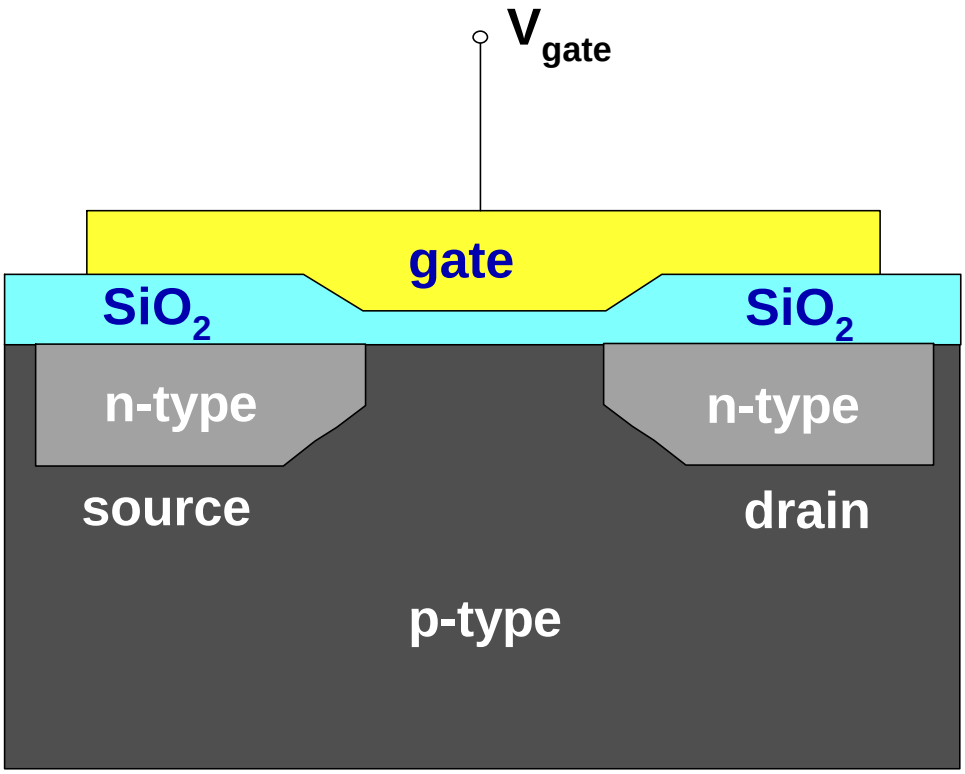

Figure 1.4. Schematic diagram of a field effect transistor (FET).

There are various types of FETs, with the broadest class of FETs being the CHEMFET. Depending upon the type of chemically selective layer deposited onto the SiO_2 insulating layer, this classification can be broken down further. ISFETs are ion-selective FETs and are based upon standard ISE technology integrated with traditional FET instrumentation. Chemically selective phases used with ISFET devices exist for many types of ions, including NH_4^+ [19] and other cations.[20-26] BioFETS are designed using biological membranes or other biospecific films to measure biologically important molecules. One such device uses the antenna from a beetle as the selective "film" for chemical sensing.[27] There are also devices for measuring enzymes (ENFETs) and immuno-chemicals (IMFETs).[24]

Voltammetric sensors are based upon the measurement of current as a function of voltage. This type of measurement relies on the applied voltage to drive a redox reaction to occur at the surface of an electrode.[28] The reaction that occurs at the surface of the electrode is of the general type given by Equation 1.5,

$$\mathbf{O_x + ne^- \rightarrow R_{ed}} \qquad (1.5)$$

where O_x is the oxidized species, ne^- is the number of electrons transferred, and R_{ed} is the reduced species. Depending upon how that voltage is applied to the system, the technique can either be amperometric or voltammetric in nature. In amperometry, the voltage is maintained at a fixed value and the analyte solution is swept through a cell containing the electrode. By selecting the appropriate voltage, the redox reaction of interest can be forced to occur. A reference and a working electrode are used in this type of measurement, with the fixed voltage being applied between these two electrodes. As the analyte diffuses to the working electrode surface, a current is generated as the

material is oxidized or reduced. The amount of charge used to drive the redox reaction is given by Equation 1.6,

$$\mathbf{Q = n_e\ F\ N_m} \qquad (1.6)$$

where Q is the number of coulombs used to convert N_m moles of analyte, n_e is the number of moles of electrons used in the process, and F is Faraday's constant. Differentiating 1.6 with respect to time yields Equation 1.7,

$$\mathbf{I = -n_e F A_r D}\left(\frac{\mathbf{dc}}{\mathbf{dx}}\right)_{\mathbf{x=0}} \qquad (1.7)$$

where I is the current, A_r is the area of the electrode, D is the diffusion coefficient of the analyte, and $\left(\frac{\mathbf{dc}}{\mathbf{dx}}\right)_{\mathbf{x=0}}$ is the change in concentration with distance measured at the electrode surface.[29] Selectivity is achieved in part by the applied voltage needed to drive the redox reaction and by the fact that only electroactive species can be measured using this technique. Added selectivity can be achieved by coating the electrode surface with a chemically selective film that "attracts" the analyte towards the electrode surface.[30, 31]

In voltammetry, the rate of the redox reaction occurring at the electrode surface is proportional to the current flowing through the electrode.[28] In contrast to amperometry, the voltage is generally varied and the resulting current is measured.[32] Another difference is that a third, or counter electrode, is used. The typical cell arrangement is shown in Figure 1.5. Different voltammetric techniques arise based upon the way in which the voltage is applied. However, the general theory is the same for all of the various techniques. If the reaction in Equation 1.2 is reversible, then the application of a

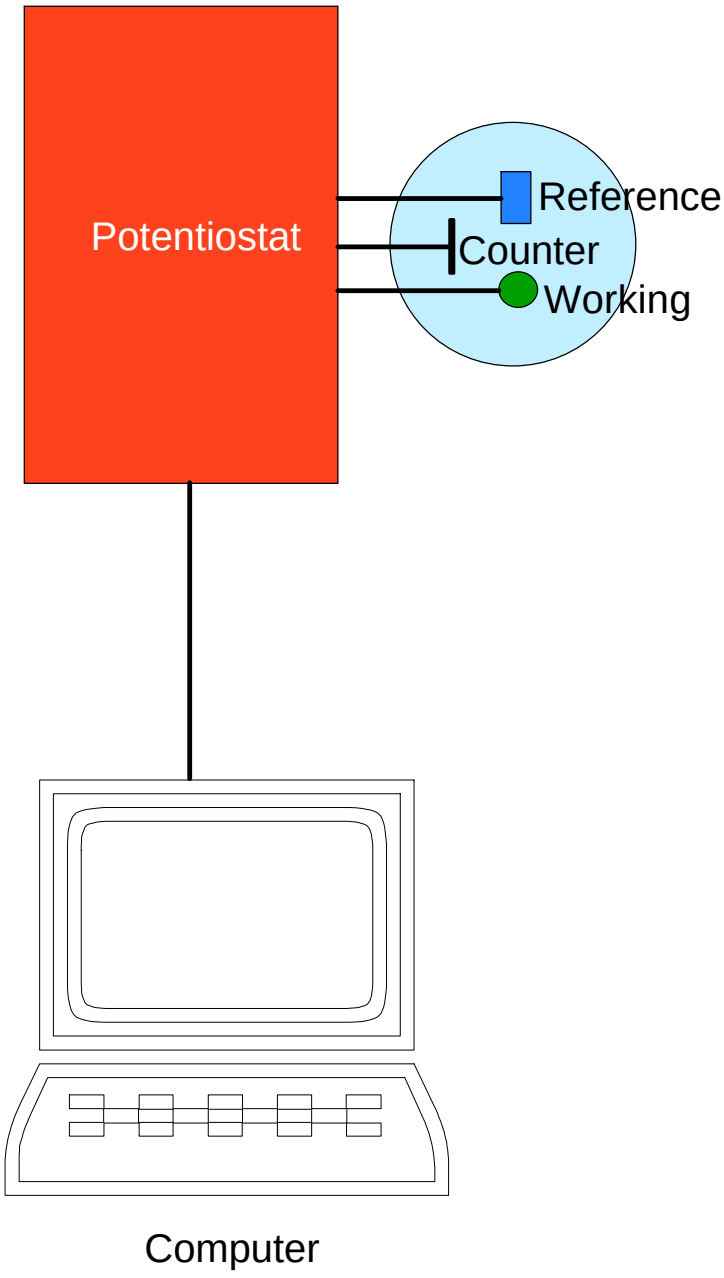

Figure 1.5. Typical cell arrangement used in voltammetric measurements.

potential E causes the ratio of the oxidized and reduced species to comply with Equation 1.8,

$$\mathbf{E = E^{o} - \frac{RT}{ne^{-}F} \ln \frac{C_R^{o}}{C_O^{o}}} \qquad (1.8)$$

where E^o is the standard redox potential for the pair, R is the gas constant, T is the temperature, ne^- is the number of electrons transferred, F is Faraday's constant, and C_R^o and C_O^o are the concentrations of the reduced and oxidized species at the electrode, respectively. The measured current is also affected by the flux of analyte to the electrode surface. This flux is then defined by Equation 1.9,

$$F = -\mathbf{A_r D_O}\left(\partial \mathbf{c_O} \big/ \partial \mathbf{x}\right) \qquad (1.9)$$

where Φ is the flux, D_o is the diffusion coefficient of the oxidized species, and x is the distance from the electrode surface.[33] Equation 1.9 can also be written in terms of the reduced species for anodic processes. In practice, this type of measurement yields a peak in the plot of current versus voltage. This peak shows the characteristic voltage at which the species of interest is either oxidized or reduced, depending on the direction of the voltage sweep. This response can generally be reversed by simply sweeping the voltage back in the opposite direction.

As with amperometry, some selectivity is inherent in the technique based upon the applied potential and the fact that the species must be electroactive. This selectivity can be greatly enhanced by using a chemically selective film on the working electrode. Films such as self-assembled monolayers [34], Nafion [35], and other polymers [36] have been employed to sequester the analyte near the working electrode surface.

1.3.3 Optical Sensors

Optical sensors rely on the interaction of light with the analyte to give rise to a measurable response. In most cases, light is propagated along the length of a waveguide until it reaches a region where interactions with the analyte occur. These interactions can cause changes in refractive index, absorbance, or fluorescence, among other things.[37] Optical chemical sensors can be classified as either intrinsic or extrinsic. An intrinsic optical sensor is one in which the chemically selective film is directly attached to or imbedded in the waveguide material. In contrast, an extrinsic sensor is one in which the waveguide simply acts to channel the light to a sensing region or solution containing the analyte. Many platforms of optical sensors exist, such as optical fibers, planar waveguides, and surface plasmon resonance sensors. Due to the many similarities between optical fibers and planar waveguides, only optical fibers will be discussed here.

One of the most commonly used waveguides is the optical fiber. An optical fiber is a thin cylinder of glass or plastic that efficiently channels light down its length.[38] It is composed of three distinct layers: a jacket that surrounds the entire fiber, cladding that surrounds the core, and the core. Figure 1.6 shows the three sections of a typical optical fiber. The fiber is constructed with materials in such a way that the cladding material has a lower refractive index than that of the core material. This is a critical requirement so that the light will travel down the length of the fiber by total internal reflection. Total internal reflection is governed by Snell's Law, which states that

$$\mathbf{n_1 \sin} q_1 = \mathbf{n_2 \sin} q_2 \qquad (1.10)$$

where n_1 and n_2 are the refractive indices of the core and cladding material and θ_1 and θ_2 are the angle of incidence and refracted light, respectively. For light to be propagated

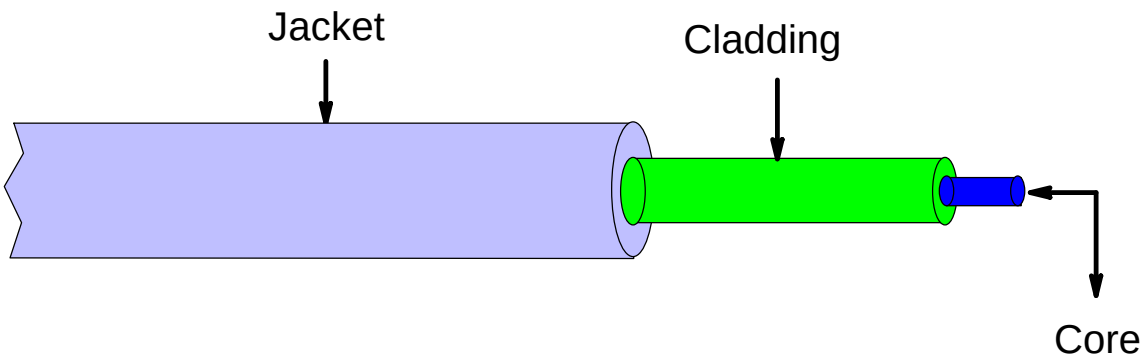

Figure 1.6. Composition of a typical optical fiber.

down the fiber, $\sin\theta_1 \geq n_2/n_1$ must be met, which occurs when $\theta_2 \geq 90°$.[39] Light enters the fiber at one end and any light that enters the fiber with angles inside the cone of acceptance will be propagated along the fiber (Figure 1.7). All other light will refract into the cladding material. This was once thought to be a limitation, but has recently been used as another method for sensing and will be discussed below. The cone of acceptance can be described in terms of the maximum half acceptance angle, β, given by Equation 1.11,

$$\sin ß = \left(n_1^{\,2} - n_2^{\,2}\right)^{1/2} \Big/ n_o \qquad (1.11)$$

where n_o is the refractive index of the medium surrounding the fiber.[39] Another way of stating this is by defining the numerical aperture, NA, of an optical fiber. The value of NA also defines the cone of acceptance and is a commonly used figure of merit for optical fibers. Equation 1.12 defines as

$$NA = n_o \sin ß \qquad (1.12)$$

Larger values of NA provide a more efficient collection of light into and down the optical fiber.

Another important aspect of sensing with optical fibers has to do with the efficiency of the total internal reflection phenomenon. For this process to be 100% efficient, there must not be any flux of energy into the cladding material.[37] However, there is always some absorption or scattering of light by the fiber that occurs. In addition, there is also a small flux present that penetrates into the cladding material. This flux is an electric field and is known as the evanescent field or evanescent wave. The evanescent

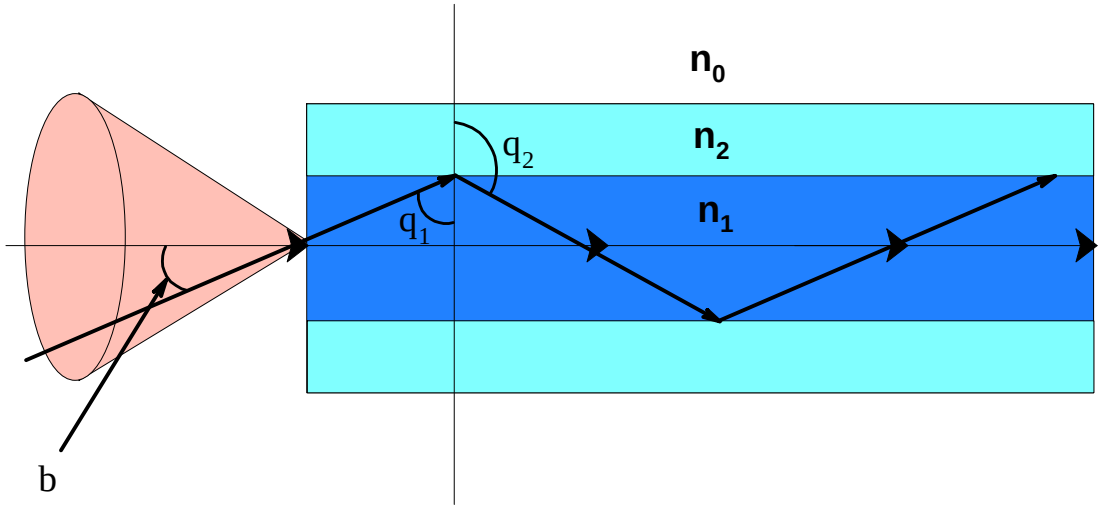

Figure 1.7. Depiction of the cone of acceptance for an optical fiber.

wave enters into the cladding material perpendicular to the reflecting surface.[38] This wave can be utilized in exciting or interrogating analyte molecules near the surface of the optical fiber. The depth of penetration, dp, of the evanescent field is dependent upon the wavelength of light used and the incidence angle as seen in Equation 1.13

$$\mathbf{dp} = \frac{l_o}{\mathbf{4}p}\left(\mathbf{n_1}^2 \sin^2 q_1 - \mathbf{n_2}^2\right)^{-1/2} \qquad (1.13)$$

where λ_o is the incident wavelength of the light used.[39] For visible light, dp is typically on the order of 100-200 nm. This is the primary mechanism by which certain intrinsic optical fibers function.

As with the other chemical sensors previously discussed, optical fibers employ a chemically selective phase to achieve the desired selectivity. Many phases exist, and most of the phases already mentioned are amenable for use with optical fibers. For example, optical fibers have been chemically coated to detect penicillin [40], biologically important compounds [41, 42], pH [43-45], drug metabolites [46], organics [47, 48], explosives [49], and metal ions.[50, 51]

Another type of optical sensor that has become popular during the last 10 years is the surface plasmon resonance (SPR) sensor. While this sensor has not been used extensively for true chemical sensing, it has been used to monitor the binding of molecules to metallic surfaces and for biological assays. SPR is based upon the interaction of a wave of surface plasmons with analytes on or near the surface of a metallic film. Surface plasmons are a collective oscillation of free electrons which travel along the surface of a metal.[52] Surface plasmons result from a charge-density oscillation at the interface of two media that have dielectric constants of opposite sign.[53] For

example, a metal film and a glass slide would satisfy this requirement. An evanescent wave is generated at the interface of the two media and decays exponentially into both media.[53] The wave has its maximum intensity at the interface of the two media and is used to probe the surface of the sensor as the analyte interacts with an immobilized film.[54] Energy from the incident light wave is absorbed by the surface plasmon wave. Because of this, SPR is sensitive to variations in the optical parameters of the transducing medium. These changes are monitored and are the basis for SPR measurements. As an example, refractive index changes as small as 10^{-4} can be detected using SPR.[55]

The widespread use of diode lasers has resulted in the use of visible wavelengths for many sensing applications. Therefore, the most commonly used light sources and metals are visible light and gold or silver, respectively. The dielectric properties of both gold and silver make them the most viable metals for interactions with visible light. The combination of these metals with visible light sources results in a good range of wave propagation lengths and penetration depths into the metal and dielectric materials. Table 1.1 summarizes some of the these values for a metal-water interface.[53]

There are different instrumental configurations used for SPR monitoring, depending upon how the light is transmitted to the metal-dielectric interface.[53] In addition to the transducer and chemically selective phase used in these systems, there are required optics and electrical components needed to collect the data.[53] Figure 1.8 shows three of the more common configurations used. The most commonly used configuration is called the Kretschmann configuration [56], which employs a prism coupled to a dielectric material coated with a metallic layer (Figure 1.8 A). There are also configurations based

Table 1.1. SPR values for various metal-water interfaces.

	Silver		Gold	
	630 nm	850 nm	630 nm	850 nm
Propagation length (mm)	19	57	3	24
Penetration depth into metal (mm)	24	23	29	25
Penetration depth into dielectric (mm)	219	443	162	400

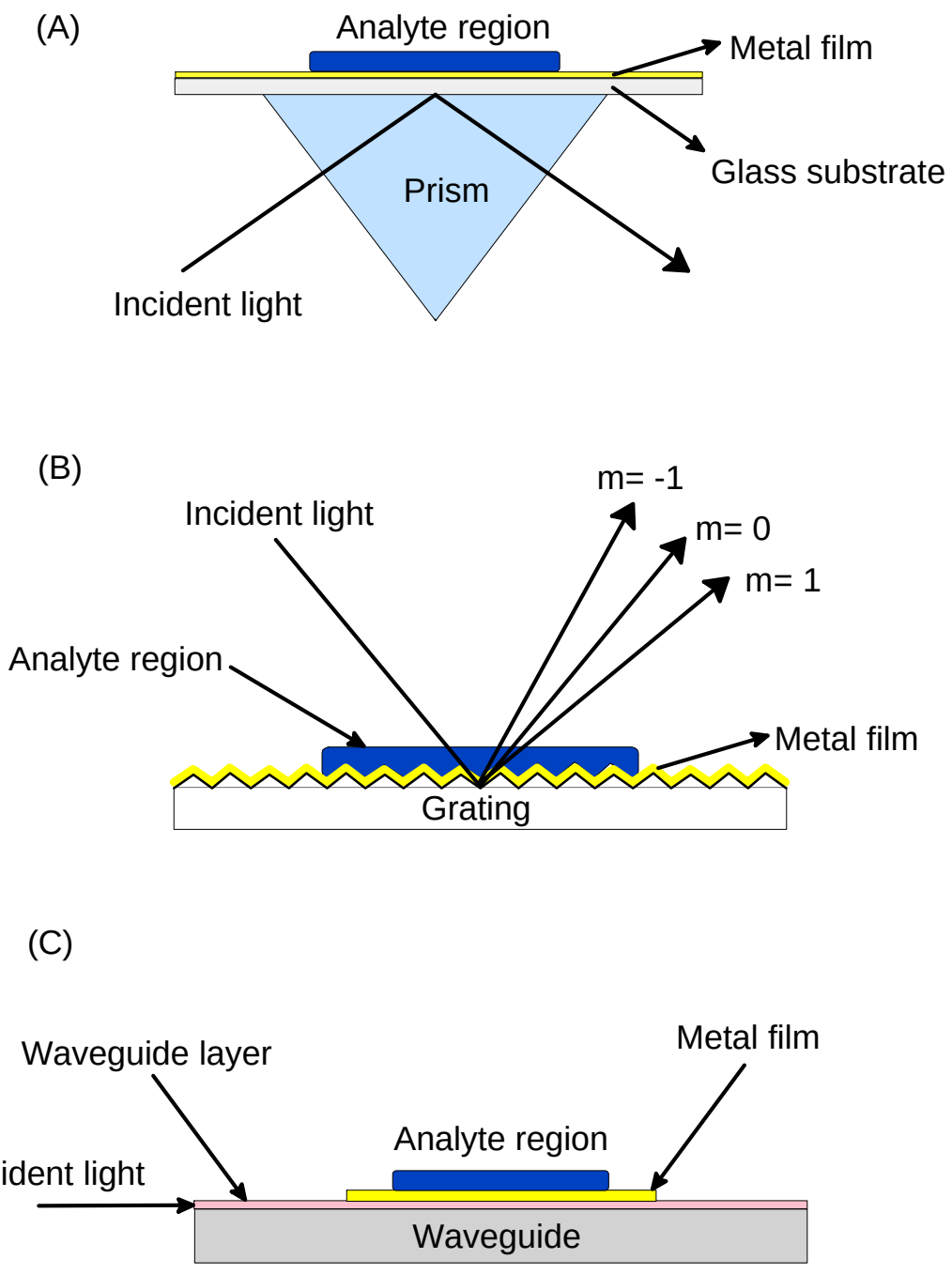

Figure 1.8. Common optical arrangements for surface plasmon resonance sensors. (A) Kretschmann configuration (B) Grating based configuration and (C) Waveguide based configuration.

upon gratings (Figure 1.8 B) and planar optical waveguides (Figure 1.8 C).[52] These different configurations have evolved because each offers something the others may not be able to offer. For example, the grating based configuration allows for a more accurate measurement of wavelength when using wavelength interrogation (about 5×10^{-4} nm).[53] The waveguide based configuration allows for more flexibility in the way that the incident light is coupled to the metal-dielectric interface.[53] In addition to the different configurations of SPR, various interrogation methods also exist. SPR sensors can be probed using angular or wavelength interrogation, or intensity measurements. In angular interrogation, the incident angle of the light source is varied and the resulting change in the SPR signal measured. The same is true of the wavelength interrogation method, except the wavelength of the incident light is varied. In the intensity measurement approach, the wavelength and angle of the light source are held fixed while the intensity of the reflected light is monitored. In general, the intensity measurement is the more sensitive of the three, but is limited by the width of the SPR curve.[53]

As with the other previously mentioned sensors, there exists a wide array of chemically selective phases used to coat SPR sensors. SPR has been used to detect metal ions [52, 57], pH [55], organics [58] and biological samples.[54, 59]

1.3.4 Mass Sensors

Chemical sensors that measure changes in mass are some of the most commonly employed. Typical examples of this class of sensor are quartz crystal microbalance (QCM), surface acoustic wave (SAW), flexural plate wave (FPW) devices and microcantilever (*MC*) based sensors. QCM, SAW, and FPW sensors rely primarily on a

change in mass that can be detected by changes in factors such as frequency, amplitude, mechanical deformation or phase shift. This change in mass can result from bulk interactions (absorption) or surface confined phenomenon (adsorption). While *MC* based sensors can be used to detect mass changes, it is generally a change in surface stress that is used for *MC* chemical sensing. This will be discussed in greater detail in section 1.4.1. The above sensors are based upon a piezoelectric oscillator with a selective film applied to its surface. As the analyte interacts preferentially with the film, a measurable response is obtained. Each of these sensors will be discussed in greater detail below.

QCM based sensors employ a quartz crystal oscillator with a metallic film placed on it for electrical contact, as seen in Figure 1.9. These quartz crystals typically operate in the frequency range of 5-10 MHz, with frequency changes as little as several Hz being measurable. The crystal can then be coated with a chemical film to provide the sensor with selectivity.[60-66] In some cases, the metallic film on the crystal can itself be the selective film.[67, 68] The coated QCM crystal is then placed into an oscillation circuit where it resonates close to its fundamental resonance frequency. This fundamental frequency depends on the nature of the crystal (i.e. thickness, structure, shape, and mass). In either case, the analyte adsorbs onto the metallic surface or absorbs into the chemical film and causes the resonance frequency of the oscillator to change. This change in frequency can then be related to the change in mass using Equation 1.14, also known as the Sauerbrey equation.

$$\Delta f = -\frac{1}{r_m k_f} f_0^2 \frac{\Delta m_a}{A_{cr}} \qquad (1.14)$$

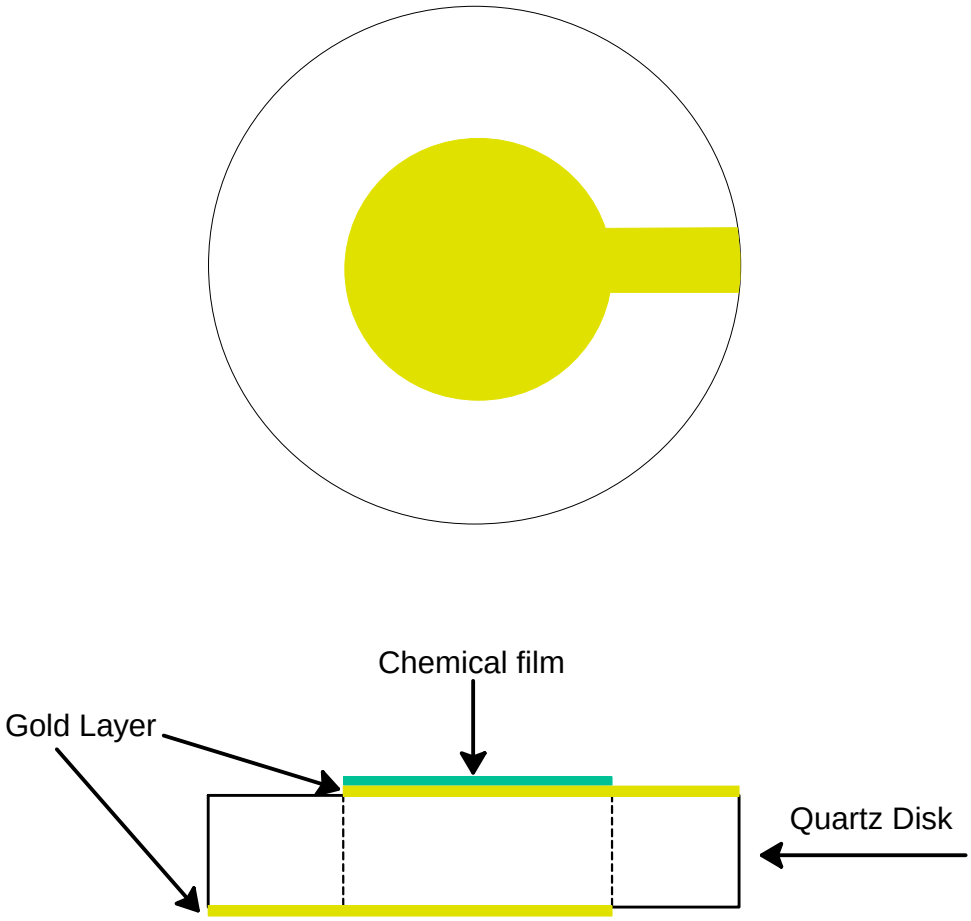

Figure 1.9. Depiction of a typical quartz crystal microbalance (QCM).

The Sauerbrey equation relates the change in frequency, Δf, to the change in mass, Δm_a, using the density of the chemical film, ρ_m, the frequency constant of the crystal, k_f, the fundamental resonance frequency of the crystal, f_o, and the cross-sectional area of the crystal, A_{cr}. As can be seen from the equation, an increase in mass results in a decrease in frequency. The above equation assumes that the measurement is being performed in the gas phase. If the measurement is being performed in a liquid environment, the properties of the surrounding solution must be considered. However, Equation 1.14 can still be used to determine the mass change as described above. The fundamental resonance frequency of the crystal is dramatically altered due to the presence of the liquid environment. This results in Equation 1.15 [69],

$$\Delta f = f_o^{3/2} \left(\frac{\eta \rho}{\pi \eta_q \rho_q} \right)^{1/2} \qquad (1.15)$$

which is used only to describe the frequency change when placing the crystal into a liquid environment. The equation relates this frequency change to the density (ρ) and viscosity (η) of the surrounding liquid and the density (ρ_q) and viscosity (η_q) of the quartz crystal. As can be expected, measurements in highly dense and/or viscous solutions dramatically dampen the fundamental resonance frequency and therefore limit the sensitivity of the sensor. This can be somewhat overcome by using thinner crystals, as the fundamental resonance frequency increases as the thickness decreases. However, the crystals become much more fragile and their thickness decreases. In addition to the density and viscosity of the solution affecting the value of f_o, crystal surface roughness, interfacial effects, and viscoelastic changes in the chemical film on the surface can also cause changes in f_o.[70]

These effects can be differentiated from "true" mass gain responses with the use of proper algorithms.

The main strengths of QCM based sensors are their low cost, ease of use in the gas phase, temperature stability and durability.[71] Their main limitations are that they suffer from lower sensitivity than other sensors and are very problematic in liquid environments.

SAW chemical sensors are based upon a pair of interdigital transducers (IDTs) deposited onto a piezoelectric substrate, as seen in Figure 1.10. In the simplest configuration, called a delay line, an alternating voltage is applied to each finger pair, which in turn creates an electric field in the piezoelectric material. Particles within the solid are displaced and a wave subsequently travels along the surface of the sensor until it interacts with a second pair of fingers. This triggers an alternating voltage in the second pair of fingers that can then be detected electrically and quantified. This configuration is called a delay line because the acoustic wave traveling along the surface does so quite slowly as compared to an electromagnetic signal.[70] A second type of SAW sensor is called the SAW resonator, where there is one interdigital system placed in the center of a resonator cavity.[72] Both configurations yield similar outputs, with the resonator configuration having higher frequency stability. Sensing with SAW devices occurs when mass loading in the region between the pairs of fingers causes the surface wave to change velocity, thus causing a reduction in frequency as described by Equation 1.16.[71]

$$\frac{\Delta n}{n_o} = -\mathbf{c}_m f_o \Delta \mathbf{m}_s \qquad (1.16)$$

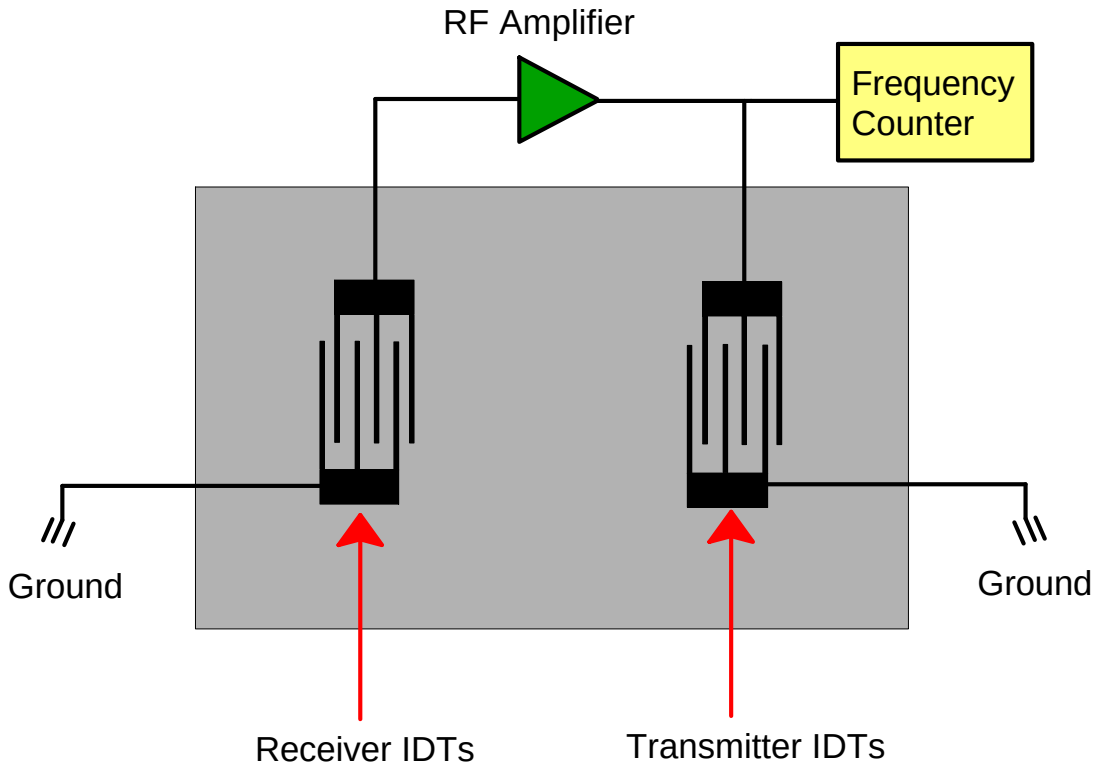

Figure 1.10. General design of a surface acoustic wave (SAW) sensor.

Equation 1.16 relates the reduction in acoustic wave phase velocity (Δv) to the acoustic wave phase velocity (v_o) using a mass sensitivity factor (c_m), the resonance frequency (f_o), and the areal mass loading on the sensor surface (m_s). This change in acoustic wave phase velocity leads to a concomitant change in resonance frequency of the sensor. This change in resonance frequency can be given by Equation 1.17, assuming the interaction of the analyte does not alter the mechanical properties of the film,

$$\Delta f = (k_1 + k_2) f_o^2 t_f r_m \qquad (1.17)$$

where k_1 and k_2 are material constants of the substrate, t_f is the film thickness, and ρ_m is the density of the film. Changes in mass can be calculated from frequency changes using Equation 1.14 because SAW devices use quartz crystals as the substrate. Since SAW devices operate at frequencies of 30-300 MHz, much higher than QCM sensors, they are more sensitive than QCM sensors.

As with QCM based sensors, the application of a chemically selective film to the SAW surface is vital for achieving the needed selectivity to make chemical measurements, and a variety have been used.[73-80] The change in acoustic wave phase velocity and hence, frequency, is a combination of mass loading and physical changes in the sensing film. Depending upon the nature of the film, the observed change in frequency can be much larger than predicted for simple mass loading. This occurs when the sensing film employed is conductive in nature. Because an electric wave is also associated with the acoustic wave, the interaction of this electric wave with conducting films creates an acoustoelectric effect. This effect has a profound impact on the resonance frequency of the device.[70] Therefore, particular attention must be paid to the

type of film being used. Another interesting aspect of SAW sensors is that they generally employ a reference set of interdigital transducers. This reference set acts to reduce temperature effects and other environmental sources of noise.

SAW sensors have some decided strengths over QCM sensors. The biggest strength is their higher sensitivity due to their higher resonance frequency. Another key strength is that SAW sensors are built on a planar geometry that can easily incorporate array type structures to enhance selectivity.[72] One of the key limitations of SAW sensors is their very limited applicability in liquid environments. Because surface launched waves are highly attenuated by the liquid environment [72], their usefulness in this environment has been limited. While there have been a few reports of sensing using SAW systems in liquid environments [81-83], much more work needs to be done to improve the reliability of these types of measurements.

FPW based sensors are similar to SAW sensors in that they rely upon the attenuation of waves propagating along the surface of the sensor to provide an analytical signal, as shown in Figure 1.11. However, in FPW devices, the waves are of a completely different nature (see Figure 1.12).[72] The waves being utilized in FPW devices are called Lamb waves. Lamb waves are only excited in very thin solid plates, where the thickness of the plate is typically a fraction of the acoustic wavelength. These waves can either be symmetric or antisymmetric, depending upon the movement of the excited particles in the solid. When certain conditions are met, such as the waves being present at both sides of the plate, the antisymmetric waves are called flexural plate waves. This is due to the fact that they cause a mechanical "flexing" of the thin plate.[84] This type of wave is quite interesting because its velocity actually decreases as the thickness of the

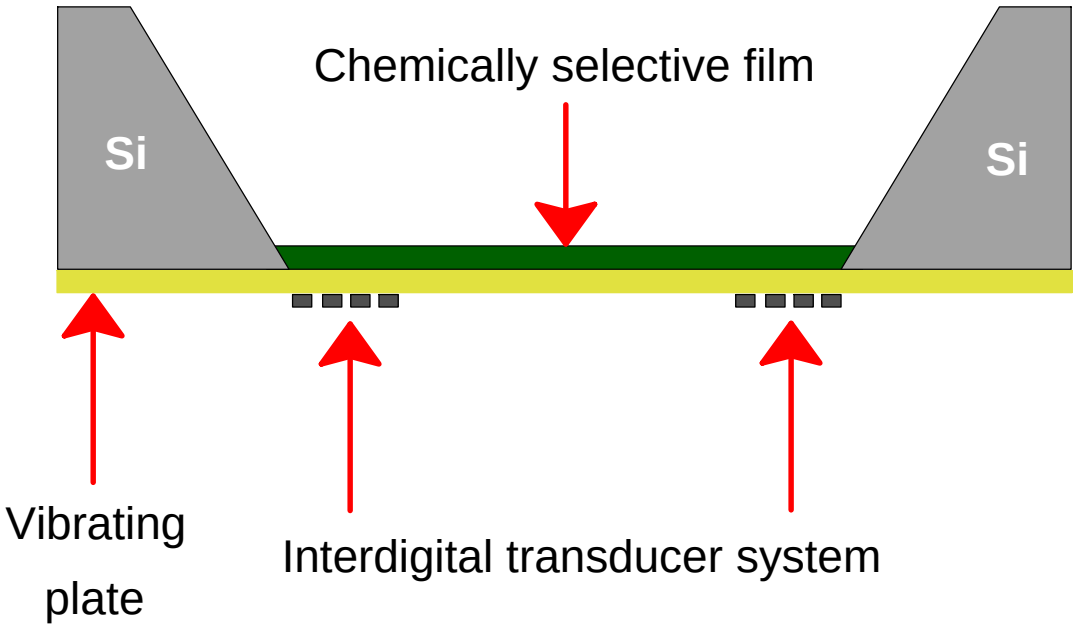

Figure 1.11. Illustration of a general flexural plate wave (FPW) sensor.

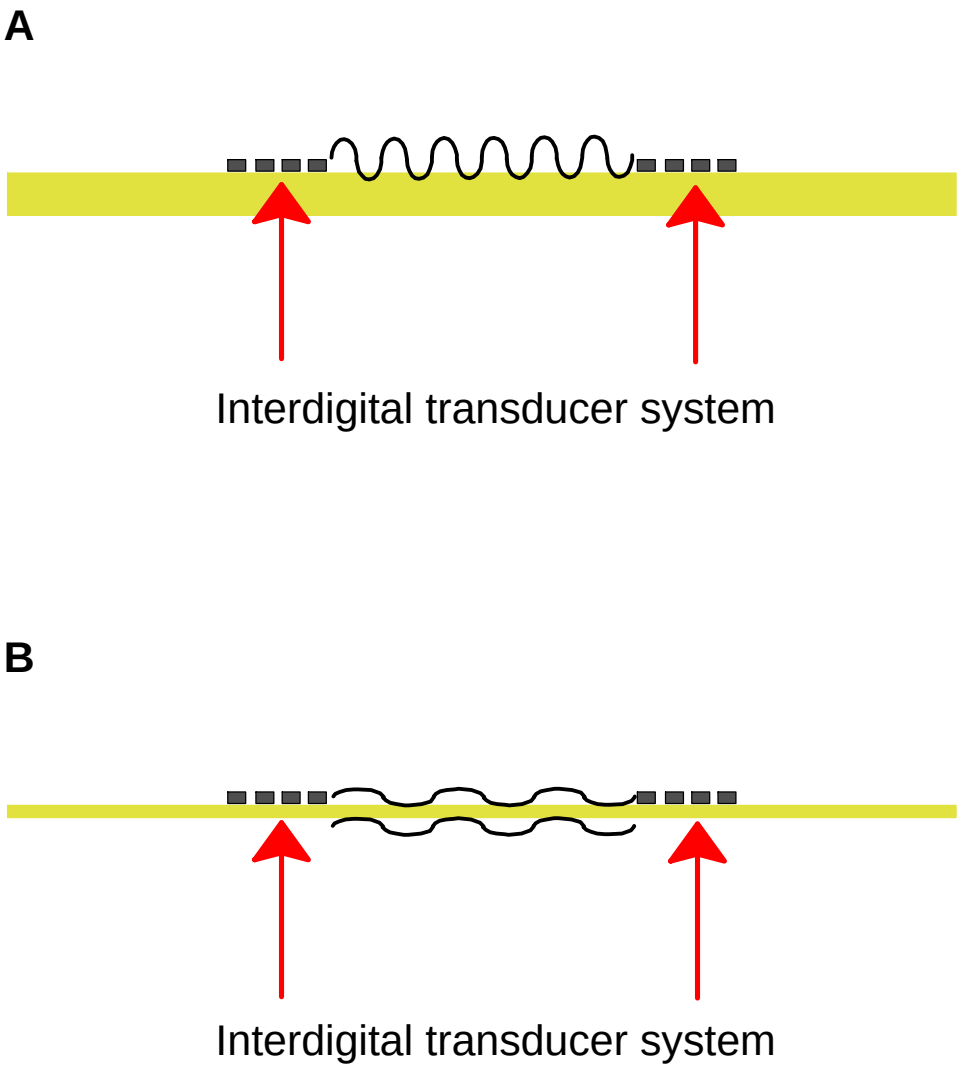

Figure 1.12. Depiction of waves in a (A) SAW device and a (B) FPW device.

plate decreases.[72] Therefore, this type of sensor has an easily tunable resonance frequency. The typical operation of FPW sensors is very similar to that of most SAW sensors and a wide variety of chemically selective phases have also been employed.[84-86]

FPW sensors do exhibit several strengths over SAW based sensors. The biggest strength of FPW sensors over SAW sensors is that they are easily used in a liquid environment since their surface waves are not emitted into the liquid.[72] This is possible because a phase velocity smaller than that of the surrounding liquid is employed, which traps the acoustic wave in the plate.[71] This results in a minimal energy loss to the surrounding liquid. A strength that falls out of this principle is that the electrical components of the sensor can be put on the face opposite of that used for the sensing, effectively separating it from the sensing medium.[84] This can prevent damage from occurring to the electrical components. FPW sensors also have a higher inherent mass sensitivity, even though they have a lower operating frequency than SAW sensors. This is because the Lamb waves generated by FPW sensors are more easily influenced by mass loading due to their unique nature (evidenced by the fact that they do not penetrate into liquids as SAW waves do). One final strength of FPW sensors is that they are based upon silicon technologies and can be easily fabricated in large quantities. Potential limitations are that the sensing regions are very thin and thus relatively fragile and that they are composed of multilayers that can be hard to precisely define. Their preparation also involves a more complicated fabrication process, making them slightly more costly than other mass sensors.

The final type of mass sensor to be discussed is the *MC* based sensor. This will be done in greater detail in the following sections of the chapter.

1.4 MICROCANTILEVER BASED SENSORS

*MC*s have traditionally found use as scanning force microscopy probes, such as in atomic force microscopy (AFM). Figure 1.13 shows some examples of typical *MC* devices. It has only been during the past 10-15 years that their application into the chemical sensing realm has begun. This is due to their intrinsically high sensitivity to slight changes in mass, surface energy, or displacement. Displacements have been measured as small as 10^{-10} m in AFM. This sensitivity makes them prime candidates as transducers in chemical sensing systems. There are several different physical phenomena that lead to cantilever motion, and as such, several different detection modes have emerged. In addition to this, there are a wide variety of chemically selective phases that have been employed on several different types of underlying metallic films.

1.4.1 Sensing Strategies

*MC*s have two primary modes of generating response: frequency based and bending based modes. These various responses can be classified as either dynamic or static in nature. Dynamic measurements involve monitoring parameters such as frequency that are measured continuously (AC type measurements). Static measurements involve parameters such as bending that are measured at a given time (DC type measurements). Figure 1.14 is a flow chart showing the two modes of *MC* response and some of the causes of each.[87] The unique nature of both types of technique allows for dual sensing to occur, specifically in cases where parameters such as bending and frequency can be measured simultaneously.[88]

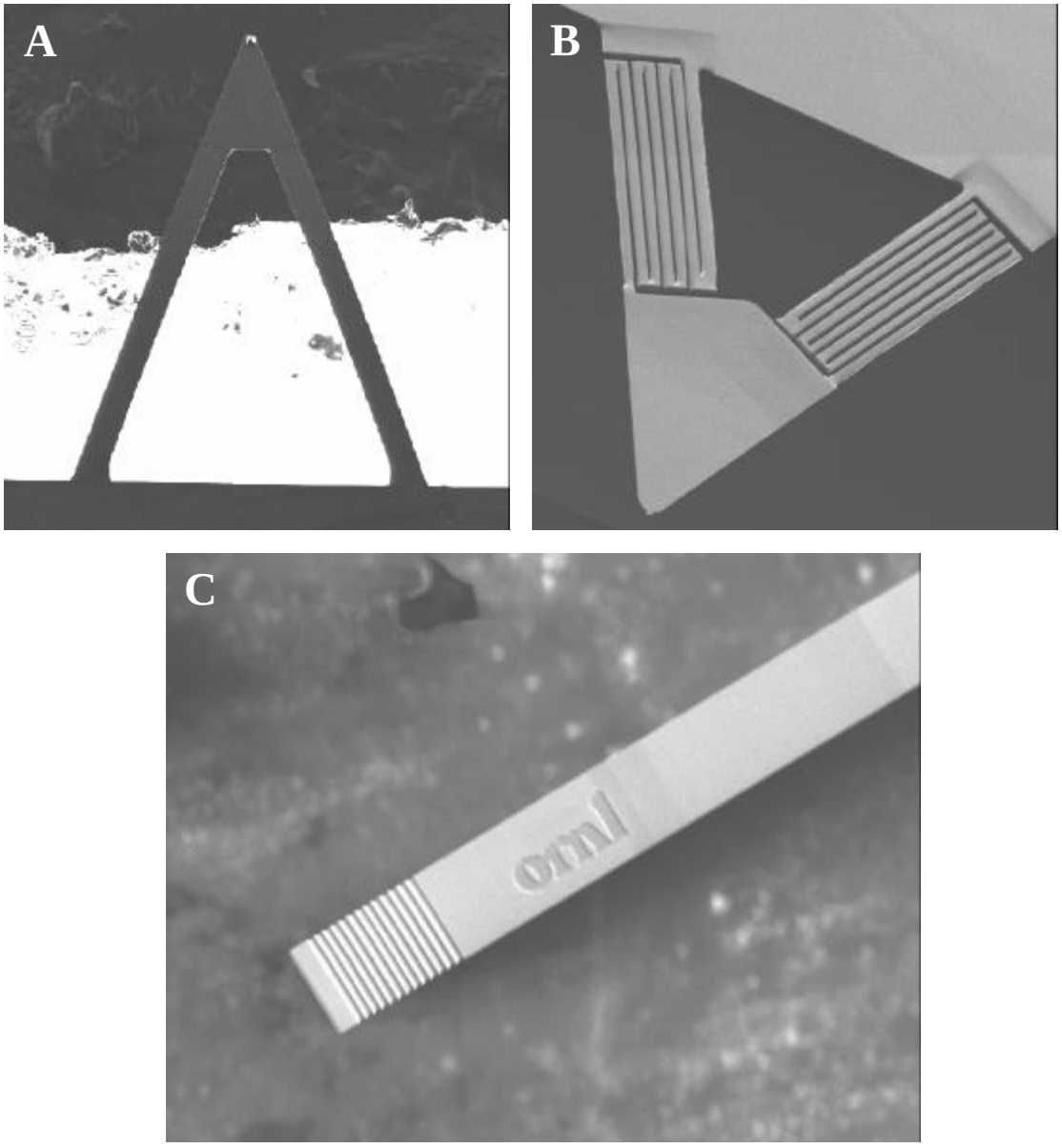

Figure 1.13. Examples of microcantilever (*MC*) devices. (A) traditional Si_3N_x AFM *MC* (B) silicon *MC* with 7 times the normal leg length (heptalever) (C) rectangular *MC* with grating ion beam milled onto the tip.

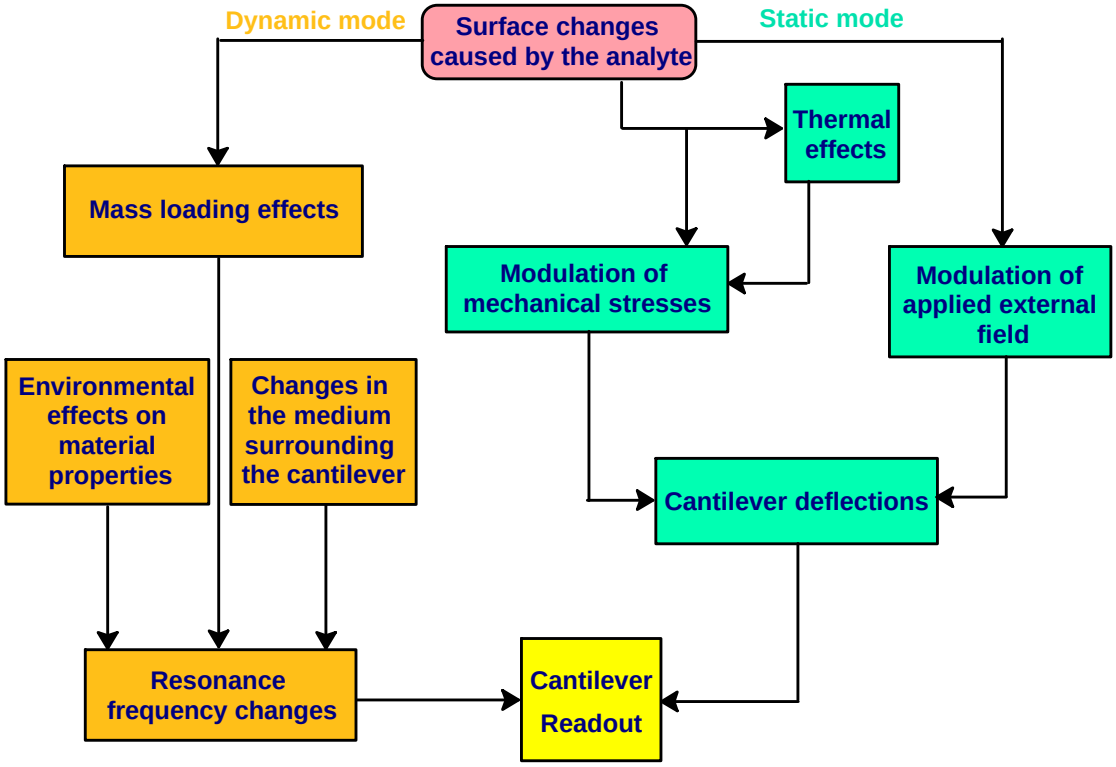

Figure 1.14. Primary modes of microcantilever measurements.

Frequency based measurements are one of the most commonly used measurements for *MC* sensing. Frequency measurements are sensitive to minute changes in the mass of the *MC*, with adsorbed masses in the nanogram to picogram range having been detected.[89-93] This type of measurement can be used for both chemical sensing and characterizing the amount of a chemically selective phase placed onto the *MC*. The resonance frequency of a *MC* is dependent upon many factors, but one of the most important factors is the spring constant of the *MC*. The spring constant, k, is given by Equation 1.18,

$$\mathbf{k} = \frac{\mathbf{Y\,w\,t^3}}{\mathbf{4}\,\boldsymbol{l}^3} \tag{1.18}$$

where Y is the Young's modulus and w, t, and *l* are the width, thickness, and length of the *MC*, respectively.[94] The Young's modulus is an intrinsic property of the *MC* material relating to its elastic properties. The relationship between the resonance frequency (f_o) and the spring constant of the *MC* can be seen in Equation 1.19,

$$\boldsymbol{f}_o = \frac{\mathbf{1}}{\mathbf{2}\boldsymbol{p}}\sqrt{\frac{\mathbf{k}}{\mathbf{m}^*}} \tag{1.19}$$

where m^* is the effective mass of the *MC*.[94] As material sorbs onto the *MC* surface, there is a concomitant change in resonance frequency. This is also true for analytes that absorb into chemical films applied to the *MC* surface. The relationship between the change in f_o and the change in mass can be seen in Equation 1.20,

$$\Delta\mathbf{m}_a = \frac{\mathbf{k}}{\mathbf{4\,n}\,\boldsymbol{p}^2}\left(\frac{1}{\boldsymbol{f}_1^{\,2}} - \frac{1}{\boldsymbol{f}_0^{\,2}}\right) \tag{1.20}$$

where n is a geometrical factor (n=0.24 for rectangular *MC*s) and f_o and f_1 are the resonance frequencies before and after the mass has been added, respectively.[88] As can be seen from the above equation, an increase in mass will be characterized by a decrease in resonance frequency. This result is very important in differentiating mass-loading related events from changes in the material properties of the *MC*.

As can be seen in Eq. 1.20, any change in the spring constant of the *MC* will also lead to a direct effect on the resonance frequency of the *MC*. There are certain circumstances in which the spring constant of the *MC* can change during a chemical measurement. For example, if the material properties of the selective film or metallic film applied to the *MC* alter its spring constant appreciably, a change in resonance frequency will be observed. This can occur when the thickness of the selective film or metallic layer approaches the thickness of the *MC* or when these films are innately stiff. Under certain circumstances, such as when the stiffness of the *MC* increases, the resonance frequency can actually increase.[95] This is in direct opposition to what Equation 1.20 predicts for the frequency response of a *MC* upon mass loading. In general, if the resonance frequency increases, it is due to a combination of mass loading and changes in the spring constant of the *MC*. By measuring the bending and resonance frequency simultaneously, any changes in spring constant can be quantified using Equation 1.21

$$\Delta \mathbf{k} = p^2 \mathbf{n} \left(\frac{\Delta s_1 - \Delta s_2}{4 \mathbf{n}_g} \right) \qquad (1.21)$$

where σ_1 and σ_2 are the stresses on the *MC* and n_g is another geometric factor.[94] One way of ensuring that no changes in spring constant occur is to only coat the apex of the *MC*. However, when this is done the sensitivity is reduced.[96]

It is useful to be able to compare the mass sensitivity of *MC* sensors to those of the other mass sensors just discussed. The mass sensitivity of frequency based *MC* measurements, S_m, can be calculated using Equation 1.22,

$$\mathbf{S_m} = \frac{1}{\boldsymbol{f}} \frac{\mathrm{D}\boldsymbol{f}}{\mathrm{D}\mathbf{m_a}} \qquad (1.22)$$

where Δm is normalized to the active sensing area of the device.[94] Another related measure of the sensitivity is the minimum detectable surface mass density, Δm_s^{min}, given by Equation 1.23,

$$\mathrm{D}\mathbf{m_s}^{\mathbf{min}} = \frac{1}{\mathbf{S_m}} \frac{\mathrm{D}\boldsymbol{f}}{\boldsymbol{f}} \qquad (1.23)$$

which is the minimum detectable mass over the active sensing area of the sensor.[97] Ward and Buttry have tabulated the values of sensitivities for various different mass sensors.[98] Table 1.2 summarizes their findings. As can be seen from the table, *MC* sensitivities can be as much as 10 times greater than the next most sensitive mass sensor. This makes them a very attractive alternative to other mass sensors. However, resonance frequency measurements are severely dampened in aqueous media, which limits the overall usefulness of this detection method. However, there has been at least one report of a system designed with a quality factor (resonance frequency divided by the width of resonance peak) that is up to three orders of magnitude better than the quality factor that is normally observed when monitoring frequency in liquid environments.[91] The authors

Table 1.2. Sensitivities of various mass sensors.

Sensor Type	f_o (MHz)	s_m (cm^2/g)	Δm_s^{min} (ng/cm^2)
SAW	112	151	1.2
QCM	6	14	10
FPW	2.6	951	0.4
MC	0.02-5	10,000	0.02

use either magnetic or acoustic energy to drive the resonance frequency of the *MC* back up to an acceptable value (10-15 kHz). However, more work needs to be done in this area if frequency measurements are going to play a major role in liquid phase sensing.

In addition to the measurement of frequency as a means of *MC* interrogation, *MC* bending is also used. This is the most widely used detection method because of its excellent sensitivity in both liquids and gases. In contrast to frequency measurements that rely upon mass loading, *MC* bending relies upon a differential surface stress on the two sides of the *MC*. There are three different models that explain what leads to the generation of surface stress needed to generate *MC* bending. The first model is one that is purely surface confined. The type of interaction described by this model is best illustrated by the self-assembly of an alkane thiol on a gold surface. The adsorption of the thiol molecule on the metallic surface causes the surface to expand to relieve the generated stress. Another example of this concept of *MC* bending comes partly from the idea of the "bimetallic effect". When two materials with different coefficients of thermal expansion are exposed to heat, the two materials expand to different degrees and cause a stress between the materials. If a beam composed of these materials is used, the beam will bend to relieve the stress. Using this concept as a starting point, *MC* bending principles were more thoroughly described in the early 1900s when G. G. Stoney studied the tension of metallic films on thin plates. He showed that metals deposited under tension caused the thin beams that the metals were deposited on to bend.[99] Stoney used beams 102 mm long, 12 mm wide, and 0.32 mm thick. When he coated these beams with nickel, they bent up to 4 mm, a very large degree of bending considering their length.

Using his findings it can be seen that a uniform surface stress acting on an isotropic material acts to either increase or decrease the surface area, which is called compressive and tensile stress, respectively.[100] If this stress is not compensated by an equal stress on the opposite side of a thin beam, the beam will bend to relieve the stress, as seen in Figure 1.15.[96, 101] This type of surface stress is described as a true surface stress, as it is generated in the surface of the *MC*.

The second model that leads to the generation of stress, and thereby *MC* bending, builds upon the first model. Whereas the first model dealt with the adsorption of a molecule on a metallic surface, the second model is governed by the absorption of molecules into the bulk of a thin film. In general, the absorption of molecules into a thin film causes the thin film to either contract or swell due to changes in the forces acting within the film. These forces can be dispersive, osmotic, electrostatic, and steric in nature. As with the case above, this leads to a stress being generated in the film that is then transmitted to the underlying surface. This again leads to the differential surface stress needed to generate *MC* bending. However, this is not a true surface stress as is the case with the interactions in the first model. Instead, it is an apparent surface stress that has been generated in the film and transmitted to the surface as described above. This apparent surface stress will then scale with the thickness of the thin film, up to a certain point, at which time the swelling of the film will not be transmitted to the surface.

The third model, which is the least understood, deals with surfaces that are colloidal or heterogeneous in nature. These surfaces contain nanometer-sized crevices that are accessible to analytes. It is believed that physical or chemical interactions of the

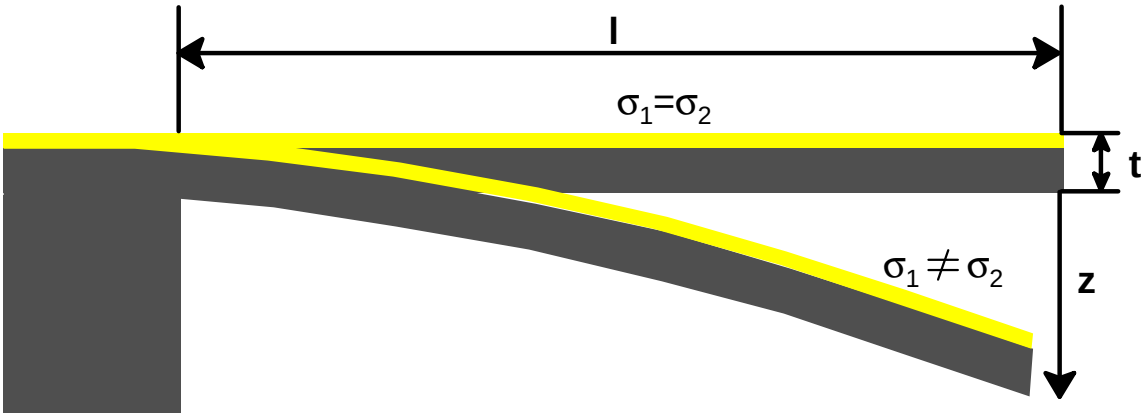

Figure 1.15. Thin beam bending described by Stoney.

analytes between adjacent particles (i.e. in the crevices) cause the particles to be either pulled together or pushed apart lead, which leads to the generation of the stress in the surface. It is therefore thought that bulk, surface, and intersurface interactions can play a considerable role in the response of *MC*s coated with these types of films. While the exact mechanism of stress is not completely known, it has been shown that this type of surface generates a considerable amount of stress.

All three models discussed above ultimately result in the bending of the *MC*. Stoney derived an equation for the bending of the thin beams he studied, which when applied to *MC* sensors can be written as Equation 1.24, also known as Stoney's equation,

$$\frac{\mathbf{1}}{\mathbf{R_c}} = \frac{\mathbf{6}\left(\mathbf{1}-n_{\mathbf{p}}\right)}{\mathbf{Y}\,\mathbf{t}^{\mathbf{2}}}\left(\mathrm{D}s\right) \tag{1.24}$$

where R_c is the radius of curvature, ν_p is the Poisson's ratio, Y is the Young's modulus, t is the *MC* thickness, and $\Delta\sigma$ is the differential surface stress on the two sides of the *MC*. The radius of curvature of the *MC* due to bending is related to the *MC* tip deflection and the length of the *MC* through Equation 1.25

$$\mathbf{z_{max}} = \frac{\mathbf{3}\left(\mathbf{1}-n_{\mathbf{p}}\right)\boldsymbol{l}^{\mathbf{2}}}{\mathbf{Y}\,\mathbf{t}^{\mathbf{2}}}\,\mathrm{D}s \tag{1.25}$$

where z_{max} is the maximum deflection and *l* is the *MC* length. The differential surface stress is maximized when adsorbates interact preferentially with one side of the *MC*, which is one of the main reasons chemically selective films are applied to one side of the *MC*s. In addition to this, attempts to passivate the "inactive" side of the *MC* can be made. One of the most interesting results of this is that any changes in the Gibbs free energy due

to analyte interactions with a selective film on the *MC* surface is directly converted into a change in surface stress.[102]

Another way to describe the surface of an *MC* is to define it in terms of its surface free energy. The surface free energy is defined as the reversible work per unit area needed to create new surface plastically (i.e. by cleaving a crystal), while surface stress is defined as the reversible work per unit area required to create new surface through elastic stretching (i.e. the pre-existing surface is stretched elastically).[100] Surface stress and surface free energy are related to one another by the Shuttleworth equation, Equation 1.26,

$$s = g + \frac{\mathbf{d}g}{\mathbf{d}e_{\mathbf{e}}} \qquad (1.26)$$

where σ is the surface stress, γ is the surface free energy, ε_e is the elastic surface strain defined as dA_s/A_s where A_s is the surface area and dA_s is the elastic increase in surface area.[103, 104] A clean, solid surface will exhibit a tensile surface stress (i.e. it seeks to minimize its surface area) if left undisturbed and this state is the upper boundary for how much energy a surface contains. Upon exposure to an adsorbate or application of a chemically selective layer, the atoms of the surface are caused to rearrange. This rearrangement causes a reduction in the surface stress of the solid. Therefore, the achievable surface stress is directly dependent upon the initial surface free energy available. A surface free energy of 1 N m^{-1} is typical of a clean, smooth gold surface in air. This value drops significantly when a metal/liquid interface is considered and even further for nonmetallic surfaces in water, with surface free energies on the order of 0.05 N m^{-1} being observed.[101] It is important then to maximize the initial surface free energy

so that a higher degree of surface stress attenuation can occur, which improves the dynamic range of the sensor.

1.4.2 Detection Methods

There are several different means by which to interrogate the above-mentioned modes of *MC* response. The four main methods that have been used to date are capacitance, piezoresistance, interferometry, and optical deflection. Each has its own strengths and limitations, which will be discussed in greater detail below.

Interrogation of *MC*s based upon capacitance measurements has found limited applicability.[105-107] In these measurements, the *MC* is used as one of the plates of a capacitor. The capacitance is highly sensitive to the movement of the *MC* and provides a direct measurement of displacement, as no voltage to deflection conversion is needed. Capacitance values as low as 1×10^{-18} F have been detected using this approach, which correspond to sub-Å deflections.[107] The ability to directly measure deflection without a displacement calibration, as is needed in optical and piezoresistance measurements, is one of the main strengths of using the capacitance to monitor *MC* deflection. One of the main reasons why this technique has not found widespread use is because it is not suitable for use in liquid environments. Faradaic currents develop between the plates, which makes it much more difficult to measure the capacitance. Another reason it has not been used as much for gas phase sensing is it suffers from a limited dynamic range, as very large deflections will result in the loss of capacitance due to the two plates being too far apart. Also, if the *MC* approaches the other plate of the capacitor too closely, the electrostatic force between the two objects can break the *MC*. There are also many

difficulties with integrating the required electronics onto the *MC* sensor in order to make the measurements, such as the high cost of fabrication of such a device.

Another method for measuring changes in *MC* deflection is to use piezoresistance measurements. Piezoresistance measurements are based upon the fact that as the *MC* bends, its resistance changes. Usually, the *MC* is made of a piezoelectric material or will have a piezoelectric channel inside of its surface. The *MC*s can then be encapsulated into another material that comprises a flow channel around the sensor or used in a traditional configuration. One strength of piezoresistance measurements, as compared to capacitance measurements, are that they give a direct measure of the change in surface stress when molecules interact with the surface of the *MC*.[108] In some cases, a piezoelectric material is deposited onto the *MC* [109-111], while in others the *MC* is composed solely of a piezoelectric material.[112-114] These measurements are generally made using one of two approaches: a coating on the *MC* surface or the *MC* physically attached to a sensing film. Using a coating on the *MC* is straightforward and will be discussed later. In the method where the *MC* is physically placed in contact with the sensing film, the tip of the *MC* is placed onto the sensing film. As the sensing film swells the *MC* bends and the resulting change in resistance is measured. This only works for a sensing film that swells primarily in the vertical direction. Piezoresistance measurements offer several unique strengths. One of these is that by using a simple Wheatstone bridge configuration, the resistance of the *MC* can be measured quite accurately and sensitively. This configuration also allows for differential measurements to be made in which one *MC* is used as the sensing *MC* and a second *MC* is used to subtract out sources of noise affecting both *MC*s.[108] Piezoresistive measurements, unlike capacitance measurements,

can also be made in both liquids and gases, making this type of measurement amenable to many sensing applications. Unlike optical measurements, piezoresistance can be measured in opaque solutions such as blood or environmental water samples. Another interesting strength as compared to the other approaches is that the circuits involved permit control of the surface temperature, which allows for the desorption of molecules from the surface of the *MC*.[100] *MC*s based upon piezoresistance can also quite easily be organized into arrays, which ultimately lead to a higher degree of selectivity. One limitation of this type of measurement as compared to capacitance or interferometric measurements is that the measured resistance must be calibrated in terms of deflection. The manufacture of this type of *MC* can also be quite challenging and depends upon lithographic techniques that increase the cost substantially. The sensitivity of this type of measurement is also lower than the optical techniques to be discussed next.

A third method for interrogating *MC*s is by using interferometry. This approach is based upon the interference of a reference laser beam with the one being reflected by the *MC*.[100] An interference pattern is created, which provides a direct measurement of *MC* deflection without the need to calibrate the measured response in terms of bending. This is possible because the movement of the rings in the pattern is easily given in terms of length, making a voltage to deflection conversion unnecessary. A second approach is to use an array of interdigitated *MC*s to form an optical diffraction grating. The light reflected off of the *MC*s forms a diffraction pattern in which the intensity changes as the *MC* bends. One limitation that this method suffers from is a more complex optical arrangement. The cantilever must be positioned extremely close to the optical components in order to collect the interference pattern. On the other hand, one strength

to this method is that an array of *MC*s can be interrogated by using the appropriate optics. This allows for much more information rich sensing to be performed.

The last interrogation approach is the most commonly used and is called the optical beam bending technique. This is the technique that has been utilized in all of the studies presented in this dissertation. The approach is derived from the principles governing the use of the atomic force microscope. In this method a laser beam is focused onto the tip of an *MC*, which acts as a mirror and reflects the laser beam. There are no special requirements for the laser, except that it must be able to be focused onto the area of the *MC*. The wavelength of the laser does not play an important role in most sensing circumstances. Diode lasers operating in the visible region are the most commonly used lasers for this approach. The reflected beam is then directed onto a position sensitive detector (PSD), which monitors the movement of the reflected laser beam across its surface. The PSD is composed of silicon and divided into four quadrants (see page 62). Because of this, different outputs are possible (i.e horizontal, vertical, and total). The PSD operates by measuring the voltage in each quadrant independently and then using mathematical relationships to obtain the three different outputs mentioned above. In addition, the signals for the horizontal and vertical outputs are divided by the total signal to help compensate for changes in laser intensity and other minor effects. As the reflected laser beam moves across the surface of the PSD, a voltage is generated based on the magnitude of the movement. This voltage is recorded and can be used to calibrate the *MC* response in terms of *MC* deflection, which is given in terms of nanometers of bending. *MC* responses will be reported in terms of voltage and deflection, depending upon the circumstance. In general, reporting the signal in terms of voltage is less

ambiguous because it does not rely upon any conversions from voltage to deflection that can depend heavily upon how the conversion is made. However, as optical systems among different research groups are bound to be different, reporting results in terms of nanometers of bending gives a means of comparing the different systems used, and ultimately the sensitivity that each group can attain.

1.4.3 Chemically Selective Coatings

Many types of chemically selective coatings have been applied to the surface of *MC* sensors. A brief review of some of the broad types of films that have been used will be presented here. One of the simplest selective coatings is the metallic layer deposited onto the *MC* that is generally used as a reflective coating. For instance, gold films have been used to selectively bind thiolated compounds [97, 115-118], palladium films have been used to detect hydrogen in air [119, 120], and both gold and platinum films have been used to detect photons [121] and charged particles.[122] These films are relatively simple to prepare and the reaction between the metal (i.e. gold or silver) and thiolated compounds is well established. Self-assembled monolayers specific for a wide range of analytes, such as metal and inorganic ions and DNA have also been formed on gold coated *MC*s.[123-126] These films have also been used to detect hydrocarbons and changes in pH. Cavitand receptors such as cyclodextrins and calixarenes have also been used.[101, 127, 128] There have also been many different types of polymers applied to the surface of *MC*s to make them selective for a class of analytes.[88, 92, 93, 129-133] Analytes studied range from environmental contaminants, organic solvents, chemical warfare agents, simple hydrocarbons, metal ions, and many more. Several groups have employed sol-gels as

chemically selective phases [109, 134] to monitor many of the same analytes. In the past several years, the application of biologically important selective films and/or reagents have also been applied to *MC* surfaces.[91, 101, 135-139] These films have been used to study DNA hybridization, biological warfare agents, and more.

1.5 STATEMENT OF PROBLEM

As previously mentioned, the need for more sensitive and selective measurements is a major driving force for research in the realm of chemical sensors. These two factors are directly related to the limit of detection that is achievable for a given analyte, which is the most common measuring stick for a chemical sensor. This work seeks to enhance both the selectivity and sensitivity, and hence the limits of detection that can be achieved using *MC* based sensors. Several different types of chemically selective films have been studied during the course of this work. Methods for coating *MC*s, as well as selectivity patterns, have been studied and capitalized upon. The selectivity has also been improved through the use of two different systems: a differential based system that both eliminates unwanted sources of noise as well as allows for response patterns to be obtained and a system based on an array of lasers that allows for the simultaneous interrogation of five *MC*s, which leads to unique response patterns. In addition, the sensitivity has been improved through the use of thicker selective films combined with nanostructured interfaces.

CHAPTER 2

CHEMICALLY SELECTIVE POLYMERIC FILMS ON MICROCANTILEVER SURFACES

2.1 INTRODUCTION

Recently, there has been an increasing interest in the development of miniature chemical sensors using micro-cantilevers (*MC*s) such as those commonly used in scanning force microscopy (SFM). *MC*s have been used in the past for a variety of physical and chemical applications. For example, bimaterial *MC*s have been used as miniature physical sensors for infrared radiation detection and temperature measurements [116, 140-144] and as chemical sensors.[89, 90, 93, 97, 116, 120, 131, 144-147]

In Chapter 1, *MC* chemical sensors were shown to offer a considerable increase in chemical sensitivity. Another distinct strength of the *MC* chemical sensors is the relatively small size of the sensing element. The *MC*s used in the present work have an active sensing area (~10^{-5} cm^2) that is about five orders of magnitude smaller than that of SAW, QCM and FPW devices (that have an active sensor area on the order of ~cm^2). Chemical sensing using SAW [148-150], QCM [151, 152] and FPW [150] devices fall under the general category of mass load transducers or gravimetric sensors [153] and achieve sensing by monitoring the sorption processes on the sensing element that result in mass changes. This is also possible using *MC*s, but the bending of *MC*s due to the generation of a differential surface stress is more commonly employed. Therefore, for any practical chemical sensing application, a chemically selective layer must be deposited on the sensor that can also provide a reversible binding of the analyte to the coated surface and

real-time monitoring. Selectivity is a common problem with chemical sensing devices and attempts to overcome this shortcoming have focused on coating the surface of individual sensing elements with analyte-selective films to provide the specificity for the target species.[151, 154-156]

In order to enhance the sensitivity of an *MC* sensor for a particular analyte, a variety of coatings have been applied to the cantilever surfaces. Phosphoric acid and bovine skin gelatin have been applied to the tips of cantilevers to detect humidity.[145] Gold-coated cantilevers were used to detect mercury vapor [146] and alkanethiols.[116] A polymethylmethacrylate coating was used to detect short-chain primary alcohols.[89] Polydimethylsiloxane was applied to the tips of cantilevers to adsorb volatile organic compounds.[93] These sensors have proven to be very sensitive with mass resolution down to the picogram range. However, the selectivity of these sensors has not been sufficiently investigated.

In the present studies, we investigated silicon *MC*s coated with thin films of polymeric chromatographic stationary phases (SP-2340 and OV-25). We investigated how a thin polar polymer coating of poly(bis-cyanopropylsiloxane) (SP-2340) affects both the sensitivity and selectivity of a microcantilever to analytes that vary greatly in their mode of interaction with coated and uncoated sides of an *MC*. The relation of film thickness and *MC* thickness on sensitivity and selectivity were investigated. An *MC* with a relatively nonpolar coating of poly(phenyl-methyl dimethylsiloxane) (OV-25) was compared to the polar coating. Because these phases are also used as GC phases, McReynolds constants were used to correlate *MC* response to analyte-phase interactions.

We also used focused ion beam (FIB) milling to modify the existing *MC*s and optimize their geometric characteristics.

Both the resonance frequency and bending of *MC*s have been found to vary reproducibly and sensitively as a consequence of adsorption of analytes on their surfaces.[143, 145-147] In the present studies, we utilized stress-induced changes in the bending of *MC*s [97, 143, 145-147, 157-160] coated with chemically selective films. As discussed in section 1.4.1, *MC*s coated with chemically selective films produce stress through the contraction or swelling of the film applied to the *MC*. This is the response mode that is utilized in the studies presented in this chapter. When a specific analyte is absorbed into the surface coating, an additional differential surface stress ($\Delta\sigma = \sigma_c - \sigma_{si}$, where σ_c and σ_{si} are the stresses on the coated and uncoated silicon surfaces) is induced, as well as a mass change. This in turn results in changes in the bending and resonance frequency of the microcantilever, respectively, that can be measured very sensitively using optical, piezoresistive or capacitive detection means.[143] In the present work we used an optical beam bending detection technique. The bending, z, depends linearly on the differential surface stress, $\Delta\sigma$ and is given by Equation 2.1 [143, 161],

$$\mathbf{z} = \frac{3\boldsymbol{l}}{\mathbf{t}_1 + \mathbf{t}_2}\left[\frac{1+(\mathbf{t}_1/\mathbf{t}_2)}{3(1+\mathbf{t}_1+\mathbf{t}_2)^2 + (1+\mathbf{t}_1\mathbf{Y}_1/\mathbf{t}_2\mathbf{Y}_2)(\mathbf{t}^2{}_1/\mathbf{t}^2{}_2 + \mathbf{t}_2\mathbf{Y}_2/\mathbf{t}_1\mathbf{Y}_1)}\right]\times\frac{\mathrm{D}s}{\mathbf{Y}^*} \quad (2.1)$$

where t_1 and t_2 are the thickness of the coating and *MC* substrate, *l* is the *MC* length, Y_1 and Y_2 are the Young's moduli of the coating and *MC*, and $Y^*=[Y_1Y_2/(Y_1+Y_2)]$ is the effective Young's modulus of the coated *MC*. Equation 2.1 was used in this work as opposed to Equation 1.25 due to the thicknesses of the selective films used in this work. When the film thickness approaches that of the *MC* thickness, contributions from the

material properties of the film must be taken into account, hence the additional thickness and Young's modulus terms.

2.2 EXPERIMENTAL

Thin films of gas chromatography stationary phases (SP-2340 and OV-25, Supelco Co., Bellefonte, PA, USA) were deposited onto micro-machined, V-shaped, silicon cantilevers (Park Scientific Instruments, Sunnyvale, CA, USA). The 600 nm thick silicon cantilevers had a 120 μm height, 90 μm base, and legs with a width of 26 μm. As supplied, the *MC*s had a 50 nm coating of gold on one side. In some cases, the gold coating was removed using aqua regia (75% HNO_3, 25% HCl) or the *MC* surface was cleaned with piranha solution (75% H_2SO_4, 25% H_2O_2). Thin films were cast on the *MC*s using a spin-coating procedure. SP-2340 dissolved in acetone (350 μl) was deposited on a *MC* spinning on a Teflon mount at 400 rpm during a 10 s time window. After spinning at 400 rpm for 10 s, the spinning rate was increased at 30,000 rpm/s to a final spin rate of 4000 rpm and maintained at that spinning rate for 2 minutes. After the spin coating process, coated *MC*s were placed in an oven at 70°C for at least 5 hours. Control of film thickness was achieved by varying the concentration of the SP-2340 solution. SP-2340 solutions ranged from 0.03 to 3 wt.% resulting in films from 50 to 500 nm thick. Films of OV-25 were cast in the same manner except this polymer was dissolved in methylene chloride.

Film thickness was measured by profilometry (Dektak 8000, Veeco/Sloan Technology, Santa Barbara, CA, USA) on films cast under the conditions described

above on silicon wafers. The flexibility of the *MC*s prevented us from dragging the profilometer stylus across the *MC* surface. Therefore, the film thickness measured on the wafer was used as an estimate of the thickness on the *MC*. The validity of this estimation of thickness was confirmed for one spin coated *MC* using changes in the resonance frequency of the coated cantilevers. The mounted *MC* was excited near its resonance frequency (35 kHz) by a piezoelectric speaker. Detection of the resonance amplitude was accomplished with a lock-in amplifier as the excitation frequency was swept across the resonance frequency range. As shown in Equation 1.20, the mass change can be determined by monitoring the change in resonance frequency upon mass loading. The thickness of the layer can then be calculated from the density of the phase and the geometric area of the coated surface. This calculation indicated that a *MC* coated with a 0.6% solution of SP-2340 was ~150 nm, whereas the value from a plot of thickness obtained by profilometry versus % SP-2340 was ~140 nm.

In an effort to enhance the sensitivity of the cantilever to gaseous analytes, the entire surface of the *MC* was coated with polymer rather than only the tip. By coating the entire surface of the cantilever legs, absorption-induced differential stress (i.e. $\Delta\sigma_c$-$\Delta\sigma_{si}$) was enhanced.[147]

Because both the top and bottom of the cantilever was coated during the film-casting process, the polymeric phase was removed from the bottom side of the cantilever legs with a FIB mill (FIB 200, FEI Co., Hillsboro, OR, USA). The FIB was used to remove unwanted polymeric phase and also to thin the cantilever legs. Typical conditions for the FIB were a 600 nm aperture resulting in a beam current of approximately 11,500 pA and a dwell time of 1 ms with 25% overlap. The depth of ion

etching was calibrated by determining the time required to etch a square hole completely through a 600 nm thick silicon cantilever. The depth of etching over a specified time can be determined by considering the difference in areas of the calibration hole and the sample. Figure 2.1 shows a *MC* in which the thin film was removed from one side of one of the legs. Before the cantilever was used as a sensor, the thin film was removed from the same side of the second leg.

*MC*s were mounted in an optical system that has the physical arrangement as shown in Figure 2.2. A 5 mW diode laser (Coherent Laser Corp., Auburn, CA, USA) operating at 635 nm was spatially filtered and focused onto the triangular pad at the tip of the *MC* using a video microscope to visualize the process. The reflected beam was focused using a bi-convex lens (focal length of 10 cm) onto a quad-cell, position-sensitive detector built in house.[121] Deflection of the cantilever was measured using the output of the position-sensitive detector that corresponded to vertical beam deflection. The amplified voltage from the position-sensitive detector was recorded and stored using a SRS 850 DSP lock-in amplifier as a digital recorder (Stanford Research Systems, Sunnyvale, CA, USA).

A flow cell was mounted over the *MC* to allow the flow of gaseous analytes across the *MC* surface. A constant flow of ultra high purity nitrogen of 1.5 ml/min was achieved using a digital mass flow controller (MKS Instruments, Inc., Andover, MA, USA). Nitrogen flow was directed first through a fixed loop sample injection valve (Model 5020, Rheodyne, Inc., Cotati, CA, USA) that had a volume of 1.0 ml and then through the *MC* flow cell. This configuration allowed reproducible injections of gaseous analytes under controlled nitrogen flow. The volume of the flow cell containing the *MC*

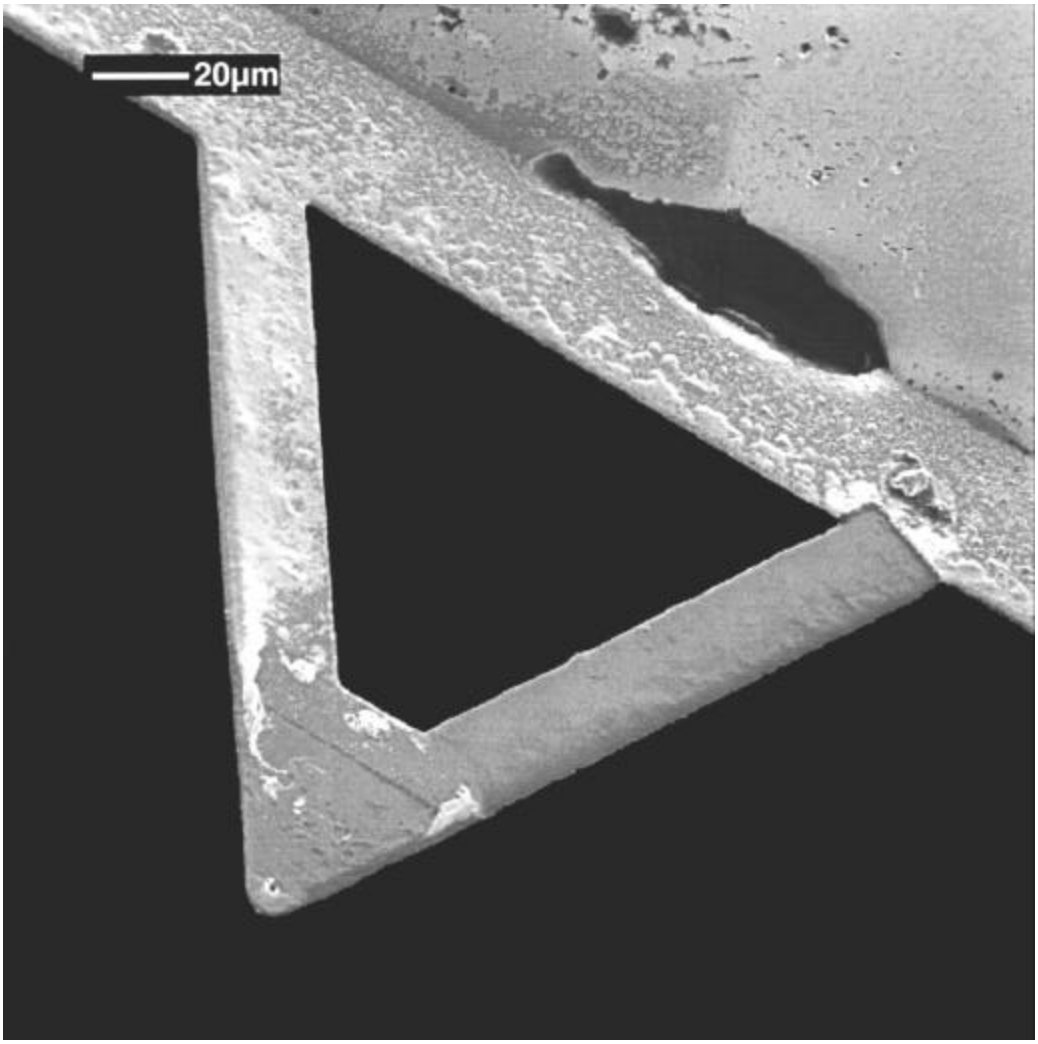

Figure 2.1. Focused ion beam (FIB) image of a coated V-shaped *MC*. The side shown in the image is the bottom of the *MC*. The top side was the spin coated side of the *MC*.

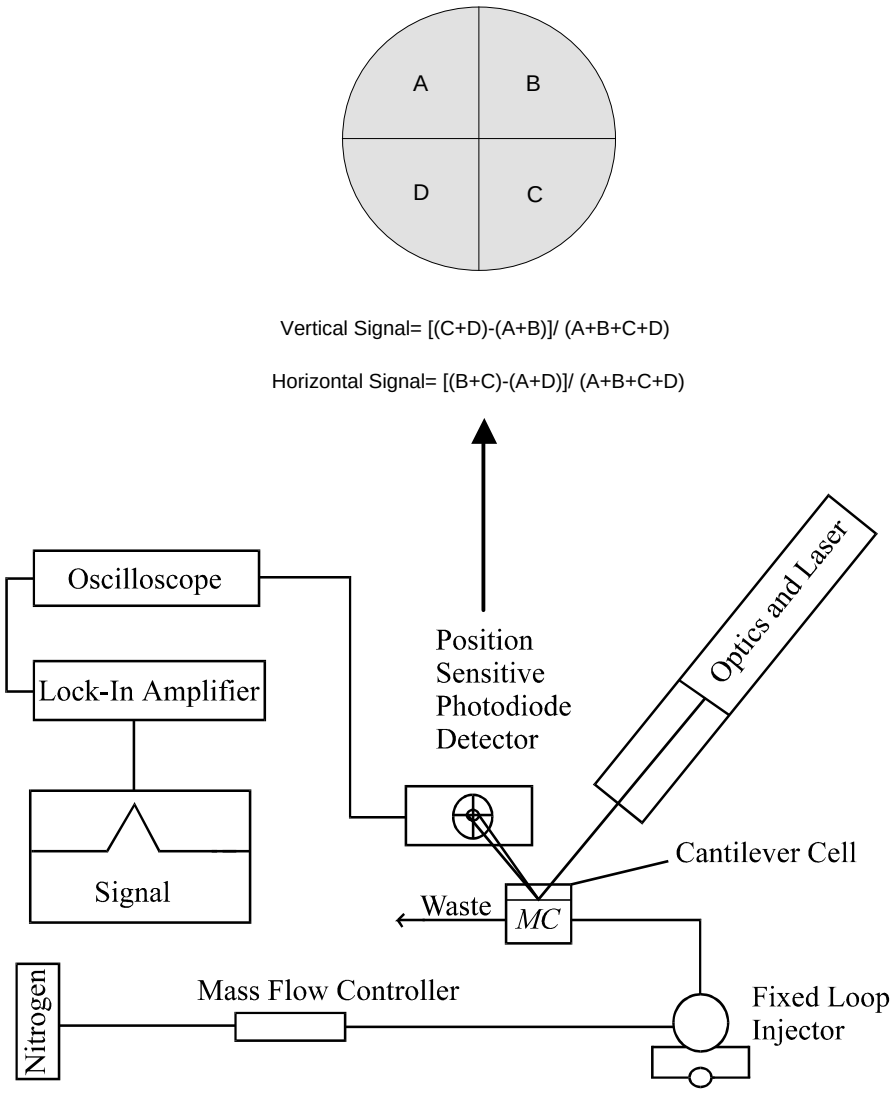

Figure 2.2. Physical arrangement of the *MC* optical setup used. The top portion of the figure shows the arrangement of the PSD and how the signals are generated.

is approximately 3 ml and consequently significant dilution of the injected analyte vapor is experienced.

Headspace above analyte solutions was developed in 40 ml headspace vials fitted with Teflon septa. To remove air and water vapor from the samples, the vial headspace was purged with nitrogen prior to development of analyte headspace. This was necessary to insure that the analyte was the only difference between the flowing nitrogen stream and the injected headspace sample. Sampling and subsequent injection into the fixed loop injector was accomplished using a gas-tight syringe. For preparation of different analyte vapor concentrations, a measured volume of headspace was diluted in nitrogen.

2.3 RESULTS AND DISCUSSION

A primary goal of this work was to enhance response and impart selectivity to *MC* chemical detection systems by coating cantilevers with thin films of gas chromatographic stationary phases. In addition, studies of the effects of film and cantilever thickness on sensor performance were also conducted. The thin films chosen for this work were selected to create a sensor that would be capable of distinguishing analytes in a general sense based on polarity. The following analytes, all monitored in the vapor phase, and potential modes of molecular interaction with the films were employed: pentane (very non-polar compound, dispersive interactions only), toluene (aromatic system with high polarizability), aniline (aromatic weakly basic compound with H-bonding capabilities), ethanol (very weakly acidic compound with strong H-bonded characteristics), methylene chloride (modest dipole moment compound with weak H-bonding acceptor

characteristics), and H_2O. Sensors were evaluated based on responses to this set of test analytes.

Figure 2.3 compares the response of three different *MC*s to the test analytes. The three cantilevers were the same shape and dimensions but their surfaces were modified in three different manners. One of the cantilevers (Figure 2.3, green) was treated with aqua regia to remove the thin gold layer, leaving nearly identical silicon surfaces on both sides of the *MC*. Because deflection depends upon the difference in the analyte-induced stress on either side of the *MC* legs, this particular cantilever shows little response to the analytes.

The second *MC* was first cleaned in piranha solution. Then the gold layer was removed from the surface of one side of the legs via FIB milling. The resulting *MC* had legs that were composed solely of silicon, but the surfaces of the legs were prepared differently. The fact that significant bending occurs upon exposure to chemical vapors (Figure 2.3, blue) indicates that the stress induced on the legs by analyte adsorption is different on either side of this cantilever. Assuming that the stress is expansive in nature, the direction of the bending (as indicated by the direction of the signal) indicates that the expansive stress on the FIB modified side is greater than that on the untreated side. It is well known that silicon can develop an overlayer of silicon oxide when exposed to air.[162] It is possible that FIB treatment alters the chemical nature and roughness of the silicon surface, thus making it a more active surface than undisturbed silicon.

The third *MC* was cleaned with piranha solution, and then spin coated to produce a 150 nm thick film of SP-2340. SP-2340 is a very polar gas chromatographic stationary

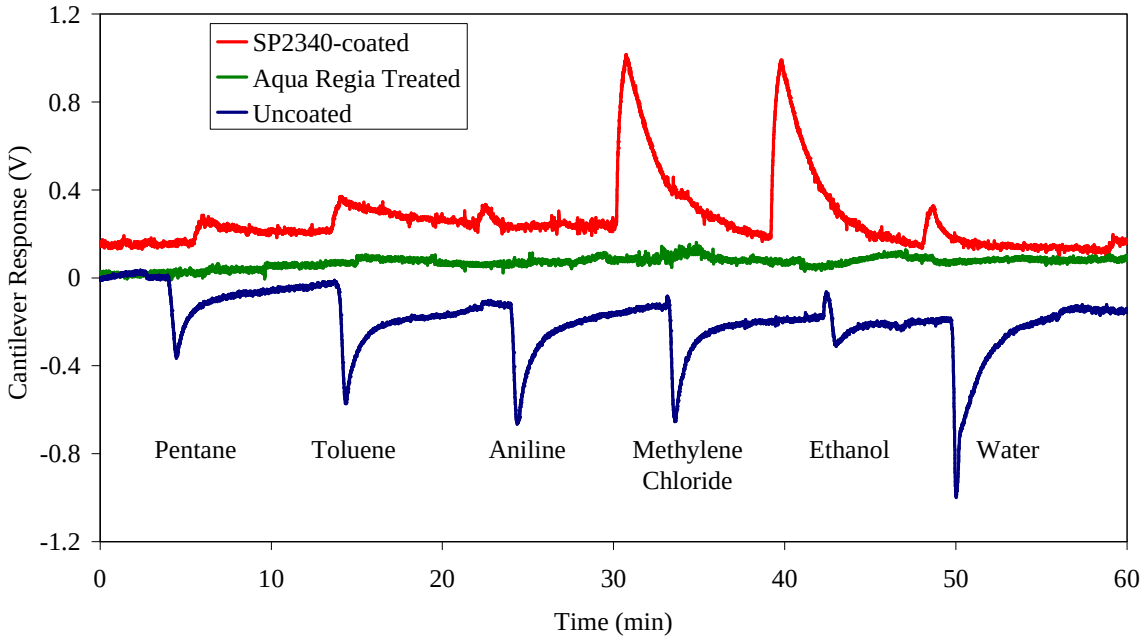

Figure 2.3. Effect of surface modification on *MC* response.

phase (100% cyano) with an average McReynolds constant, I_{ave}, of 736 (by contrast OV-25, a 25% phenyl and 75% methyl phase, (see below) has an I_{ave} of only 235). Any coating that ended up on the bottom of the cantilever surface was removed using FIB milling (see Figure 2.1). The thin layer of gold was also removed from the bottom of the cantilever surface at this time. With the exception of the thin stationary phase coating, the resulting *MC* was identical to the uncoated cantilever that produced the blue trace in Figure 2.3. The response of this coated cantilever to the test analytes is shown as the red trace in the figure. The presence of the thin film caused the *MC* to deflect in the opposite direction of the uncoated *MC* when exposed to the same chemical vapors. In order for the signal to change direction, the polymeric phase must first counter the stress on the side cleaned by the ion beam, then exert an even greater stress to cause it to bend in the opposite direction. The direction of cantilever deflection indicates that the expansive stress induced by absorption of vapors on the coated side is greater than adsorption of vapors on the uncoated side. The change in deflection direction resulting from the presence of the thin polymeric coating shows that we have been able to dramatically modify response characteristics via the coating procedure.

Both coated and uncoated *MC*s (Figure 2.3, blue and red) bend shortly after injection of analyte. After a sharp increase, the signal begins to decrease slowly owing to the desorption of analyte from the cantilever surface under continuous nitrogen flow. The return of the *MC* to its original position after exposure is important because it shows that the absorption is reversible and allows the sensor to be reused. However, no studies concerning the reproducibility of sensor response were made in this chapter (see Chapter

3, page 109 for liquid phase reproducibility data). It should also be possible to alter the dynamics of the *MC* response via ambient or resistively induced temperature changes.

The responses of each *MC* sensor to analytes of different polarity and molecular characteristics are quite different. Because the gaseous analytes used in this study have different vapor pressures, Table 2.1 presents the peak responses normalized to the known room temperature, atmospheric pressure, and vapor pressures of the analytes. Since the injected analyte headspace vapors were developed in a fixed volume container for which the vapor pressure increases beyond 1 atm, this procedure should not be taken as a strict normalization to the relative concentrations of the analytes in their respective headspaces. However, we feel this approach is adequate for initial illustrations of coating-induced *MC* response and selectivity effects. The selectivity factors presented in Table 2.1 are all relative to pentane and calculated by dividing each response factor by the response factor of pentane. Because the magnitude of the signal depends on many variables present in the optical arrangement, it is difficult to compare absolute signal magnitude between two separate *MC*s. The signals in this work are reported in voltage output of the detector. In general, this has not been converted to actual cantilever displacement since the focus of this work was selectivity not sensitivity. Moreover, the volts to displacement conversion would vary as the optical alignment (e.g. distance between *MC* and position sensitive detector) was slightly altered during the course of these experiments. However, for a typical optical configuration (not optimized for sensitivity) the conversion is roughly 80 nm/V based on a relationship presented in an earlier report by Datskos and Sauers.[97] The high frequency noise that appears in the traces presented could be diminished greatly

Table 2.1. Normalized responses of the analytes used in this study.

Analyte	**Normalized Response Factor** (maximum signal/vapor pressure) V/atm			**Selectivity Factor (Relative to pentane)**	
	Uncoated	SP-2340 Coated	Δ	Uncoated	SP-2340 Coated
Pentane	-0.54	0.15	0.69	1	1
Toluene	-15	4.6	20	27	31
Aniline	-690	120	810	1300	820
Methylene Chloride	-1	1.8	2.8	1.8	12
Ethanol	-1.6	11	13	3.0	75
Water	-26	5.5	31	48	37

with filtering. The baseline drifts in those traces that exhibit time frames comparable to the transient signals, hence limiting detection of injected analyte bands, correspond to approximately 2 nm deflections (e.g. see small negative baseline disturbance in blue trace in Figure 2.3).

Table 2.1 shows a modest correlation between response factors for SP-2340 coated and uncoated *MC* sensors. This may reflect the similarity between the adsorption strengths of the analytes onto a silicon oxide surface and absorption into a thin coating of the highly polar SP-2340 phase. The deviation in this trend for water is also consistent with the large adsorption strength of water on silica. The values in the table indicate the overall stress due to interaction of an analyte with the polymeric phase. Aside from selectivity effects, it is clear that the polymeric phase enhances the overall response to the analytes; in all cases the analyte-induced expansion on the polymeric side overcomes the negative uncoated response.

The thickness of the film also influenced the response of the *MC*. Figure 2.4 shows the signal-to-noise levels of silicon cantilevers in which the gold was removed from one side of the legs by ion beam etching. Each of the cantilevers used in this diagram was prepared in the same fashion except for the thickness of the SP-2340 film. All of the *MC*s had legs that were 360 nm thick, but the SP-2340 films on one side of the legs ranged from 50 to 500 nm thick. It is apparent that SP-2340 film thickness affects both sensitivity and selectivity. A quantitative analysis of the sensitivity and selectivity is presented in Figure 2.4 and Figure 2.5, respectively. As the film thickness increases, the signal-to-noise ratio decreases quite dramatically (see Figure 2.4). For ethanol, the

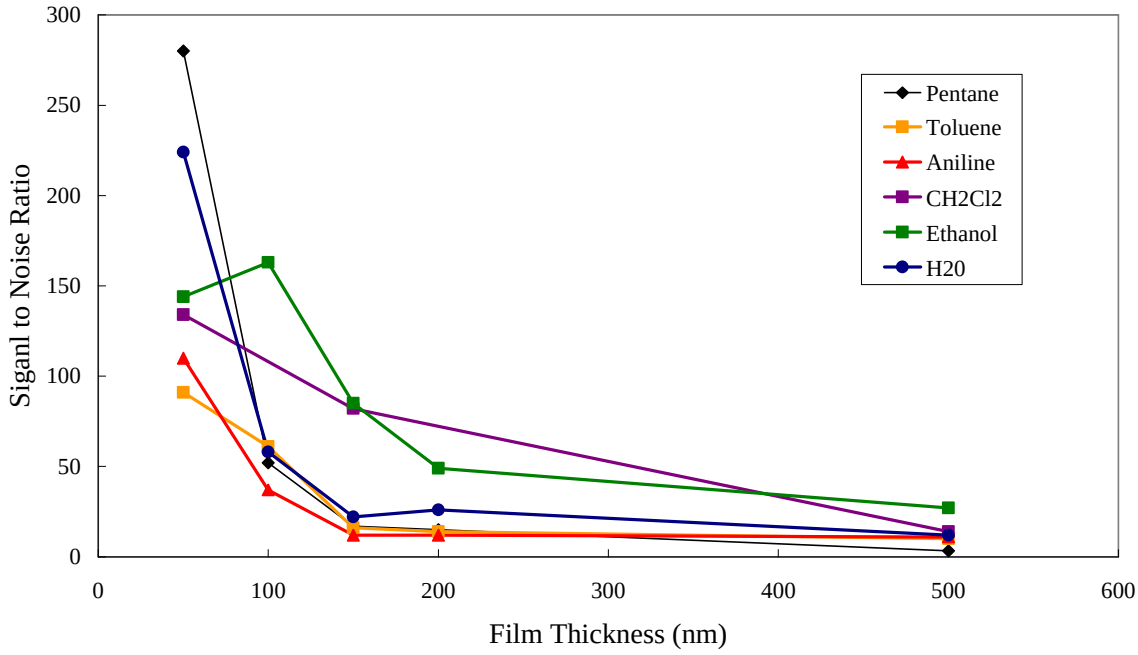

Figure 2.4. Effect of film thickness on *MC* response. The *MC* had legs that were 360 nm thick for this study.

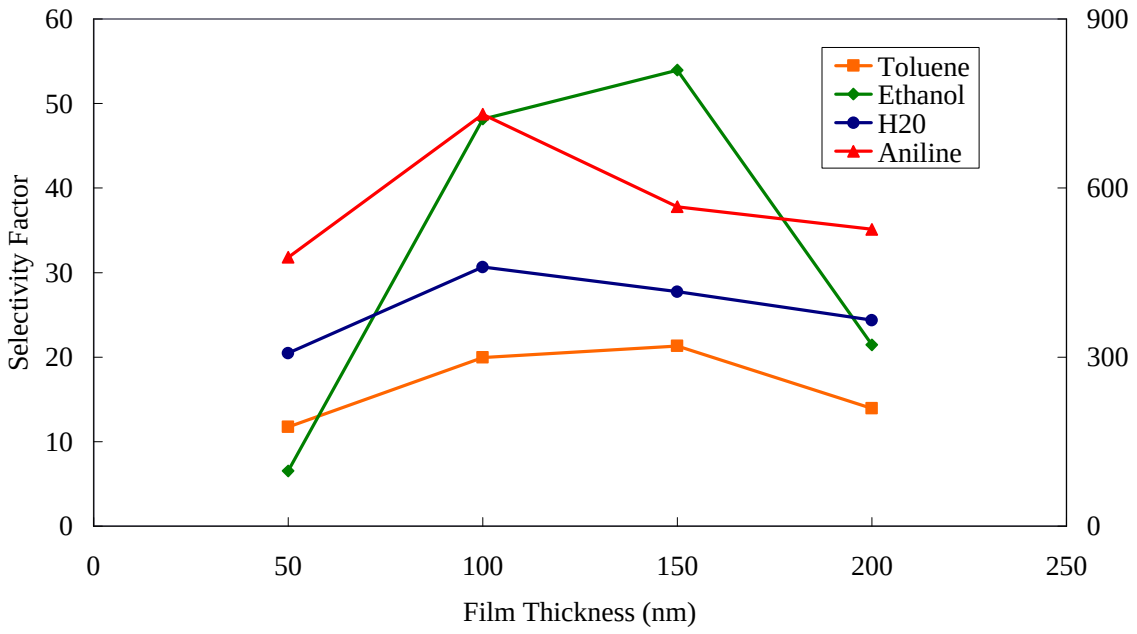

Figure 2.5. Plot of selectivity factors for various analytes and coatings. The left Y-axis is for all analytes except aniline, which is on the right. The *MC* had legs that were 360 nm thick for this study.

signal-to-noise ratio increases then sharply decreases above a 100 nm film. The low signal-to-noise ratio at large film thicknesses could be due to the additional mass on the cantilever legs restricting the bending of the cantilever, effectively altering t_1 and/or Y_1 in Equation 2.1. Alternatively, there may be a "dilution" of the stress since the mole fraction of analyte in the coated film resulting from injection of a fixed amount decreases as the amount of coating is increased. As was mentioned in section 1.4.1 in conjunction with the second model, there will be a point in which the swelling of the film will not be transmitted to the surface. This is the case for relatively thick films in which the analyte may not penetrate deep enough into the film to cause swelling close enough to the *MC* surface to cause the apparent surface stress.

The selectivity factors plotted in Figure 2.5 are calculated by dividing the response factor of each analyte by the response factor of pentane. The apparent change in selectivity with film thickness is caused by the differential nature of the response. The stress on the uncoated side of the SP-2340 *MC* is probably constant as film thickness is altered. However, the coated side response is sensitive to film thickness. Hence, as thickness is varied the net response to the analytes varies depending on the constant values of σ_{si} and changes in σ_c (see Equation 2.1).

Another means to alter the response of the *MC* sensor is to modify the thickness of the cantilever legs. The commercial cantilevers used had a leg thickness of 600 nm. By FIB milling it is possible to etch the cantilever surface in a very controlled fashion. Figure 2.6 depicts the response of a single cantilever sensor with a 150 nm thick film of SP-2340. Each trace shows the response of the cantilever after successive thinning of the legs by FIB milling. The 480 nm thick legs (Figure 2.6, green trace) show little response

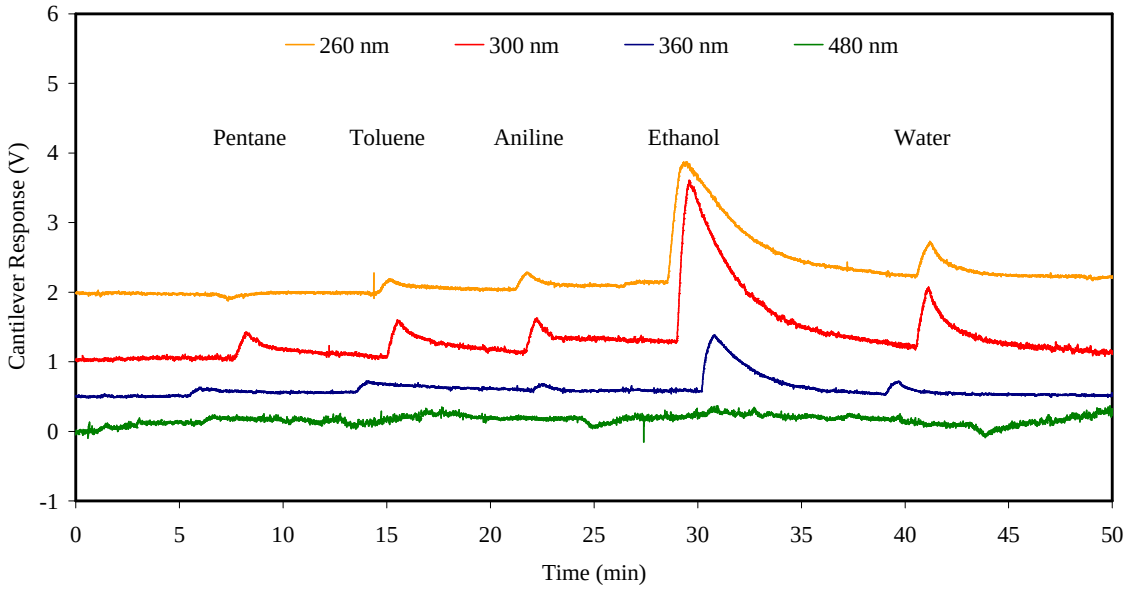

Figure 2.6. Effect of *MC* thickness on response.

when exposed to analyte vapors. The relatively thick legs are not flexible enough to allow adequate bending of the cantilever to provide a reasonable signal-to- noise ratio. As the legs were thinned (blue, red, and orange traces), the signal levels are increased. The differences in the baseline noise shown in Figure 2.6 may be a result (at least in part) of differences in optical alignment rather than changes in sensitivity. Curiously, the cantilever with 260 nm thick legs (orange trace) actually bends in opposite directions as opposed to other solvents when exposed to pentane, indicating again that the differential nature of *MC* response can create unique changes in selectivity. Cantilevers with legs thinner than 260 nm were extremely unstable.

*MC*s are also capable of providing quantitative information. By diluting analyte headspace with nitrogen in a gas-tight syringe, and passing the diluted vapor across the surface of a SP-2340 coated cantilever, we were able to calibrate the SP-2340 coated *MC* for two analytes as shown in Figure 2.7. The response of the cantilever increased with increasing analyte concentration.

By coating the cantilever surfaces with a variety of thin films it may be possible to impart a different selectivity to individual *MC* elements in an array. A recent report of this approach involved coating eight *MC*s in an array with common polymers (e.g. polystyrene, polymethylmethacrylate, etc.) or mixtures of these polymers.[131] When creating such an array it is desirable to use coatings that respond differently for the analytes of interest. A potential strength of using gas chromatographic phases as coatings, as reported herein, is that there is a wealth of information on the selectivity of these phases. This should facilitate the rational design of arrays containing elements exhibiting orthogonal response characteristics. We have investigated another gas

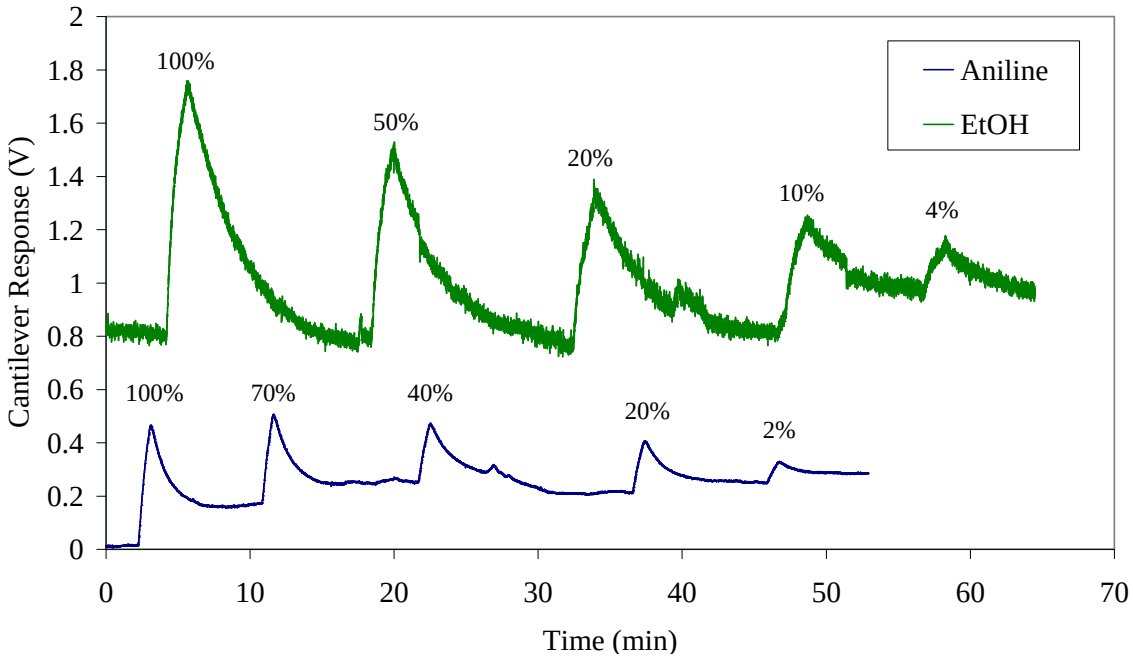

Figure 2.7. Concentration based *MC* bending for aniline and ethanol. The percentages represent the amount of analyte in the sample that was injected.

chromatographic stationary phase, OV-25, as a cantilever coating to alter selectivity. Methods of classifying stationary phases often involve measuring the Kovat's indices of selected test compounds on columns prepared using the phase.[163] Characteristic constants are generated by subtracting indices determined for these test compounds using a column prepared with a reference stationary phase such as squalane from the indices determined using a column prepared with the stationary phase of interest. McReynolds constants are created in such a classification scheme.[163] The McReynolds constants for SP-2340 and OV-25 phases, expressed as percent of the average value for the test compounds, appear in Table 2.2. The higher the value (or percent in Table 2.2) the greater the relative absorption strength of the test compound (or compounds with related structural features) for the phase.

Figure 2.8 compares the responses of OV-25 and SP-2340 coated *MC*s to the test analyte vapors used in these studies. Although the response of a coated *MC* is governed by more than the absorption strength of the coating for the analyte, there are still trends in the responses seen in Figure 2.8 that are consistent with the data in Table 2.2 and worth noting. Based on the possibility of similar molecular interactions, the responses of the test analytes methylene chloride, aniline, and ethanol might be expected to mimic the data presented in the table for 2-pentanone (z'), pyridine (s'), and butanol (y'), respectively. The z' values for the two phases are similar. However, the ratio of s' to z' is considerably larger for OV-25 than SP-2340. Similarly, the ratio of responses for the aromatic base aniline (s' mimic) to the dipole moment compound methylene chloride (z' mimic) is substantially greater for OV-25 (0.29) than SP-2340 (0.089). Conversely, the

Table 2.2. Relative McReynolds constants for SP-2340 and OV-25 phases. The values in the table are listed as percent relative to a squalane coated column. These test compounds represent broad classes of compounds based upon their mode of interaction with the specified phase. The actual analytes used in these studies are similar to these test analytes, so the values in this table are expected to be similar for the analytes used.

Phase	**Test compounds used in classification**				
	Benzene (x')	Butanol (y')	2-pentanone (z')	Nitropropane (u')	Pyridine (s')
SP-2340	71	103	90	128	108
OV-25	76	87	89	130	120

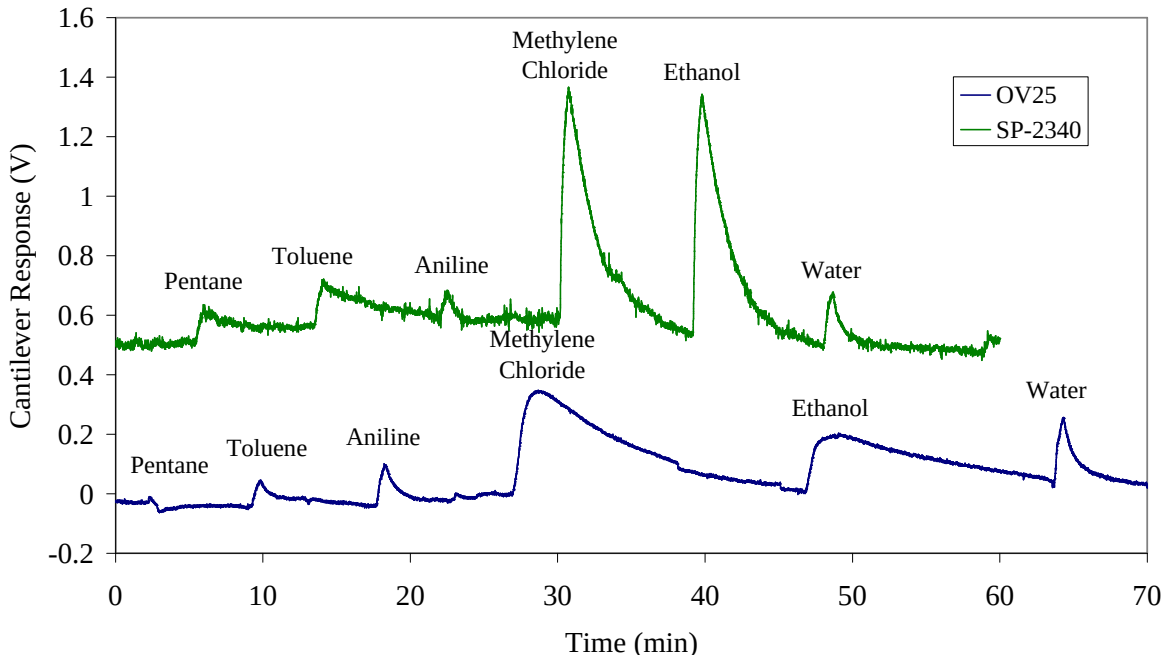

Figure 2.8. Response comparison between OV-25 and SP-2340 coated *MC*s. Responses are shown at 100% analyte composition. Both *MC*s had leg thicknesses of 360 nm.

ratio of y' to z' is greater for SP-2340 than OV-25. In agreement, the ratio of responses of the alcohol ethanol (y' mimic) to methylene chloride is greater for SP-2340 (1.0) than OV-25 (0.52).

This work shows that depositing thin films of gas chromatographic-type polysiloxane phases on the surfaces of *MC*s dramatically influences sensitivity and selectivity toward analytes that possess different possible modes of molecular recognition. Moreover, common classification schemes such as McReynolds constants appear to have some value in predicting response characteristics and, hence, may aid in the rational design of *MC* elements in arrays. Film and *MC* leg thickness are shown to be important parameters in optimizing *MC* performance.

CHAPTER 3

INVESTIGATION OF THE EFFECTS OF CAVITAND FILM TYPE AND THICKNESS ON THE PERFORMANCE OF SMOOTH AND NANOSTRUCTURED MICROCANTILEVER SENSORS

3.1 INTRODUCTION

Recent reports from several research groups [92, 101, 109, 115, 120, 126, 129-131, 134, 138, 164, 165] confirm that sensors based on *MC*s have a substantial potential for various analytical applications. In order to fully realize this potential, however, further optimization of *MC*s designs is required. A clean smooth solid surface generally exhibits a tensile (positive) surface stress due to the electronic arrangement of the atoms composing the surface and, significantly, changes in stress on that surface can occur when the surface atoms are caused to rearrange due to adsorption by a chemical species.[104] The change in stress can be either compressive (negative) or tensile depending upon the nature of the adsorbed species. As discussed earlier, the surface stress and surface free energy are related by the Shuttleworth equation (Equation 1.26).[103, 104, 117] In principle, the second term in Equation 1.26 can be comparable to the surface free energy and assume a positive or negative value.[117] However, a general trend is that if the initial surface free energy is large, then modulation in surface stress and, hence, *MC* response can be large. For example, pure gold surfaces in contact with air have large surface free energies, typically exceeding 1 N m^{-1}. Not surprisingly, when *MC*s coated on one side with gold are exposed to alkylthiols in the gas phase very large total responses are observed as the thiol compounds covalently bond to the gold.[97, 116]

In order to impart selectivity when *MC*s are used in analytical sensing, chemically selective receptor phases (e.g., self assembled monolayers, SAM) are immobilized on one of the sides of the cantilever. Ideally, the interaction of the analyte with the receptor phase, while being selective, is reversible and exhibits reasonable kinetics for sensing applications. We have shown this in a previous work using gas phase analytes in which we employed films of thiolated cyclodextrins on nanostructured surfaces.[127] Reasonable response times as well as reversible binding of the analytes with the cyclodextrin film was observed for gas phase measurements. The use of *MC*s with reversible receptor phases for measurements in liquids (e.g., aqueous solutions) has not received a great deal of attention. In part, this is because organic receptor phases in water possess surface free energies that are more than an order of magnitude smaller than the gold-gas phase case mentioned above. Therefore, modulation of surface stress is small and often within an order of magnitude of the inherent noise of *MC*s mounted in aqueous environments.[101] This gives rise to low signal-to-noise levels and somewhat limited dynamic range.

We report herein two approaches to improved performance for liquid phase measurements using receptor modified *MC*s. In both cases, we use cantilevers with nanostructured surfaces to overcome limitations of smooth surfaces (see page 48). Our idea of *MCs* with nanostructured surfaces is derived from the models that have been a focus in colloidal science.[166] Although our experimental findings indicate that the smooth surface model, the first model mentioned in 1.4.1, does not strictly apply to nanostructured *MC* surfaces, it is also true that classical colloidal models may not fit all the details of this system. It is therefore some combination of the second and third models discussed in section 1.4.1 that govern the results presented in this chapter.

In the first approach, the limitations of smooth surface *MC*s are circumvented via nanostructuring of one side of the cantilever and modifying it with a SAM phase. The nanostucturing increases the available surface for SAM phases and analyte binding and creates a quasi-3-D structure that is colloidal in nature. Importantly, the short-range forces associated with intermolecular interactions in the tight interstitial spaces of colloidal systems can be very large.[166] It has also been shown that stresses induced by solvation forces in sol-gels are most pronounced when the interstitial spaces are on the order of several nanometers or smaller.[167, 168] Figure 3.1 illustrates how analytes binding within sterically confined interstitial spaces (third model from section 1.4.1) may give rise to an enhancement in cantilever bending. The in-plane component of these forces can serve to efficiently convert the chemical energy associated with analyte-receptor binding into *MC* static bending. In our previous work, gas phase measurements with nanostructured, cyclodextrin (CD)-modified *MC*s provided two orders of magnitude improvement in chemi-mechanical response (bending) relative to similarly modified smooth *MC*s.[127]

A second method to circumvent the limitations of smooth surfaces is to employ films thicker than SAMs as receptor phases [130] anchored by nanoscale features to a *MC* surface. Here, in analogy to polymeric phases used previously [130, 134], the stress that gives rise to bending of the *MC* results from bulk phase swelling or contractions of the film upon absorption of analyte (second model from section 1.4.1).[116, 169] There are several forces involved in film swelling, including steric, electrostatic, and hydration forces. The integral force that causes swelling-induced *MC* bending upon analyte absorption

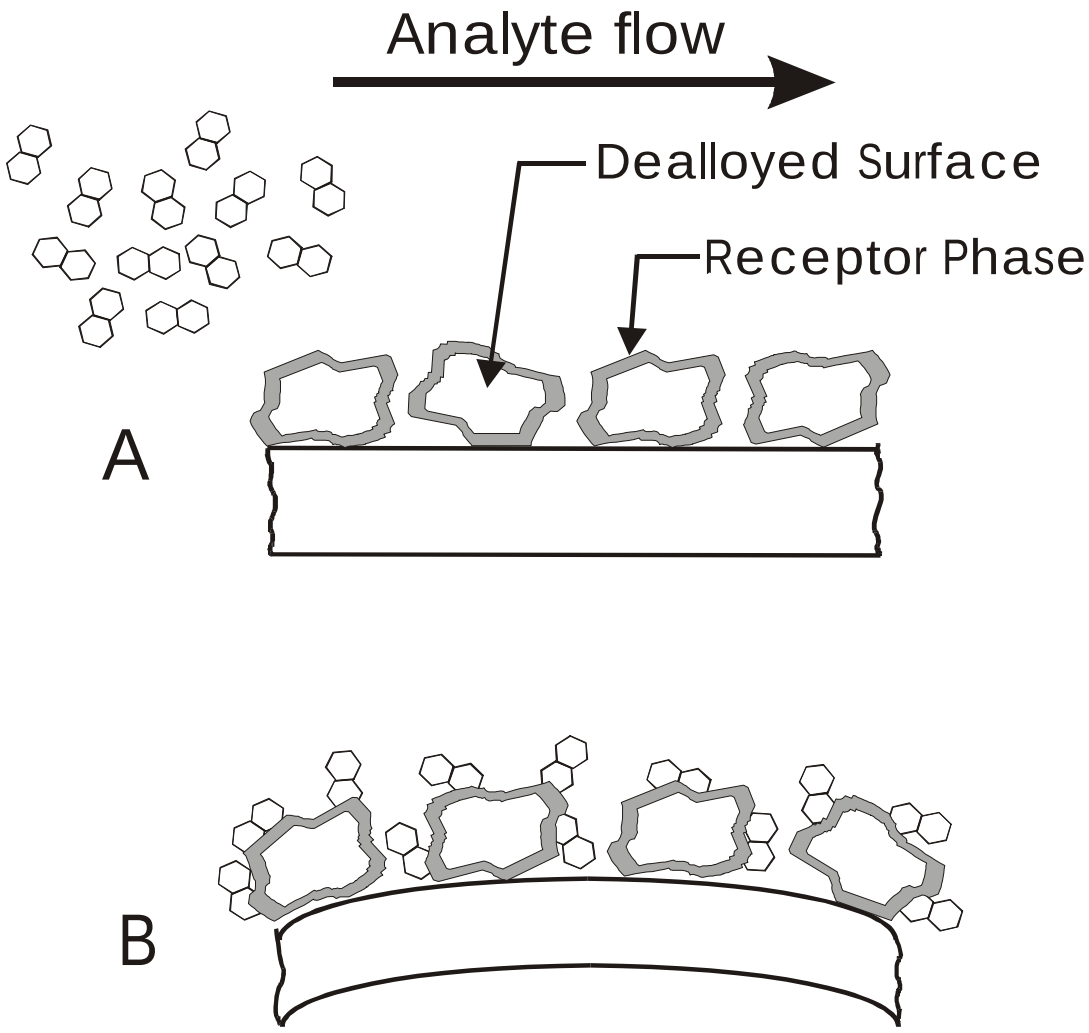

Figure 3.1. Analyte binding within sterically confined interstitial spaces.

should scale with film thickness. In the case of smooth surfaces and weakly adhering receptor phases, however, a large *stress* gradient generated at the cantilever-coating interface would ultimately result in a stress-slip condition (i.e. when a large stress causes the coating to freely slide along the surface of the *MC*). This may be evidenced by the results shown in Figure 2.4. We demonstrate in this work the strengths of using nanostructured surfaces with non-monolayer receptor films to reduce stress-related slippage. Films of synthetically-modified cyclodextrins (CDs) that are both thinner and thicker than the root mean square (RMS) roughness of the supporting surface are investigated. To our knowledge, this is the first report of a CD receptor phase that can be vapor deposited intact on sensor surfaces.

3.2 EXPERIMENTAL

The *MC*s used in this work were commercially available, V-shaped, 0.55 μm thick, and composed of silicon nitride coated with a 0.05 μm layer of gold (Park Scientific Instruments, Sunnyvale, CA). The length and leg width of the microcantilevers were 350 and 20 μm, respectively. For measurements made using cantilevers coated with smooth gold, the cantilever was cleaned in piranha solution for 45 seconds before chemical treatment. The process of creating the nanostructured *MC*s having a dealloyed surface is described in greater detail elsewhere.[127] Briefly, the thin gold layer was removed from the commercially obtained cantilevers by immersing them in aqua regia for 3 minutes. The *MC*s were then placed into a physical vapor deposition (PVD) chamber (Cooke Vacuum Products, Model CVE 301, South Norwalk, CT) to be coated

on one side with the appropriate metallic films using thermal deposition. To create a nanostructured *MC*, a thin film (~3.5 nm) of chromium was applied to the surface to act as an adhesion layer. A thin film of gold (~15 nm) was then applied to the cantilever surface, followed by a film consisting of codeposited gold and silver. The silver was subsequently chemically removed via oxidation from the film using an aqueous solution of $HAuCl_3 \bullet 3H_20$, leaving a gold surface with nano-sized, colloid-like features. The thickness of the dealloyed gold layer was approximately 50 nm in these studies. The smooth *MC*s were prepared by depositing gold onto the chromium layer until a total thickness of approximately 50 nm was achieved. These two types of *MC*s (smooth and nanostructured) were then chemically modified with receptor phases as described below.

The cantilevers used in our studies were chemically modified using two distinct methods. In the first method, a SAM of heptakis-6-mercapto-β-cyclodextrin (HM-β-CD) (see Figure 3.2) was formed on the cantilever surface. A 1.50 mM solution of HM-β-CD was prepared in 60/40 deaerated DMSO/H_2O. The *MC* was then immersed in the HM-β-CD solution for 18-20 hours, after which it was rinsed with copious amounts of the DMSO/H_2O solvent. The chemically treated cantilever was then allowed to soak in the DMSO/H_2O solution for at least an hour to remove any nonspecifically bound cyclodextrin. The second method involved the physical vapor deposition of the compound heptakis (2,3-O-diacetyl-6-O-tertbutyl-dimethylsilyl)-β-cyclodextrin (HDATB-β-CD) (see Figure 3.2) onto the cantilever surface. The HDATB-β-CD was placed into a quartz crucible in the PVD chamber that was then electrically heated in

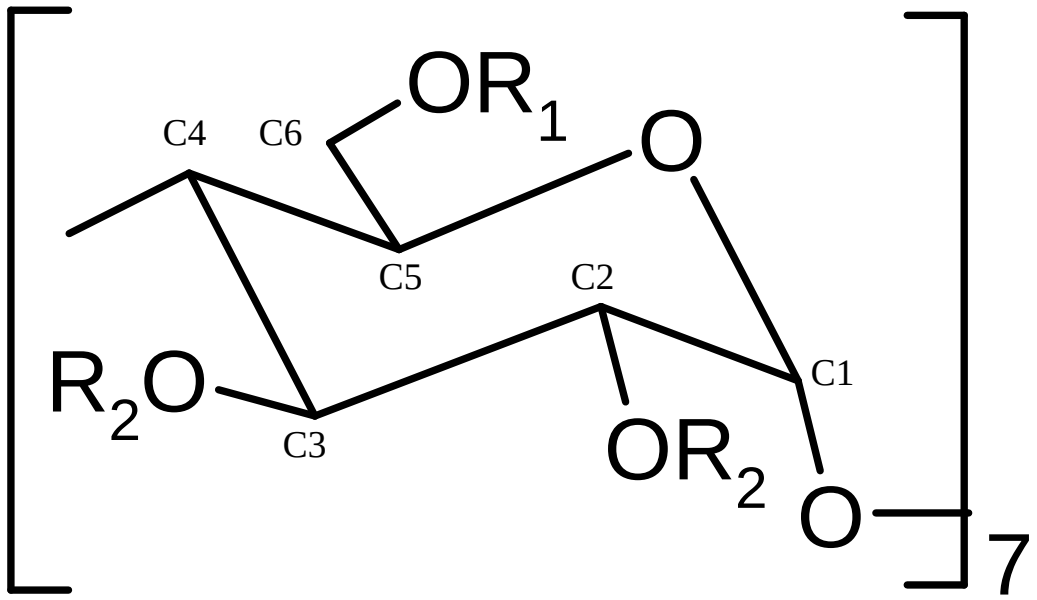

Figure 3.2. Monomeric units of the functionalized cyclodextrins used as *MC* receptor phases. R_1 and R_2 for the self assembled monolayer of HM-β-CD are SH and H, respectively. R_1 and R_2 for the vapor deposited film of HDATB-β-CD are $(CH_3)_3CSi(CH_3)_3$ and $COOCH_3$, respectively.

vacuum causing the cyclodextrin to evaporate onto the *MC* surface. The thickness of the resulting film was measured using a conventional quartz crystal microbalance (Maxtek, Model TM-100R, Santa Fe Springs, CA). Vapor deposited films with QCM-based thicknesses of approximately 18 and 50 nm were used. With both types of chemically modified cantilevers, the cantilever was allowed to equilibrate in the background solution until a stable baseline (usually less than an hour) was achieved before any measurements were attempted.

The deflection of the *MC* was measured using an optical beam-bending technique as shown in Figure 3.3. The system employed in this chapter differs from that in Figure 2.2 in that the optics have been simplified, a different flow cell was used, and the analytes were delivered via a different mechanism. Deflection of the cantilever is measured in the same manner (with the exceptions noted above) as it was measured in Chapter 2 (see page 60). The conversion factor for converting output voltage to *MC* deflection was determined by displacing the detector using a micrometer and measuring the resulting change in output voltage. The output signal was fed into a TDS 220 digital oscilloscope (Tektronix, Beaverton, OR) to facilitate optical alignment. The *MC* flow cell (Figure 3.4) was imaged using a Watec CCD camera for alignment of the laser beam on the cantilever tip (Edmund Industrial Optics, Barrington, NJ). The readout accuracy of our system was approximately 0.25 nm and the noise associated with the measurement under flow was less than 10 nm in most experiments. The *MC* was mounted in a 100 μL Teflon flow cell and exposed to various solutions at a flow rate of 0.85 ml/min. The analytes were delivered to the cell via a 10 ml syringe connected to a 2-way valve. This valve was

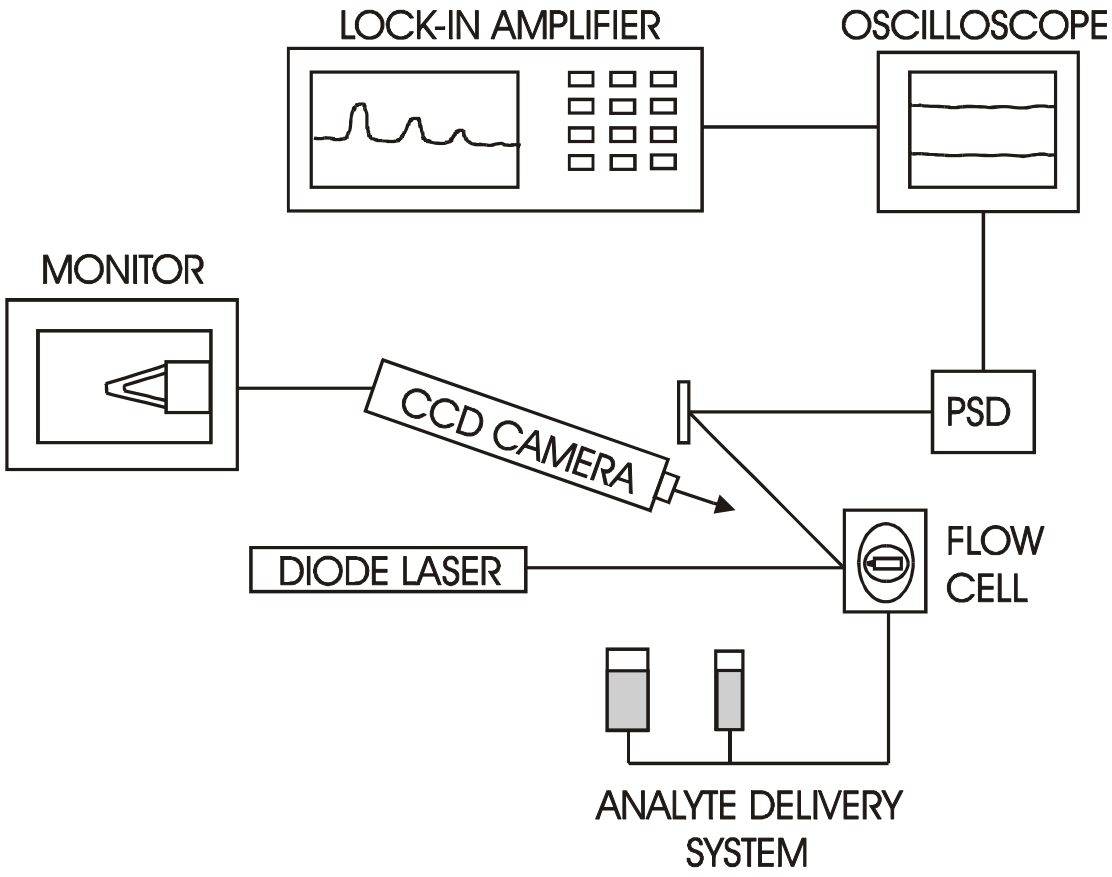

Figure 3.3. Optical arrangement used in these studies. The analyte delivery system is composed of two syringes (50 and 10 ml) placed in series and connected via 2-way valves.

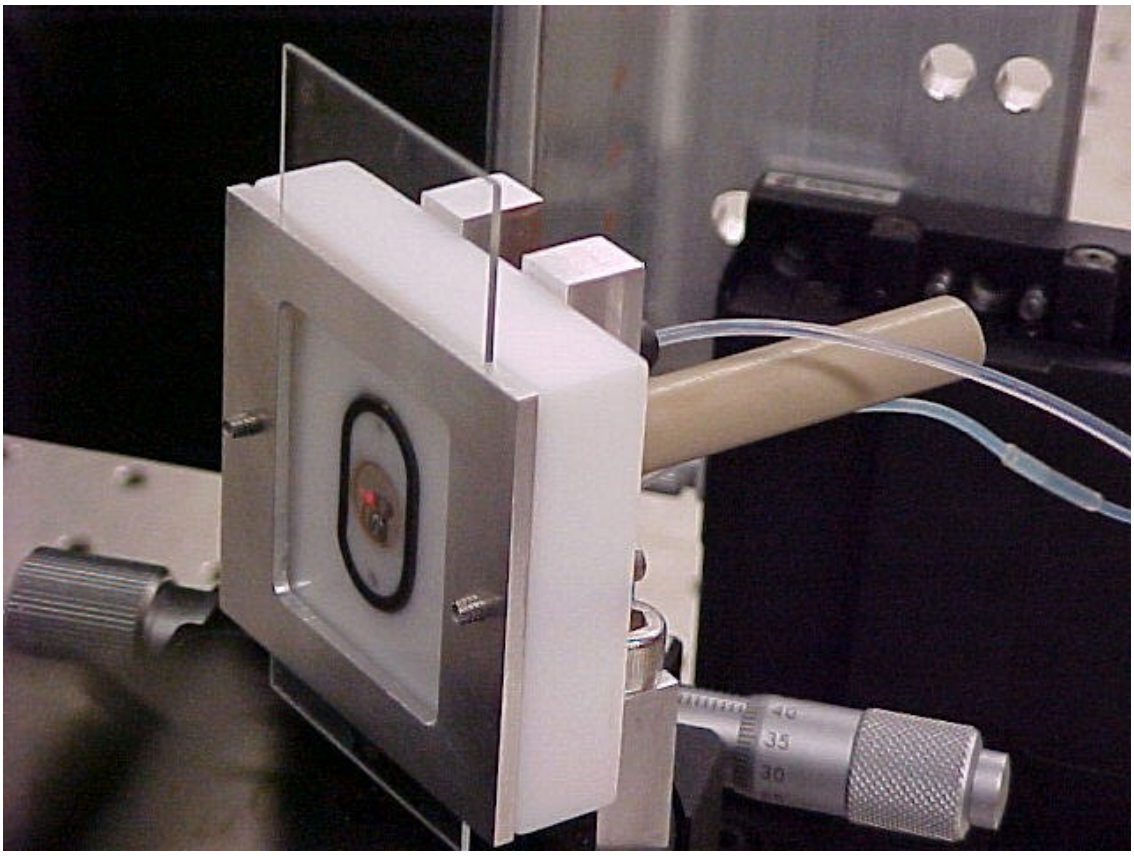

Figure 3.4. 100 μL Teflon liquid flow cell used for these studies. The *MC* is mounted onto the brown PEEK rod shown protruding from the back of the cell.

placed in series with a second 2-way valve connected to a 50 ml syringe that was used to flow background solution into the cell. The analytes were diluted in the syringe using the flowing background solution that was a 0.025 M phosphate buffer at pH 7 to ensure the analyte solution and the background solution were at the same temperature. Measurement of pH was performed using an Orion SA 520 pH meter (Thermo Orion, Beverly, MA).

Film and *MC* surface characterization was performed using both spectroscopic and surface imaging techniques. Spectroscopic information was obtained using C^{13} nuclear magnetic resonance spectroscopy (NMR), Fourier-Transform infrared spectroscopy (FTIR), and X-ray photoelectron spectroscopy (XPS). Surface images were obtained using atomic force microscopy (AFM). The NMR experiments were performed using a Varian Mercury 300 MHz NMR spectrometer (Varian Inc., Palo Alto, CA), the FTIR experiments using a Bio-Rad FTS-60A infrared spectrometer (Bio-Rad, Hercules, CA), the AFM images were obtained using the tapping mode of a Digital Instruments Multimode AFM (Digital Instruments, Santa Barbara, CA) and the XPS spectra were obtained using a Perkin Elmer PHI 5000 Series ESCA (Perkin Elmer, Wellesley, MA).

The metals used in the coating process of the cantilevers were purchased from Alfa Aesar (Ward Hill, MA) or the Kurt J. Lesker Company (Livermore, CA) at a purity of 99.9%. The analytes and buffer components used were obtained from Sigma (St. Louis, MO) or Aldrich (Milwaukee, WI) and used as received. All acids and bases used were obtained from Fisher Scientific (Pittsburgh, PA). Ultra pure water was obtained by using a Barnstead E-Pure water filtration system (Barnstead, Dubuque, IA). The HM-β-CD was synthesized using the method of Stoddart et al. [170] and the HDATB-β-CD was

synthesized using the method of Takeo et al.[171] All buffer solutions consisted of monobasic and dibasic sodium phosphate dissolved in ultrapure water. The ratio of the two components was fixed to yield a buffer at pH 7. All analyte solutions were prepared in this buffer solution that is also called the background solution.

3.3 RESULTS AND DISCUSSION

3.3.1 Surface Modification and Characterization

We have applied chemical coatings to both smooth and nanostructured *MC* surfaces in an attempt to study the effect of morphology on sensor response. Nanostructuring the cantilever surface creates three important results: a larger surface area compared to a *MC* with the same geometric area, spatially confined spaces, and stabilization of thicker films applied to its surface. In some cases the nanostructuring itself has led to slight changes in selectivity for gas phase measurements based upon the size of the features and the analyte.[127] To study these effects for liquid phase measurements, we have exposed these various *MC*s to aqueous solutions of a set of analytes previously observed to reversibly interact with β-CD cavitands. We have chosen to use cyclodextrin macrocycle sugar cavitands as chemical coatings due to their established molecular recognition capabilities. Solutes interact with CDs based on size, geometry, and physichemical properties of both the solute and CD.[172] These different interactions have resulted in high levels of selectivity in chemical separations.[173-176] However, in chemical sensor work in which the CD is covalently bound or deposited on a surface as a disordered film, the molecular recognition properties of the CD may be

altered. We have used a thiolated cyclodextrin (HM-β-CD) and one that was thermally evaporated in vacuum (HDATB-β-CD) as our chemical coatings.

Although direct spectroscopic investigations of the HM-β-CD-gold *MC* surface were not performed at this time, prior reports of thiolated-CD binding to gold [31, 177] and the following experiments we performed indicate that a substantial chemically attached layer of HM-β-CD was formed on the gold surface following treatment with pure solutions of the thiolated CD. XPS measurements performed in conjunction with prior work confirm the presence of sulfur on the surface after treatment with HM-β-CD. In addition, the contact angle for water on these surfaces was substantially altered. Also, when the responses of an untreated and a HM-β-CD treated *MC* to the certain analytes were compared, the response of the former (sorption onto the active gold surface) was irreversible, while the response of the HM-β-CD treated cantilever was reversible. The response of the *MC* to pH was also measured before and after treatment with HM-β-CD. Upon treatment of the *MC* with HM-β-CD, there was a considerable decrease in response to pH, again indicating that the surface was modified with a chemical layer.

Due to the fact that HDATB-β-CD was thermally evaporated onto the cantilever surface, it was important to determine if the compound decomposed during the evaporation process. Both C^{13} NMR and FTIR spectroscopy were used to characterize the compound before and after vapor deposition. For the reference comparison, a solution of HDATB-β-CD in deuterated chloroform was prepared in bulk and the C^{13} NMR spectrum was obtained. A small droplet of this solution was placed onto a gold-coated microscope slide and allowed to dry. The surface was measured using FTIR.

Subsequently, thin films were vacuum vapor deposited onto a gold-coated microscope slide and measured as above. A C^{13} NMR spectrum was obtained by dissolving the vapor deposited film from the surface using deuterated chloroform and measuring the resulting solution. The NMR experiments showed that within experimental error the film was the same before and after the vapor deposition process. The C^{13} peaks in the spectra (before; after) for the most prominent bonds were as follows: C=O (170.5, 169.2; 170.8, 169.5), C-1 (96.5; 96.5), C-4 (75.0; 75.2), C-2,3,5 (71.6, 71.2, 71.0; 71.8, 71.5, 71.2), C-6 (61.8; 61.8), $(CH_3)_3C$ (25.9; 25.8), $COCH_3$ (20.9, 20.7; 20.9, 20.8) and $(CH_3)_2Si$ (–4.9, –5.2; -5.0, -5.3). There were very small shifts in peak positions due to instrumental variations ($\delta \pm 0.3$). However, it should be noted that some of the relative intensities of the peaks did change. This may be due to the loss of an impurity during the vaporization process or to structural degradation. Figure 3.5 shows that the FTIR spectra for bulk (blue) and vacuum vapor deposition (red) are nearly identical. The lack of bands in the region 1700-1500 cm^{-1} for the vapor deposited sample is probably due to a loss of a nonvolatile contaminant present in the bulk material. These bands in the 1700-1500 cm^{-1} region are relatively weak and do not correspond well with any known bonds in the CD compound. The reaction scheme to produce the HDATB-β-CD involves several purification steps and chromatographic isolation of the desired product, but clearly not in the highest purity [170]. It should be noted that CDs similarly functionalized at the C2, C3, and C6 hydroxyl positions have been used as stationary phases in gas chromatography at temperatures ranging up to 200°C.[178, 179]

Both AFM and XPS were used to study the thin film coated *MC*s. Figure 3.6

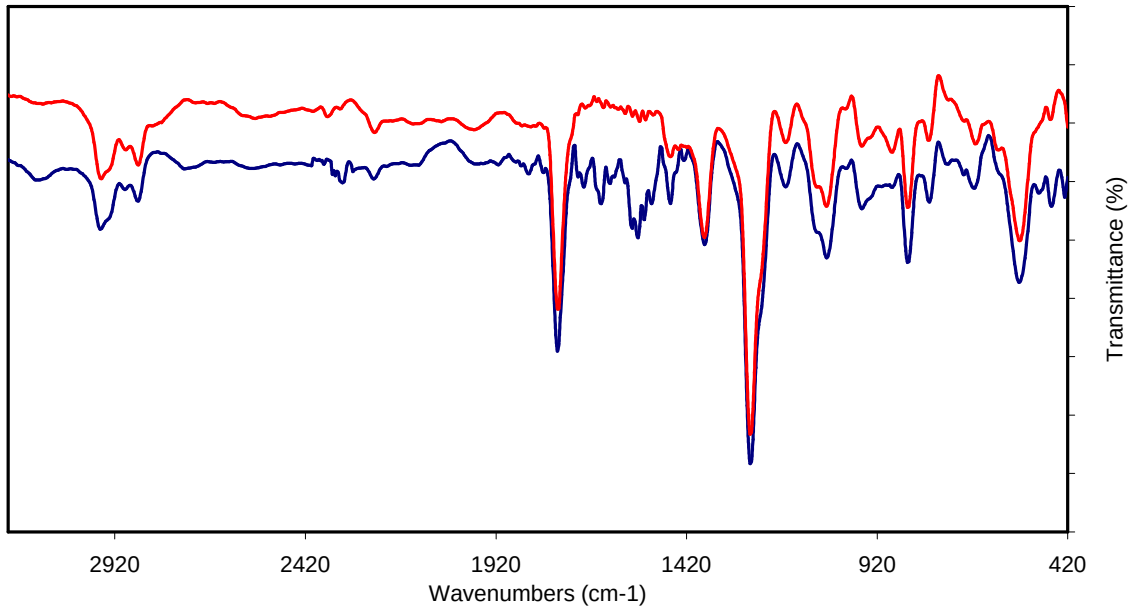

Figure 3.5. Effect of deposition method on the FTIR spectrum of a chemical film. The blue trace is that of the bulk material, while the red trace is for the vapor deposited film. The plots have been offset so that comparisons can be made more readily.

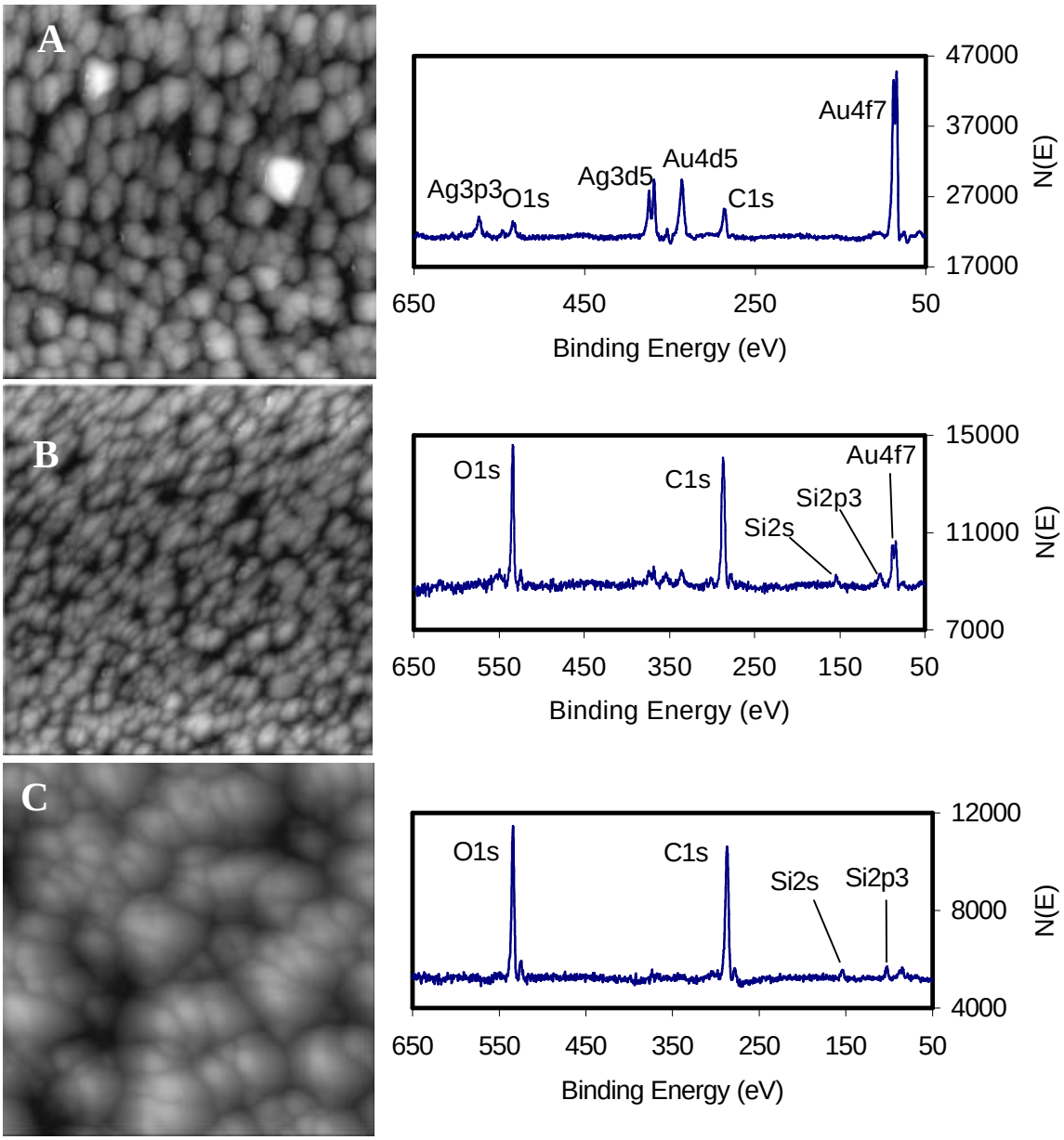

Figure 3.6. Atomic force microscopy and x-ray photoelectron spectroscopy images of coated *MC*s. (A) a bare nanostructured *MC* (B) a *MC* coated with an 18 nm film of HDATB-β-CD and (C) a *MC* coated with a 50 nm film of HDATB-β-CD. All images are of a 1×1 μm square.

shows the AFM images (left) and XPS spectra (right) for three of the nanostructured surfaces studied. The AFM images (1×1 μm) were obtained from an actual cantilever surface and show colloidal type surface for both the uncoated nanostructured surface as well as for the surface coated with the 18 nm film of HDATB-β-CD. The root mean square (RMS) roughness of the bare nanostructured surface shown in Figure 3.6 (top) is about 30 nm. There is an apparent reduction in feature size upon addition of the thin (18 nm) film (RMS roughness of 20 nm)(middle image). This may be due to a filling in of the crevices between colloidal particles of gold or the build up of small CD aggregates on top of colloidal particles. In either case it is likely there are areas where there is bare metal or a very thin (<5 nm) film on the surface, as evidenced by the XPS data. The thicker (50 nm)(bottom image) film (RMS roughness of 18 nm) shows both an increase in the size of the features and in the continuity of the features, presumably due to a complete but not smooth coverage of the nanostructured surface. Further evidence of this can be seen in the XPS spectra of the surfaces. The XPS spectrum of the bare nanostructured surface was obtained from a gold-coated microscope slide and shows both gold and silver peaks due to the presence of these metals in the coating. There is also a small amount of carbon and oxygen present due to adsorbed hydrocarbons. Upon addition of the 18 nm CD film, the gold and silver peaks are greatly diminished while the carbon and oxygen peaks show a considerable increase. There is also the presence of silicon on the surface due to the silicon in the CD. Small peaks due to gold present in the spectrum of the 18 nm coated surface indicates that there is not a complete coverage of the metallic layer by the thin film. In comparison, the metal peaks are essentially absent

in the spectrum of the nanostructured surface coated with the 50 nm film, indicating that the underlying metallic layer is more completely covered.

3.3.2 Control Experiments

Control experiments were performed in order to verify that the observed responses were principally due to the analyte binding with the chemically modified side of the *MC*s. For our purposes, tensile and compressive responses will be defined as bending away from and bending towards the silicon nitride side of the *MC*, respectively. Responses to each analyte were obtained for both smooth and nanostructured cantilevers that were not chemically modified with cyclodextrins. Upon exposure to each analyte at 1000 ppm, the uncoated *MC*s exhibited a compressive response of no more than 50 nm for the dihydroxynaphthalene series and 20 nm for the non-aromatic analytes. These responses were in the same deflection direction as for chemically modified *MC*s but far smaller in magnitude (see below). The observed blank responses were the greatest for the nanostructured surface, with the responses for the smooth surface being barely detectable. In some cases, the small blank responses were not reversible, showing no desorption from the surface.

The pH responses of non-chemically modified cantilevers were also investigated. For a smooth gold surface, tensile responses were observed for pH values < 7 and compressive responses for pH values > 7. The average value of cantilever deflection was approximately 90 nm/pH unit at pH 7, which corresponds well with previous work done by Thundat and coworkers.[126] When making these same measurements with a nanostructured surface, the results were quite different. Compressive responses were

observed for pH values < 7 and tensile responses for pH values > 7. The average value of cantilever deflection for this system was approximately 500 nm/pH unit at pH 7 over the range of pH 6-8. It is logical to surmise that increases in pH response with nanostructuring are related to increases in surface area, although the response characteristics, including the change in deflection direction, may also reflect a different chemical nature of the nanostructured surface that results from the dealloying procedure. Differences in response for smooth versus nanostructured *MC*s indicate the importance of analyte interactions with the active side but do not preclude the possibility of some interaction with the silicon nitride side. An ability to overwhelm interactions with the non-treated side of the *MC*s with very large stresses on the nanostructured side is another strength of our approach.

Finally, control experiments were performed to gauge the effect of solute-induced changes in refractive index (RI) on the responses of our system. In this work, the incident and reflected laser beams traverse RI interfaces at angles near normal and refraction effects are small. Also, it should be realized that reflection at the *MC* in our optical arrangement does not occur on the modified side. By reflecting off of the base of our *MC* chips we observed a small (30-40 nm) compressive deflection when going from pure water to our 25 mM buffer and essentially no detectable deflection when the buffer was then made to contain the highest 2,3-DHN concentration employed. Deflection measurements reported herein were performed with the plane of the incident and reflected beam in the same plane as Δz. With our apparatus, the post (PEEK rod, Figure 3.4) that holds the *MC* can be rotated 180 degrees to reverse the direction of cantilever deflection without changing any possible RI effect. Using the nanostructured *MC* with an

18 nm film of HDATB-β-CD (see below), the response to the highest concentration of 2,3-DHN was found to maintain the same magnitude of signal (within 10%) but change direction when the 180° rotation was performed. It is clear that the signals reported in this work involve negligible contributions due to RI effects even at the highest analyte concentrations. In fact, a unique 90° optical configuration is possible with our system. The cantilever can be rotated to the 90° configuration that places deflections of the cantilever in a vertical plane (see Figure 3.7a) and RI effects in the horizontal plane (see Figure 3.7b) at the PSD. Since the vertical and horizontal outputs of the PSD are separately available for processing, the two effects (true signal and RI artifacts) can be distinguished.

3.3.3 Deflection Measurements

Different type films and film thicknesses were used on both smooth and nanostructured *MC*s to study their influence on *MC* response. When comparing smooth and nanostructured *MC* surfaces, an increase in the available binding sites in rough proportion to the increase in surface area is expected. In addition to an increase in the total energy of binding due to more binding events, the strong short range intermolecular forces occurring for receptors and analytes located in narrow crevices [166-168] on the structure may yield a more efficient conversion of the energy of binding into cantilever bending. This unique feature allows for enhancements in bending greater than the increase in surface area. In prior gas phase work, it was determined that an uncoated 50 nm thick dealloyed surface has roughly a 13-fold greater surface area than a smooth gold

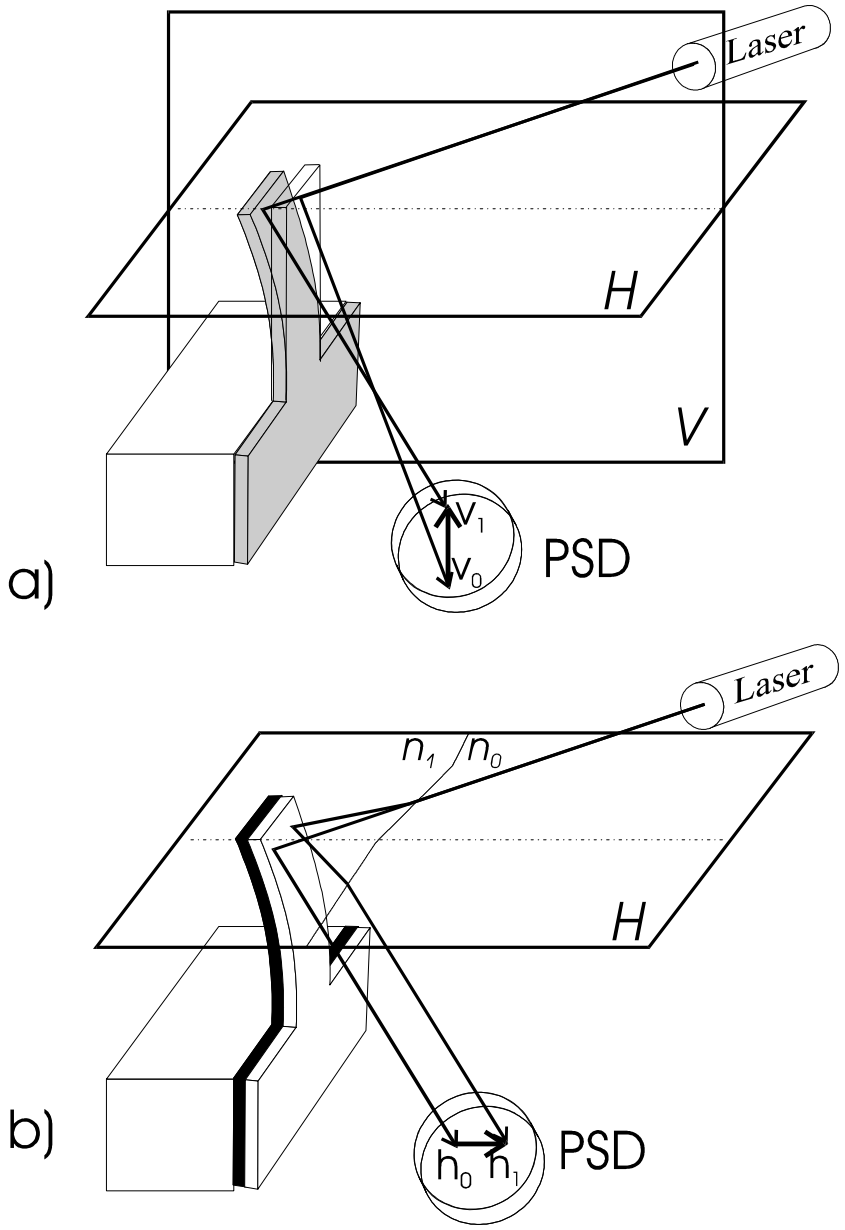

Figure 3.7. Optical arrangement for eliminating refractive index effects at the position sensitive detector (PSD). H and V represent the horizontal and vertical planes, respectively. *MC* bending and refractive index effects are shown in (a) and (b), respectively.

surface, but exhibited enhancements in response in some cases that were approximately 100-fold.[127] An object of the work reported herein was to determine if liquid phase systems, where the organic receptor phase is highly solvated, yield similar enhancements in chemi-mechanical response due to nanostructuring.

Self-assembled monolayers of HM-β-CD were formed on both smooth and nanostructured *MC*s. Cantilever deflections were measured on both *MC* systems. Figure 3.8 shows the response of the two different surfaces to 2,3-dihydroxynaphthalene (2,3-DHN). The compressive response of the nanostructured *MC* is approximately 4.5 times larger than that of the smooth one for a ten-fold less concentrated solution. This general trend (larger response on a nanostructured surface) is true of all the analytes we studied. In addition, the molecular recognition properties of the CD are evident. The aromatic molecules (DHNs) exhibit larger responses and lower limits of detection (LODs) than the non-aromatic molecules studied, where the LOD is determined to be a signal-to-noise ratio for *MC* bending of three (S/N= 3) (see Table 3.1). This may be explained by higher binding constants for the larger two-fused-ring DHN molecule relative to the other single-ring analytes. The two-fused-ring systems exhibit a better "snug" fit into the cavity of β-CD; evidence of this can be found in prior work involving cyclodextrins as running buffer additives in capillary electrophoresis and in molecular modeling studies.[172, 174, 176] However, since measurements are based on stress changes, response differences between these classes of analytes may be related to differences in intermolecular forces that are not directly related to binding constants. For example, one can envision interactions between the aromatic groups of adjacent DHNs bridging across deep crevices that contribute to the stresses observed in these studies. The LODs for all

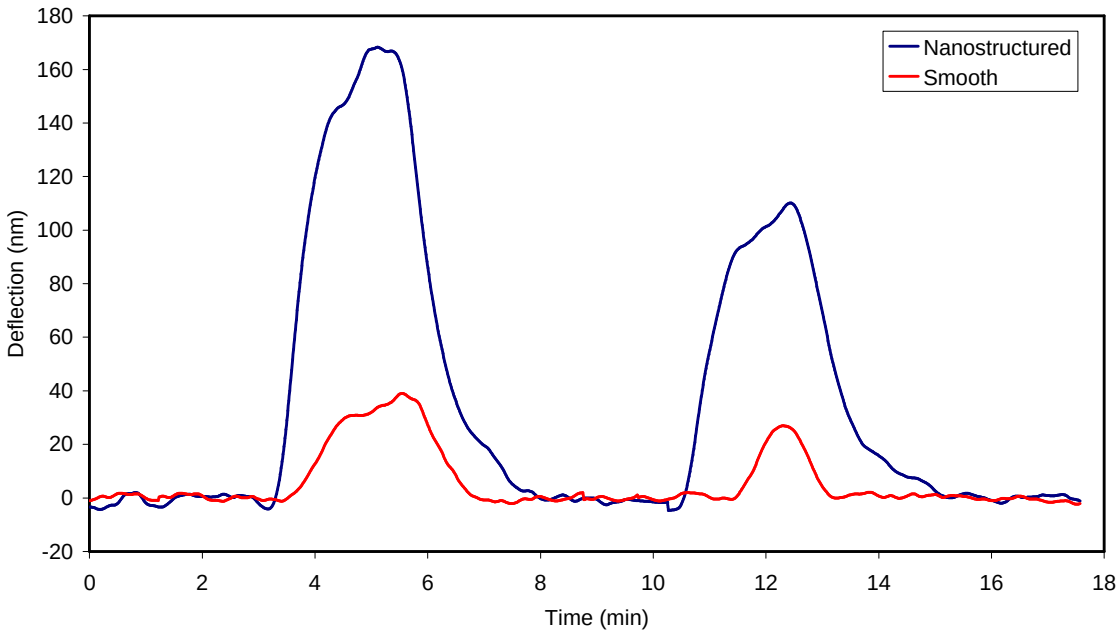

Figure 3.8. Response of a HM-β-CD treated smooth (red) and nanostructured (blue) *MC* to 2,3-DHN. The responses shown are for 1000 and 500 ppm (red) and 100 and 50 ppm (blue) analyte concentration in a 0.025 M pH 7 phosphate buffer.

Table 3.1. Summary of limits of detection for different film and surface type. All values listed in the table are given in terms of parts per million (ppm).

Compound	SAM (smooth)	SAM (nanostructured)	17 nm (smooth)	17 nm (nanostructured	50 nm (nanostructured
2,3-DHN	288	4.80	31.3	0.988	0.0248
1,7-DHN	242	8.50	22.4	4.45	0.0383
2,7-DHN	250	7.50	39.5	1.02	0.0387
Tolazoline	300	17.0	214	13.1	4.87
Ephedrine	326	31.3	93.8	15.7	14.4
Benzoic Acid	1.50×10^{3}	144	250	42.1	18.3

of the analytes on the HM-β-CD coated *MC*s range from 242 to 1.50×10^3 ppm and 4.80 to 144 ppm on the smooth and nanostructured surfaces, respectively. The average improvement in LOD upon nanostructuring for the DHNs and other compounds were 40 and 13, respectively, demonstrating that substantial enhancements in performance can be realized for liquid phase measurements.

The concept of analyte-induced modulation of the surface free energy of SAM functionalized *MC* surfaces, as a means to stress and bend the surfaces, is rendered fuzzy with nanostructuring and may be best described by theories describing stresses in colloidal systems.[166] In the case of thin films on those structures, the mechanism of stress is completely different. Analyte-induced swelling of the film leads to bending by a mechanism more akin to that observed in bimetallic devices with the two metals exhibiting different coefficients of thermal expansion.[166] However, thin organic films applied to smooth *MC* surfaces that swell with analyte absorption may "slip" or move along the surface to minimize stress. This reduces the response of the cantilever. There may also be reduced adhesion when applying films to a smooth surface. When applying films to a nanostructured surface, the phase is effectively anchored and the amount of slippage should be reduced. We have used films of thermally evaporated HDATB-β-CD that allow for facile adjustment of film thickness even on diminutive *MC*s. When 18 nm thick HDATB-β-CD films were applied to both smooth and nanostructured *MC*s, the observed LODs for all the analytes were substantially lower for the nanostructured *MC* (see Table 3.1). The average improvements in LODs were 25 and 9 for the DHN's and other compounds, respectively. This suggests that by using the nanostructured surface, the stress generated by film swelling was more effectively translated into *MC* bending.

It is interesting to note that the overall performance of the nanostructured SAM *MC* is better than the nanostructured 18 nm film *MC*. These systems differ in the disposition of CD on the surface, the actual CD on the surface, and the mechanism of analyte-induced bending. These factors make it difficult to compare selectivity patterns achieved on these cantilevers. However, it is important to note the achieved increase in sensitivity in going from a smooth surface to a nanostructured surface. It was decided to investigate two film thickness regimes, substantially less than and greater than the RMS roughness of the bare nanostructured surface. The fact that these produce different surfaces was demonstrated in conjunction with Figure 3.6. We surmise that swelling of the thin (probably discontinuous) 18 nm film within the nanostructured surface may have a large out-of-plane (of the *MC*) component that is not effectively translated into in-plane stress. For this reason, thicker (continuous) films should be, and generally are used as *MC* coatings.[88, 92, 129]

In a previous work (Chapter 2), we created relatively thick (50 nm up to 500nm) coatings of GC phases on smooth *MC* surfaces using a spin coating technique.[130] The largest responses to gas phase analytes were obtained with the thinnest (50 nm) films. The loss in response with greater film thickness may have been due to stress-induced slippage. However, since the measurements were not performed under true equilibrium conditions, it also could have been due to slow kinetics. While it is true that the mass loading of analyte increases with film thickness, bending due to increased mass is generally much smaller than that due to in-plane stress. It is for this reason that we have chosen to use a very well-controlled vacuum vapor deposition approach to deposit very thin to moderately thick layers of receptor phases on *MC* surfaces. Despite having only

limited quantities of HDATB-β-CD we were able to compare films with a thickness of 18 nm and 50 nm. As can be seen in Table 3.1 the 50 nm film performed much better (an average factor of 60 better than the 18 nm film for the DHNs). This film, as seen in Figure 3.6 (bottom), appears to be more continuous than the 18 nm film, which leads to efficient conversion of swelling to in-plane stress. With our flow system, the response kinetics for the 50 nm film *MC* was essentially the same as seen in Figure 3.8 for the SAM coated *MC*.

Figure 3.9 shows a calibration plot of the 50 nm thick HDATB-β-CD film exposed to 1,7-DHN. The system exhibits the response typical of a Langmuir type film, with the onset of saturation between 2 and 4 ppm. However, even at low concentrations the response is relatively large with a very high sensitivity. The sensitivity to each analyte as a function of film type and cantilever morphology can be seen in Figure 3.10. The highest sensitivity is achieved on the nanostructured cantilever modified with the 50 nm film of HDATB-β-CD. This indicates that using a nanostructured surface with a thicker chemical coating can greatly enhance sensor performance. It is also evident that all of the films on the nanostructured cantilevers performed better than any of the films on a smooth cantilever. Given the wide range of polymeric and other films that are widely used and characterized, this appears to be a significant finding. The films on smooth cantilevers were marked by very low sensitivities and relatively higher LODs. The LODs obtained on the 50 nm film on a nanostructured *MC* were in the parts per billion range for the DHNs. The relative standard deviation tested via replicate (n=8) consecutive measurements of a solution of 100 ppm DHN was 11% on day 1 and 9% on

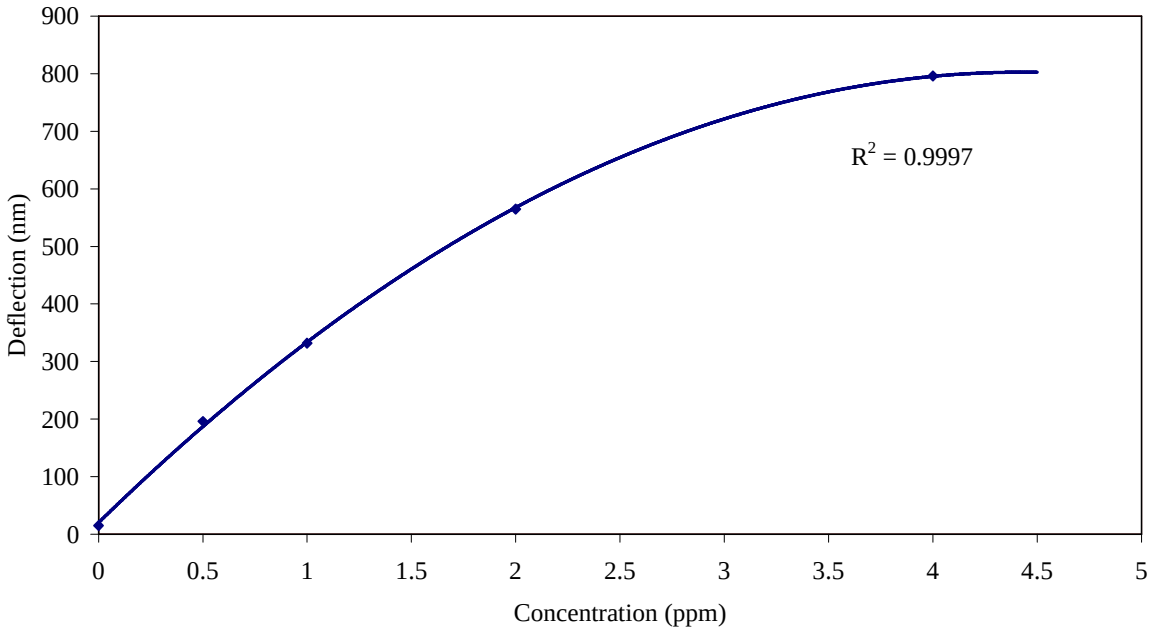

Figure 3.9. Concentration based *MC* bending to 1,7-dihydroxynaphthalene.

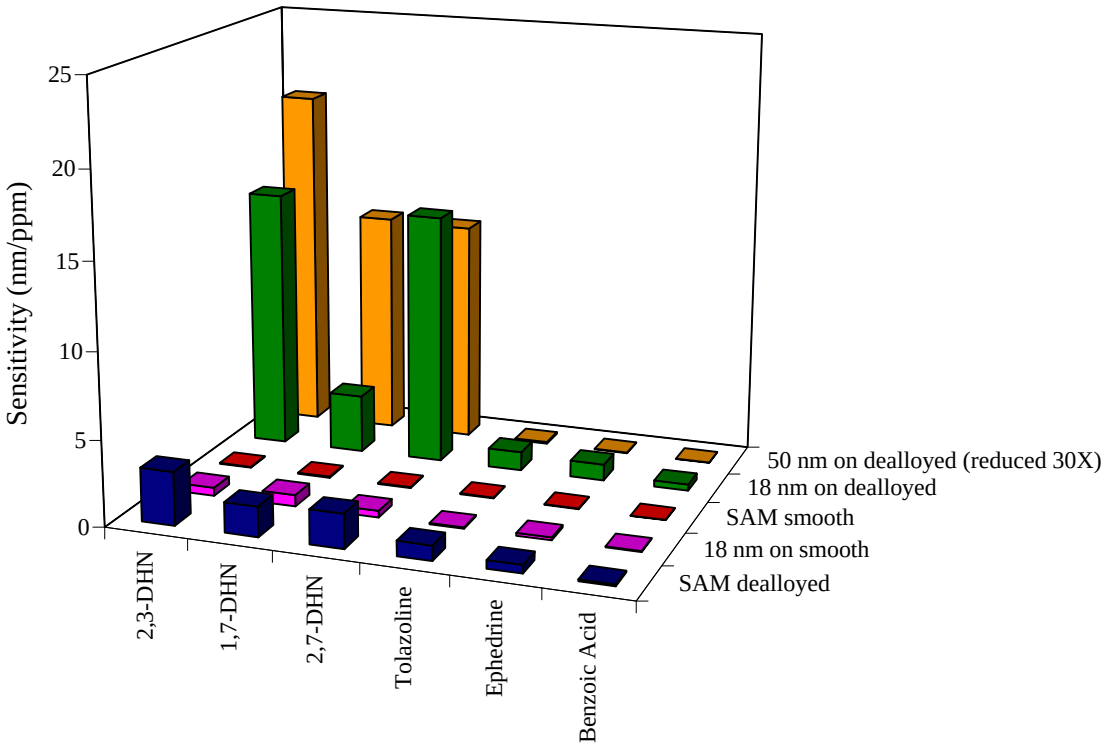

Figure 3.10. Sensitivity as a function of film type and cantilever morphology.

day 2. The average value in deflection from day 1 was approximately 76% of the average value from day 2. Thus, reasonable reproducibility is possible with this non-differential system, but calibration should be performed on at least a daily basis.

It can be envisioned that *MC* arrays can be made in this same general manner. Using vapor deposition and suitable masks it should be possible to individually coat *MC*s in an array. Up to a point, increasing film thickness may prove to enhance sensor performance even further than what we have demonstrated in this work. In addition, the larger responses achieved using nanostructured cantilevers with thick films may prove advantageous in the development of chemi-mechanical *MC* actuators.

CHAPTER 4

IMPROVED MICROCANTILEVER SENSING: A DUAL DIODE LASER BASED AND A VERTICAL CAVITY SURFACE EMITTING LASER BASED OPTICAL READOUT

4.1 INTRODUCTION

Along with the increased popularity of chemical sensors, it has become apparent that greater selectivity needs to be at the center of attention for further advances in chemical sensing to be fully realized. The research and development of a wide variety of chemically selective phases has become one of the chief means by which to increase the selectivity of chemical sensors. Films such as metal oxides [180, 181], sol-gels [134, 182, 183], conducting polymers [184-186], chromatographic phases [130, 187], calixarenes [188, 189] and cyclodextrins [75, 190, 191] have been employed as chemically selective phases. While none of these films may exhibit extremely high selectivity on their own, when used in conjunction with one another they can provide good selectivity when coupled with sophisticated data mining techniques. In addition, they can be used simultaneously to obtain "fingerprints" or unique response patterns for chemical species. This creates the ability to measure individual components in a mixture of chemicals. Overall, the use of multiple films provides more information than is available by using a single selective film.

With the recent growth in the number of chemically selective films available and the ability to mass-produce microfabricated transducers, the applicability of array-based sensors is at its highest point ever. Current fabrication techniques allow for highly

integrated and spatially dense arrays of micro-electro-mechanical systems to be formed. The overwhelming driving force for the use of sensor arrays is that they enhance the robustness and reliability of the measurement. In doing so, better limits of detection and precision can be obtained. Many groups have published reports of an array of sensors using various transducers. [88, 131, 182, 184-187, 192, 193] While these arrays can provide an abundance of information about an analytical sample, complex software packages and instrumentation are needed to garner that information. Data treatment techniques such as principal component analysis [187, 194-196] and neural networking [197-200] have been the most widely used to date. These techniques require significant programming and complex computer software with which to collect and analyze the data. In addition, these techniques often require complex optics and/or multiple lasers and detectors in order to perform the measurements. The overall sensor system may become highly complex and more time consuming to operate. Meanwhile, there have been no simple methods for collecting this same type of data published in the literature.

A logical place to begin is to use arrays consisting of only two elements. This alleviates the need for complex software to collect and analyze the data, which saves both time and money. Once a method for measuring a two-element array has been established, the technology should be readily transferable to arrays consisting of a larger number of elements. In this work, a dual diode laser (DDL) differential mode of monitoring microcantilever (*MC*) bending is described. The reference output of a lock-in detector, in combination with a simple inverter circuit, alternately powers the DDL system at an adjustable frequency. The laser beams are reflected off of adjacent *MC*s in a small linear array and onto a single position sensitive detector (PSD). The lock-in detector monitors

the synchronous output signal of the PSD. By simplifying the functions of the system, a non-differential mode of operation can be used to monitor the bending of a single *MC*. The *MC* array is mounted in a flow cell and exposed to liquid phase samples. Ideally, only specific targeted interactions between analytes and the *MC* will induce bending. Unfortunately, *MC* systems tend to bend due to a wide variety of conditions in the *MC*'s local environment. The results of studies of factors that affect the stability and reliability of *MC* based chemical sensors are reported for both modes of operation with chemically and non-chemically coated, nanostructured silicon *MC*s. Baseline disturbances resulting from changes in flow rate, temperature, refractive index, ionic strength, etc. that often mask true analyte responses are reduced by approximately an order of magnitude when comparing the differential and non-differential modes. This system has also been applied to the quantitation of individual components in a binary mixture.

Building upon the framework of the system discussed above, a second system was designed and employed for increasing selectivity. In this system, an array of vertical cavity surface emitting lasers (VCSELs) was utilized to measure five adjacent *MC*s simultaneously. This allowed for the responses of the five *MC*s to be compared to one another, which creates a distinct pattern for each analyte studied using this system.

4.2 EXPERIMENTAL

The *MC*s used in this work were custom ordered, rectangular shaped and composed of silicon (MikroMasch, Portland, OR) as seen in Figure 4.1. The length, width, and thickness of the microcantilevers were 400, 100, and 1 μm, respectively. The

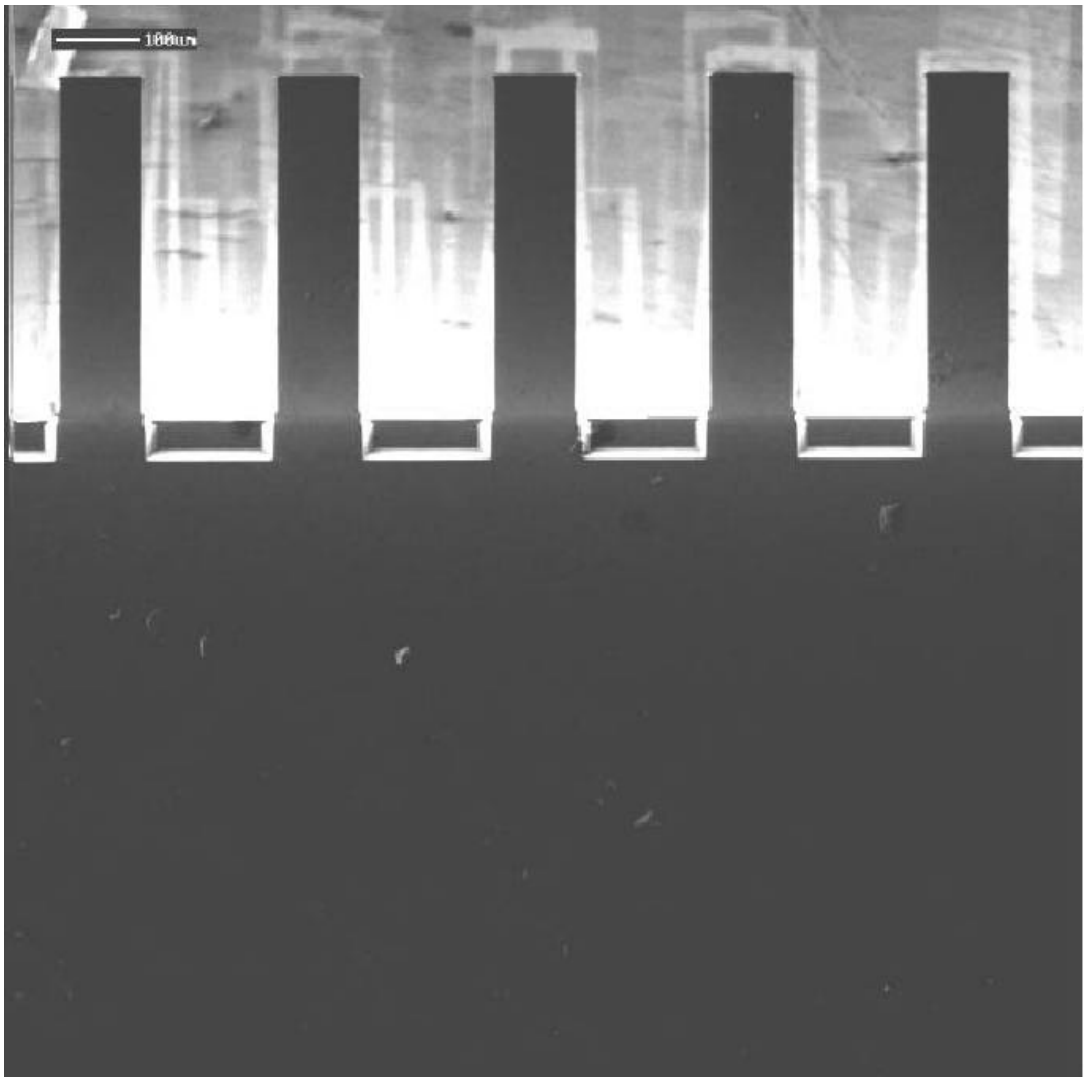

Figure 4.1. Silicon *MC*s used in the DDL and VCSEL studies. Image shows the entire array of five *MC*s (seen as black rectangles above).

*MC*s were coated with a 50 nm layer of aluminum at the time they were prepared. This aluminum layer was removed prior to their use by immersing them in aqua regia for 5 minutes. The *MC*s were then cleaned in warm piranha solution for 3 hours prior to having the dealloyed film applied to them. The process of creating nanostructured *MC*s having a dealloyed surface is described in greater detail elsewhere.[127] These dealloyed levers were then either used as is or chemically modified as described below.

The chemically modified cantilevers used in our studies were coated using traditional liquid phase reactions, nebulized solutions of polymers or physical vapor deposition. For vapor deposited films, a dealloyed *MC* was exposed to an ethanolic solution of 1.0 mM propanethiol for at least 18 hours. Following a thorough rinsing, the propanethiol treated *MC* was then coated with a selective film using physical vapor deposition of volatile organic compounds. Thin films of tert-butylcalix[4]arene (C4A), tert-butylcalix[6]arene (C6A), and tert-butylcalix[8]arene (C8A) were created by placing a small amount of the material into a quartz crucible in the PVD chamber (Figure 4.2). The crucible was then electrically heated in vacuum causing the material to evaporate onto the *MC* surface. A single *MC* on a chip could be coated by using a 120 μm slit to mask the other *MC*s on the chip, effectively exposing only the *MC* of interest to the vaporized material. The *MC* of interest was aligned under the opening of the slit using a CCD camera and held in place using double-sided tape. The thickness of the resulting film was measured using a conventional quartz crystal microbalance (Maxtek, Model TM-100R, Santa Fe Springs, CA). The polymers polydimethylsiloxane (PDMS), squalane and polyepichlorohydrin (PECH) were deposited using a nebulizer consisting of

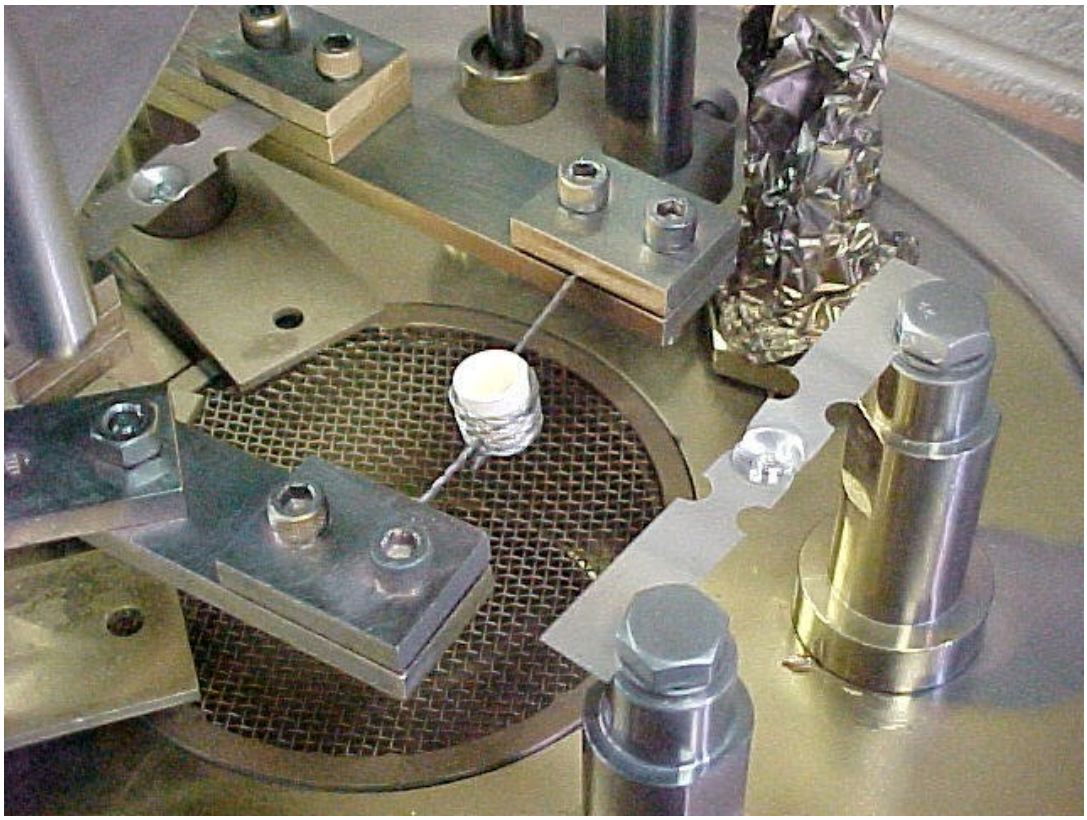

Figure 4.2. Quartz crucible used in the PVD for depositing organic materials.

a 100 μm fused silica capillary and sheathing tubing to spray solutions of the polymers in toluene onto the *MC* surface. This approach also utilized the mask used in the PVD coating approach to make arrays of coated *MC*s.

A third, and less frequently used method of coating the *MC*s was to immerse the *MC* inside of a fused silica capillary containing a solution to be placed on the surface of the *MC*. Up to two *MC*s, as shown in Figure 4.3, could be coated simultaneously using this approach by choosing the appropriate sized capillary. However, in most cases only one *MC* was coated at a time. This method was primarily used to form self-assembled monolayers of thiolated compounds on gold surfaces. This was done to create reference levers coated with different thiolated compounds. In the case of the DDL system, the *MC* was allowed to equilibrate in the background solution (25 mM phosphate buffer) until a stable baseline was achieved. Measurements using the VCSEL based system were made in the gas phase. A background flow of air at a rate of 2 ml/min was passed through the flow cell using a syringe pump. The analyte was then passed through the flow cell using a second syringe pump at different rates in order to prepare different gas phase concentrations.

In both systems the deflection of the *MC*s was measured using an optical beam-bending technique (Figure 4.4 specifically for the DDL system). In the DDL system, the deflection of the *MC* is measured by reflecting a modulatable, 3.5 mW diode laser (WSTech, Toronto, ON) operating at 670 nm off of the tip of the *MC* and onto a position sensitive detector to interrogate the different levers in the *MC* array. In the DDL system, one of two approaches was used: either the lasers were aligned to interrogate adjacent

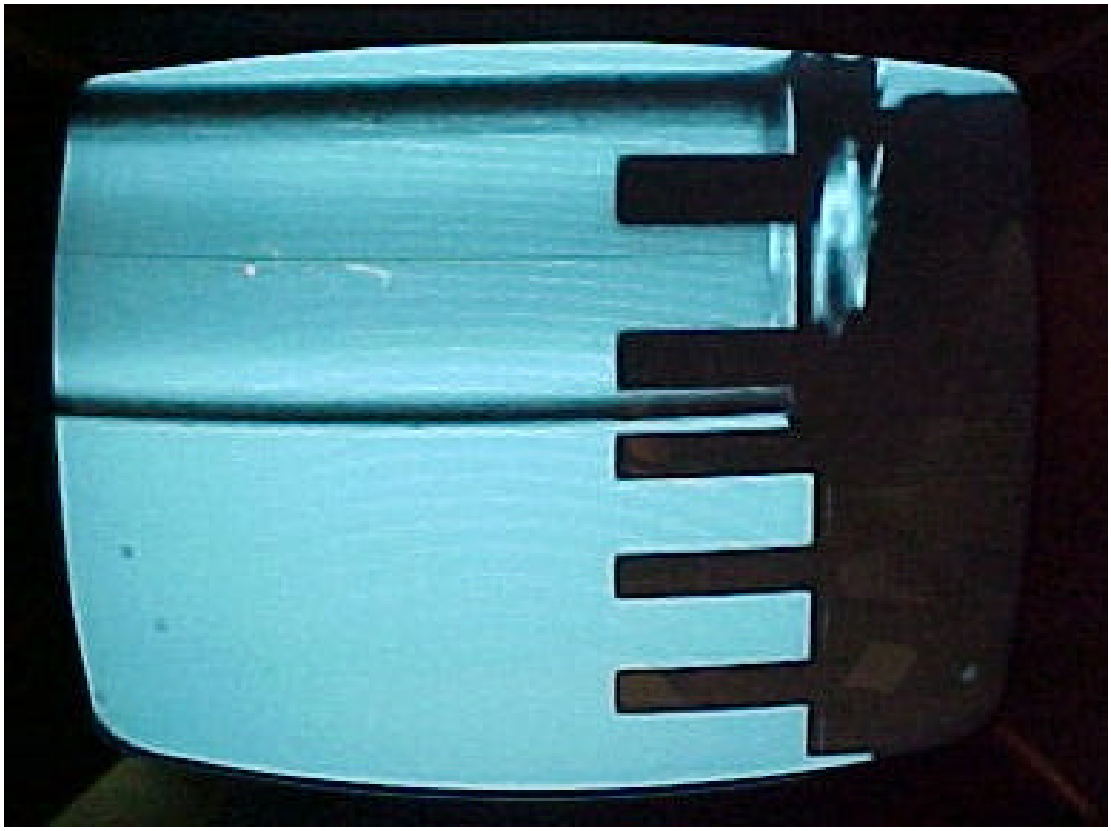

Figure 4.3. *MC* coating using a fused silica capillary.

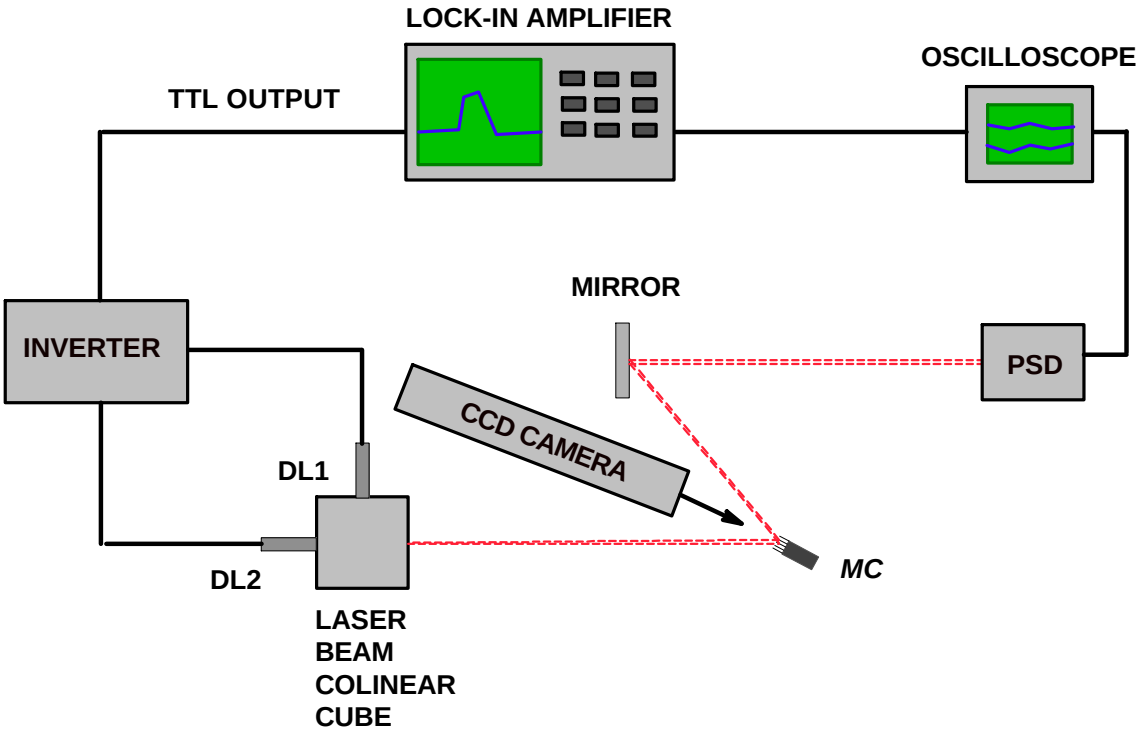

Figure 4.4. DDL optical setup.

*MC*s on a single chip. Because the lasers are mounted into a colinear beam cube, the distance between the two laser spots at the *MC*s could be easily changed. The position of the output from the laser diodes was adjusted so that the laser spots were aligned on adjacent *MC*s, as shown in Figure 4.5. This was done with respect to both the position from the base of the chip and the distance from either side of the *MC* (i.e. the spot was centered on the *MC*). The output of the detector was recorded and stored using a SRS 850 DSP lock-in amplifier (Stanford Research Systems, Sunnyvale, CA). The TTL output of the lock-in amplifier was used to modulate the two lasers at frequencies ranging from 1 to 160 Hz. This TTL signal was passed through an inverter in order to alternately power the two diode lasers. The output signal of the detector was fed through a TDS 220 digital oscilloscope (Tektronix, Beaverton, OR) to facilitate the optical alignment of the reflected laser beams onto the surface of the PSD. Upon a few simple changes in the electronics of the DDL system, the non-differential system could be restored and used to make non-differential measurements. No physical changes in the optics or lasers of the DDL system were necessary in going from the DDL to the non-differential system.

The VCSEL system used five diode lasers in a vertical array operating at 780 nm. The lasers were reflected off of five adjacent *MC*s and directed onto a single PSD. In this system, only one laser was operating at any one point in time. The lasers were pulsed in sequence (i.e. 1,2,3,4,5,1,2,3,4,5, etc) in a repetitive fashion and were separated in time by about 50 milliseconds. This cycle was continued until the user stopped the measurement. In both systems, the *MC* flow cell was imaged using a Watec CCD camera for alignment of the laser beam on the cantilever tip (Edmund Industrial Optics,

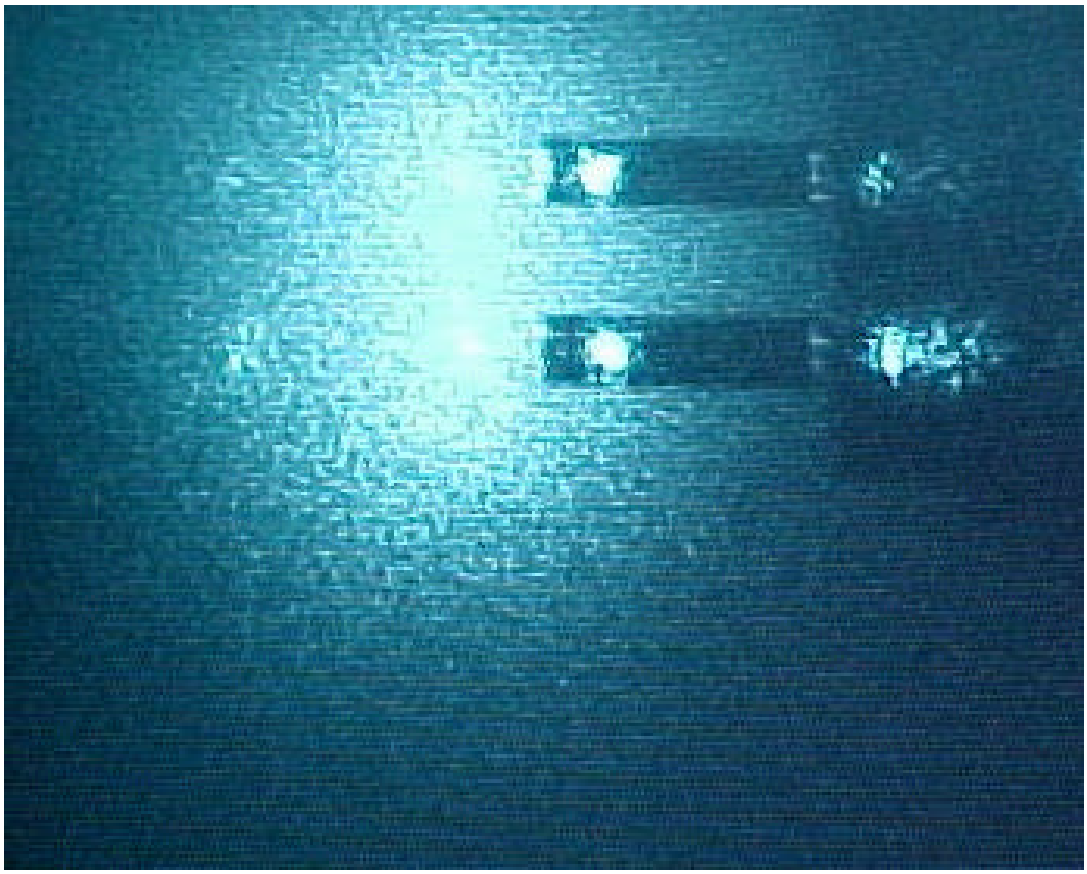

Figure 4.5. Image of both DDL lasers on adjacent *MC*s. Image shows the two laser spots on adjacent *MC*s.

Barrington, NJ). The *MC* chip was mounted in a 100 μL Teflon flow cell (Figure 3.4) and exposed to various solutions at flow rates of 0.85 ml/min or 2 ml/min, for liquid and gas phase measurements, respectively. The liquid phase analytes were delivered to the cell in the same manner as described in Chapter 3, page 87. The analytes were prepared in a 25 mM phosphate buffer, which was also used as the background solution flowing through the cell. The measurement of pH was performed using an Orion SA 520 pH meter (Thermo Orion, Beverly, MA). The gas phase analytes were contained in a 25 ml gas tight syringe and delivered to the cell using a syringe pump. Analyte headspace was collected using the 25 ml syringe from a 40 ml vial containing several milliliters of the liquid analyte. The gas mixtures were created by one of two approaches. In the first approach, equal volumes of the two analytes were placed into a syringe. In the second approach, the ratio of volumes of the two analytes was the same as the ratio of their vapor pressures, thus creating a mixture whose components had nearly equal concentrations.

The gold, silver, and chromium metals used in the coating process of the cantilevers were purchased from Gatewest (Winnipeg, Canada) or Alfa Aesar (Ward Hill, MA) at a purity of 99.9%. The analytes, squalane and buffer components were obtained from Sigma (St. Louis, MO) or Aldrich (Milwaukee, WI) and used as received. The calixarenes C4A, C6A, and C8A were obtained from Lancaster (Windham, NH). The polymer PECH was purchased from Scientific Polymer (Ontario, NY). All acids and bases and the polymer PDMS were obtained from Fisher Scientific (Pittsburgh, PA). Ultra pure water was obtained by using a Barnstead E-Pure water filtration system (Barnstead, Dubuque, IA).

4.3 RESULTS AND DISCUSSION

4.3.1 DDL System Characterization

The initial experiments performed using the DDL system were designed to test the ability of the system to eliminate unwanted sources of noise. Because two diode lasers are being directed onto a single PSD, it was important to determine if differences in the intensities of the two lasers significantly affected the measured signal. The experimental setup allows the intensity of one of the lasers to be adjusted relative to the other. This can be used to compensate for effects such as a poorly reflected spot (i.e. poor shape) or intensity fluctuations in the lasers. Experiments were performed in which the two lasers were adjusted so that their output at the PSD differed by either less than 200 mV or greater than 800 mV. A C8A coated and an uncoated *MC* were used to obtain the differential signal as a 200 ppm solution of 8-hydroxyquinoline (8-HQ) was passed through the flow cell. Figure 4.6 shows the differential response of the two levers at the two conditions described above. While the differential response in the case that the outputs differ by greater than 800 mV is slightly larger, it is not significant enough to cause major problems in making measurements when the lasers are not exactly matched, as evidenced by the slight difference in response. In cases where one of the lasers is completely dimmed as compared to the other, there may be significant effects observed due to the nature of the PSD (i.e. dividing the signal by 0).

A second factor that was investigated was the effect of the laser modulation frequency on the signal to noise ratio of the differential measurement. The same two coated levers as mentioned above, as well as the same analyte solution, were used to

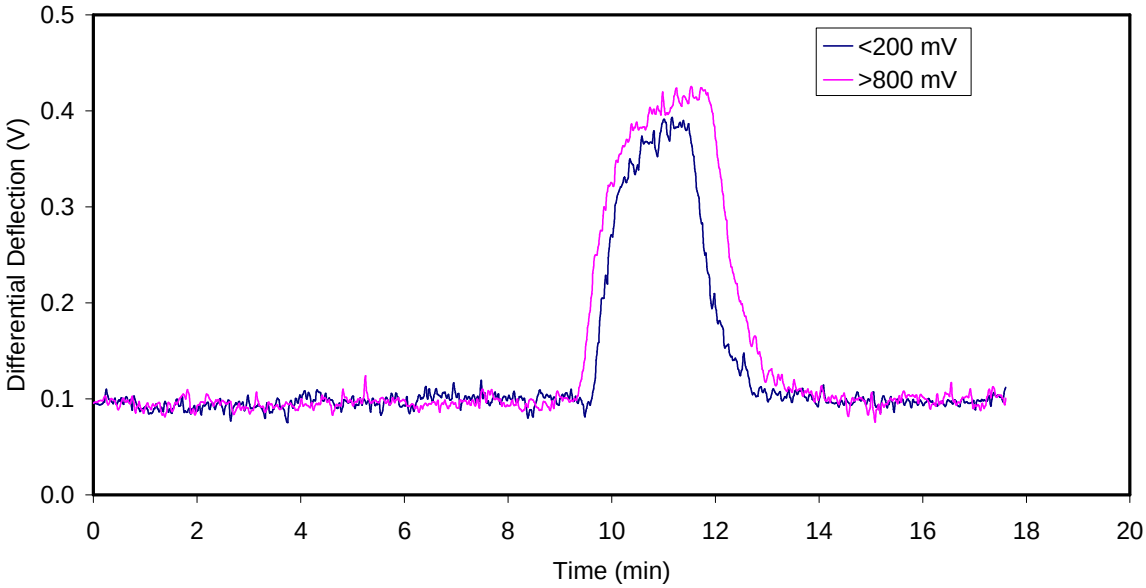

Figure 4.6. Effect of DDL laser output matching.

measure the differential response as a function of modulation frequency. The lock-in amplifier was used to drive the lasers at frequencies ranging from 1 to 160 Hz. Figure 4.7 plots the observed signal to noise (S/N) ratio as a function of frequency. As can be seen from the figure, the best S/N ratio is observed at lower frequencies. Operating at 1 Hz seems to give a better S/N ratio for this case, but it was decided to operate at a frequency of 20 Hz since interactions in this environment occur on the order of seconds. It is clearly shown that operating at higher frequencies results in a dramatic reduction in the S/N ratio and should therefore be avoided if possible. This is primarily due to the ability of the detector to measure such fast signals.

4.3.2 DDL Noise Reduction Studies

A major goal of using a differential based system is to remove unwanted sources of noise, which leads to a more stable and robust measuring system. *MC* based measurements have been traditionally plagued by various sources of artificial response (i.e. noise) and to long-term drift, which can be indistinguishable from real analytical signals. Using the DDL system, these sources of noise can be reduced significantly. These sources of noise are mainly due to changes in flow rate, temperature, refractive index, and ionic strength. Each of these sources of noise was studied using both the DDL system and the traditional non-differential *MC* system using plain silicon *MC*s. Figure 4.8 shows the reduction in *MC* response of uncoated silicon *MC*s caused from a change in flow rate by using the DDL system. There is no noticeable change in response when the flow is completely stopped using the DDL system (red trace). However, the non-

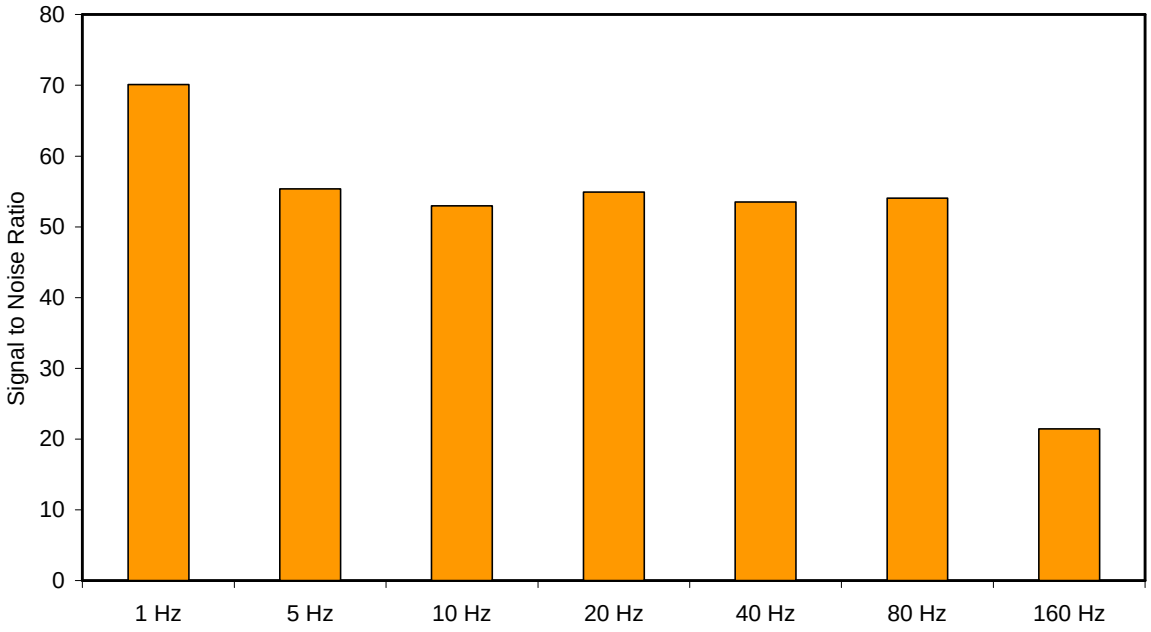

Figure 4.7. S/N ratio as a function of laser modulation frequency.

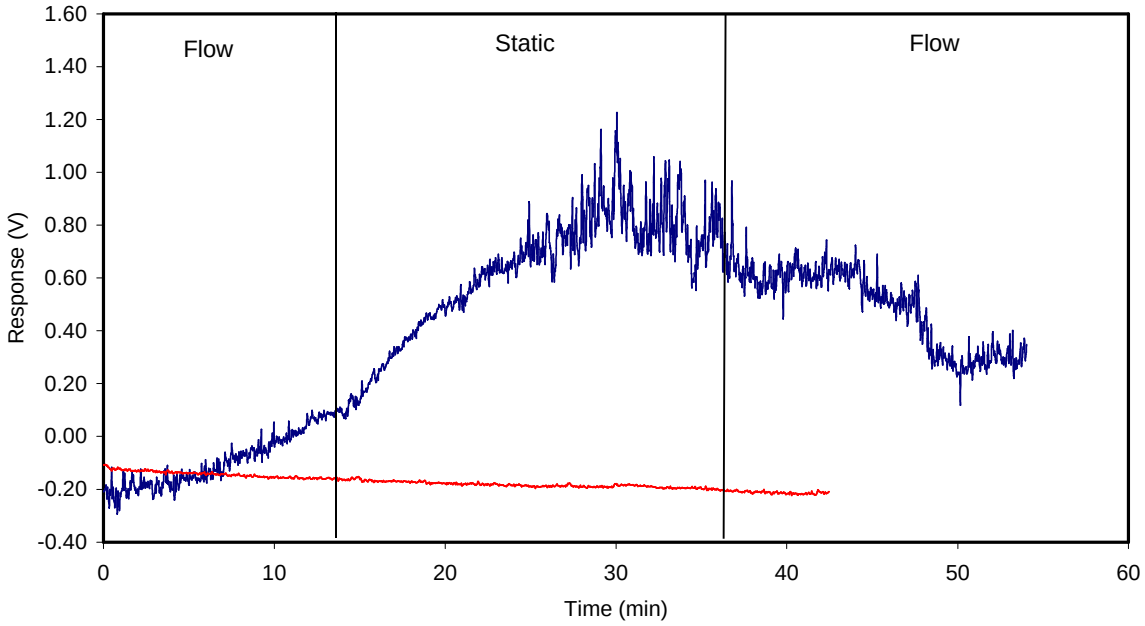

Figure 4.8. Effect of flow rate on *MC* response. The responses of the non-differential and DDL systems are shown in blue and red, respectively. The regions marked flow correspond to times in which the flow rate was 0.85 ml/min and the region marked static corresponds to the time in which the flow was completely stopped.

differential system (blue trace) responds as expected to the change in flow rate. The effect of flow is closely related to the effect of temperature, as the *MC* is heated by the laser to a greater extent when there is not a flow across its surface. Figure 4.9 shows the effect that a change in temperature in the *MC* environment has on *MC* response. To affect a change in temperature, the inlet tubing near the Teflon cell was heated using a heat gun. Both the DDL system (red trace) and the non-differential system (blue trace) respond to temperature, but it is interesting to note that the DDL system responds to a much smaller degree than does the non-differential system. This illustrates that the unique nature of each individual *MC* can affect the nature of the response. While this temperature change was more dramatic than any temperature change that may be realistically expected during a normal *MC* experiment, it demonstrates the ability of the DDL system to substantially reduce this source of noise. The effect of refractive index changes, which can be a major problem in *MC* based measurements when using the optical beam bending method (see Chapter 3), can be seen in Figure 4.10. An aqueous solution of 0.100 M quinoxaline was prepared using the background solution (0.025 M phosphate buffer) and was used to affect a change in refractive index. Both the DDL (red trace) and the non-differential system (blue trace) respond to the change in refractive index (ΔRI= 0.003), but the DDL system does limit the magnitude of the response and exhibits little baseline shift of the *MC*s. Again, a change in refractive index due to sample matrix or analyte concentration changes of this magnitude would not be expected in a typical *MC* experiment. However, it is useful for showing the ability of the DDL system to reduce this source of noise.

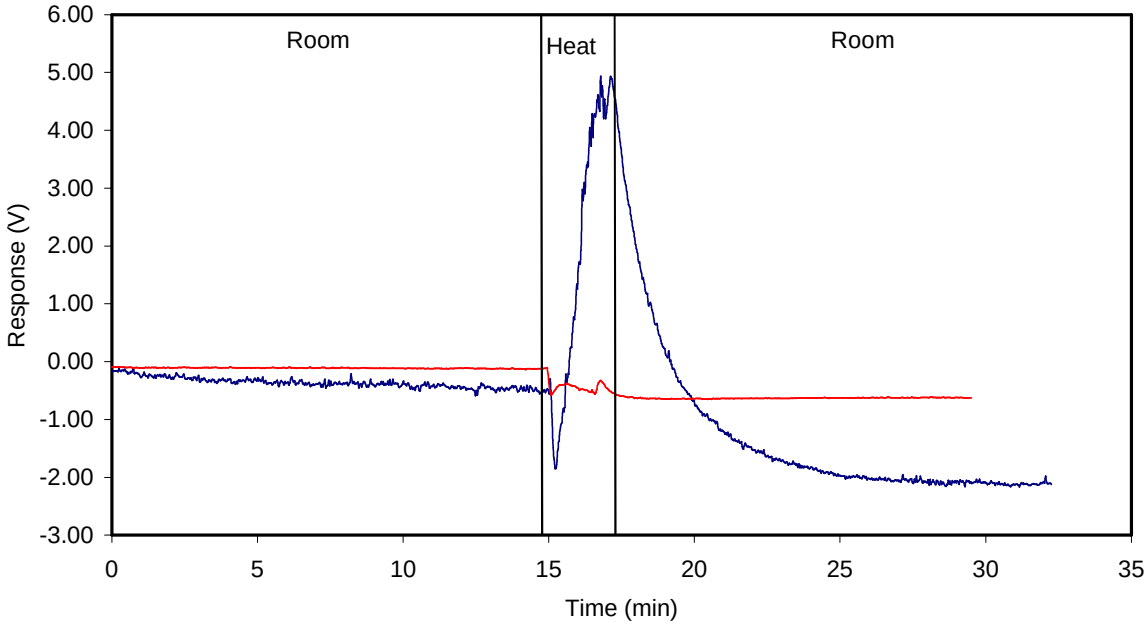

Figure 4.9. Effect of temperature on *MC* response. The responses of the non-differential and DDL systems are shown in blue and red, respectively. The regions marked room correspond to times in which the flow cell was at room temperature and the region marked heat corresponds to the time in which the flow cell was heated.

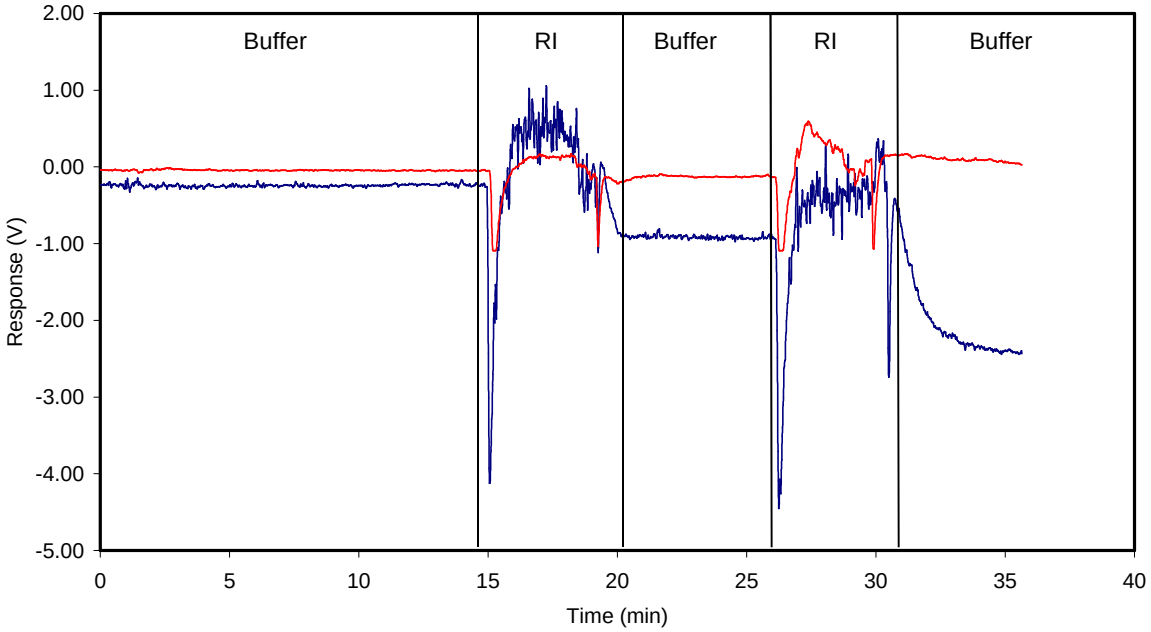

Figure 4.10. Effect of changes in refractive index on *MC* response. The responses of the non-differential and DDL systems are shown in blue and red, respectively. The regions marked buffer correspond to times in which only phosphate buffer filled the flow cell and the regions marked RI correspond to the times in which a 0.100 M quinoxaline solution filled the flow cell.

The final type of noise studied was the effect of solutions having different ionic strengths. Solutions were prepared in the background solution containing $NaNO_3$ at concentrations of 61.5, 102, and 200 mM. The solutions were injected in order of lowest to highest concentration of $NaNO_3$. Figure 4.11 shows the response of both systems to these changes in ionic strength. The non-differential system (blue trace) shows a significant response to the changes in ionic strength. In contrast, the DDL system (red trace) shows a much smaller response to the same changes in ionic strength. Table 4.1 shows the different magnitudes of the artificial responses (noise) in both systems. When taking all of the different sources of noise into account, the DDL system exhibits an average reduction in noise of approximately 22 when compared to the non-differential system. This is an important result, as this reduction can lead to better LODs and more reliable responses when making *MC* measurements. In addition, the DDL system does a better job of reducing baseline drift and shifts that occur during the span of a typical *MC* measurement.

4.3.3 DDL Binary Mixture Analysis

The DDL system was also used to perform measurements on a binary mixture of two structurally related compounds, 8-HQ and quinoxaline. These analytes were chosen due to their similar chemical structure and nature. In order to perform these measurements, two adjacent levers were used with the DDL system. Two separate cases were used in these experiments: a C6A coated lever and a propanethiol coated reference lever, as well as a C8A coated lever and a propanethiol coated reference lever. Film thicknesses for the C6A and C8A coated levers were 143 and 125 nm, respectively.

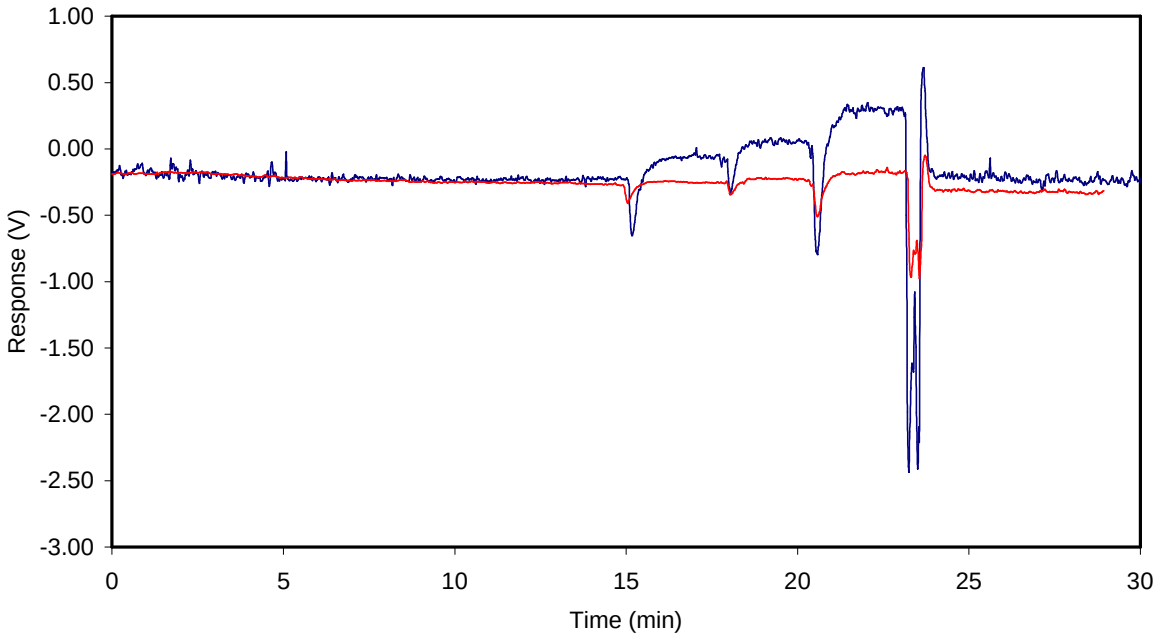

Figure 4.11. Effect of changes in ionic strength on *MC* response. The responses of the non-differential and DDL systems are shown in blue and red, respectively. The changes at 15, 18, and 21 minutes were due to the injection of solutions containing 61.5, 102, and 200 mM $NaNO_3$.

Table 4.1. Summary of the reduction in noise using the DDL system. The values in the table correspond to the response of the *MC* to the listed variable.

	DDL (V)	Non-differential (ND) (V)	Ratio of ND to DDL
Flow	0.01	0.66	66.00
Temperature	0.51	5.94	11.65
Refractive Index	0.22	1.09	4.95
Ionic Strength	0.03	0.24	8.00
Average	0.19	1.98	22.65

Calibration plots were obtained for each analyte, injected separately, using the two different coating schemes mentioned above in order to obtain response factors necessary to quantitate the individual components. Figure 4.12 shows the differential responses of both 8-HQ and quinoxaline on the C6A and C8A coated levers. The triangles and squares represent the C6A and C8A coatings, respectively, while the red and blue traces represent 8-HQ and quinoxaline, respectively. As can be seen in the figure, 8-HQ and quinoxaline exhibit moderately different responses even when using the same coating. After these initial experiments to determine the response factors for the analytes and coatings, a mixture of the 2 analytes was prepared by Dr. Jeremy Headrick. The response of the "unknown" mixture on each of the two coating systems used was then obtained in triplicate. This yielded a situation in which there were two unknown quantities in two corresponding equations, which could be solved using simple algebra. The two appropriate equations to use are Equations 4.1 and 4.2,

$$\mathbf{Response}_6 = \mathbf{RF}_{8-\mathbf{HQ}(6)}\,\mathbf{[8\text{-}HQ]} + \mathbf{RF}_{\mathbf{Quinoxaline}(6)}\,\mathbf{[Quinoxaline]} \qquad (4.1)$$

$$\mathbf{Response}_8 = \mathbf{RF}_{8\text{-}\mathbf{HQ}(8)}\,\mathbf{[8\text{-}HQ]} + \mathbf{RF}_{\mathbf{Quinoxaline}(6)}\,\mathbf{[Quinoxaline]} \qquad (4.2)$$

where the response factor for the analyte on a given film is symbolized by $RF_{Analyte\ (film)}$ and the molar concentration of each analyte is shown in brackets. Solving one of the equations in terms of one of the unknown concentrations and substituting that value into the second equation gives the unknown concentration of one of the analytes. The other concentration can then be readily determined. Using this approach, the unknown concentrations of 8-HQ and quinoxaline were determined to be 303 and 493 ppm, respectively. The actual concentrations of 8-HQ and quinoxaline used were 250 and 500

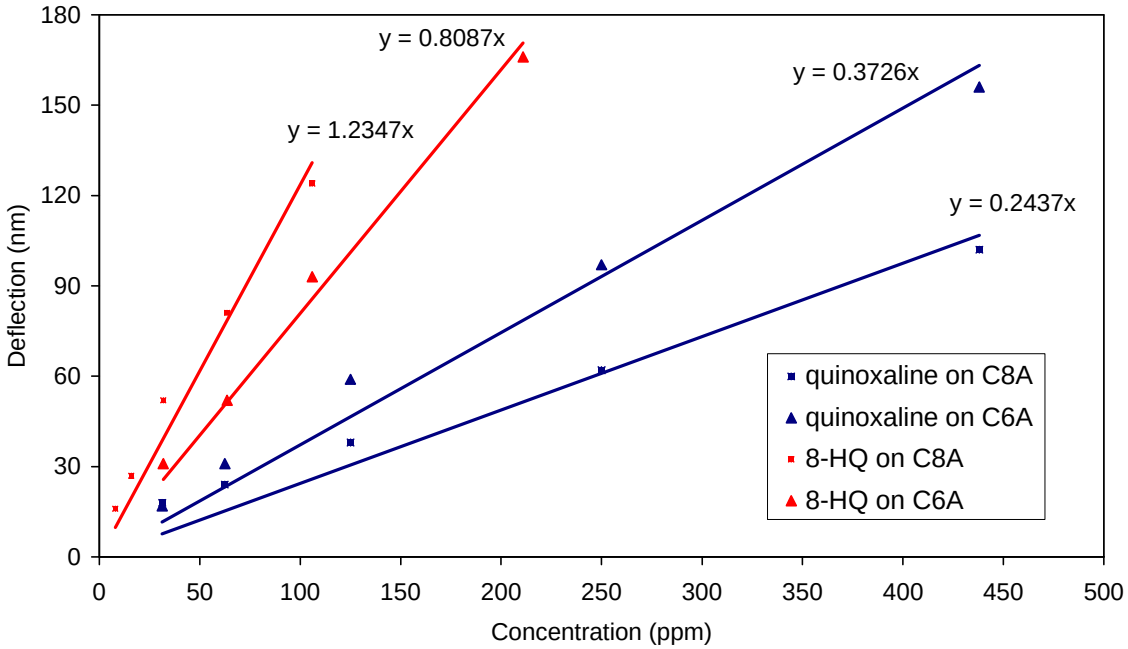

Figure 4.12. Calibration plots for 8-HQ and quinoxaline.

ppm, respectively. This results in an absolute error of 20.7 and 1.60% for 8-HQ and quinoxaline, respectively. These results show modest success for this type of data treatment combined with the DDL system.

The DDL system has proven useful for reducing the types of noise that commonly affect *MC* based measurements. It is expected that with this reduction in noise, lower LODs should be attainable. However, this has yet to be realized, as in general the LODs obtained with the DDL system mimic those obtained with the non-differential system. However, preliminary results for quantifying individual components in a binary mixture using the DDL have shown promise. These measurements could be performed using the non-differential system, but would require more time and be more prone to the sources of noise discussed in the previous section. More work does need to be done to optimize the ability of the DDL system to perform analyses on mixtures of analytes.

4.3.4 Selectivity Patterns Using the VCSEL System

The VCSEL system was used to measure several gas phase analytes in an attempt to show that unique response patterns could be obtained by using an array of chemically coated *MC*s, each with a different coating. Before this was performed, several system tests were conducted to insure that no response from artifacts was present. Changes in gas flow rate were tested by manipulating the total flow rate using a single syringe pump. The flow rate was changed from 2 to 4 ml/min with no signal being observable. In fact, measurements initiated under static flow conditions that were changed to a flow of 2 ml/min showed no significant response. This meant that the total flow rate did not need

to be carefully controlled during the experiments and the analyte flow rate could simply be changed incrementally to achieve different concentrations.

Measurements were made by collecting baseline response and then exposing the *MC* array to analyte vapor for 20 seconds. This allowed for the maximum response to be achieved. This was done for a series of analytes, including common organic solvents. For each analyte measured, the peak height was obtained and plotted against the four different chemical phases used. The four *MC*s used in these studies were coated with PDMS, squalane, PECH and a final *MC* that was not coated with any film. These films were initially selected due to their ability to detect trichloroethylene (TCE) in the gas phase. Figure 4.13 shows the actual responses of each of the four *MC*s to an injection of 50% TCE. As expected, the figure shows that the coated *MC*s respond much better than the uncoated *MC*. The responses are also shown to exhibit good kinetics and to be reversible. The actual responses for both tetrachloroethylene (TrCE) and chloroform were similar in nature to that of TCE, not surprising since all three are common chlorinated solvents. Each analyte studied was injected three times in order to show that the responses were reproducible. The overall goal of these studies was to show that the VCSEL system shows great promise for discriminating one analyte from another. Therefore, we have chosen to use the simplest data analysis method available for doing so. Methods such as principle component analysis (PCA) or neural networks are expected to yield better results, but are not necessary to achieve our goal. Using the plots of the actual responses, the peak heights of these responses were measured and used to create visual depictions of the response pattern for each analyte. Figure 4.14 shows the

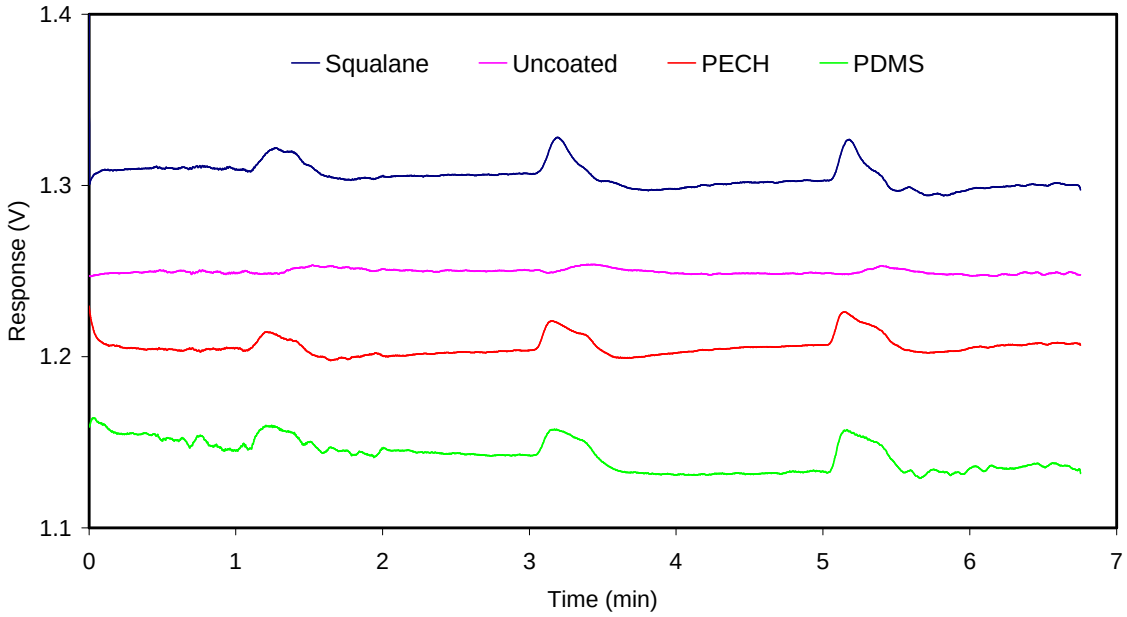

Figure 4.13. Film based responses for TCE using the VCSEL system. Triplicate injections of the same concentration were made at 1, 3, and 5 minutes.

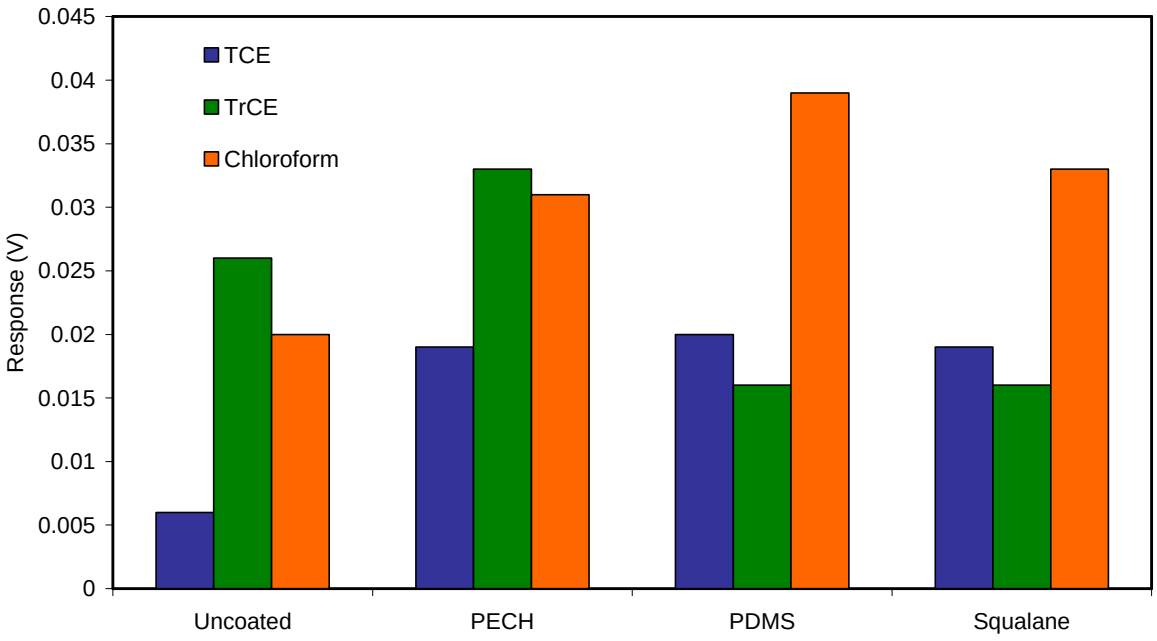

Figure 4.14. Response patterns for TCE, TrCE, and chloroform obtained using the VCSEL system.

response patterns obtained for TCE, TrCE, and chloroform. The figure shows that the patterns are quite different and can be discriminated relatively easily. This demonstrates the extreme usefulness of the VCSEL system in differentiating between different analytes. The effect of concentration on the response pattern is shown in Figure 4.15 for two different concentrations of TCE. As expected, the shapes of the two patterns are quite similar, while the overall area is smaller for the lower concentrated sample. This behavior was also observed for the other analytes studied.

In order to test the limits of the VCSEL system, a mixture of analytes was measured. A simple mixture composed of equal concentrations of trichloroethylene and chloroform was prepared by sampling the headspace above their respective vials. The mixture was composed of different volumes of TCE and chloroform, owing to their different vapor pressures (197 and 69 mm Hg for chloroform and TCE, respectively). A mixture composed of equal volumes of the two analytes was also studied. Both mixtures were injected and the response to each *MC* was collected as described above. Figure 4.16 shows the response patterns that resulted from the analysis of both mixtures. As can be seen, the pattern is very similar to that of TCE in both cases. The figure shows that at equal concentrations the pattern of the mixture is dominated by the TCE pattern. However, when equal volumes of the two components are injected, the pattern of the mixture is shifted towards the chloroform pattern. The overall shape is still much like that of TCE, showing that even when the mixture is composed of approximately 3 times more chloroform the pattern retains the character of TCE.

A key issue to investigate is how reproducible the patterns are over time.

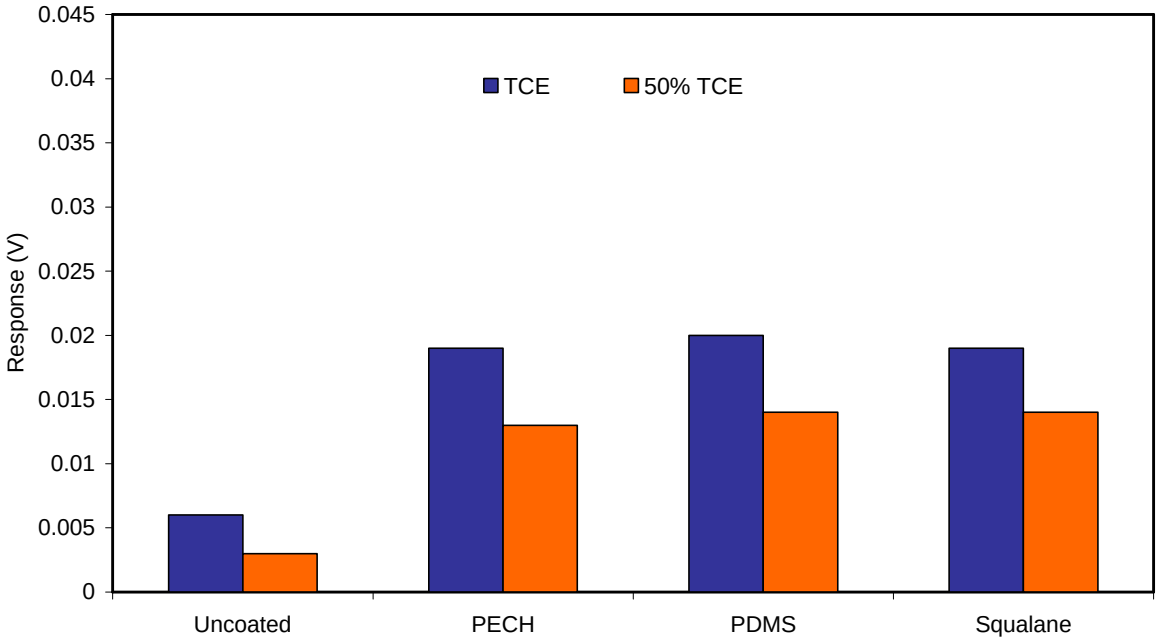

Figure 4.15. Concentration based response patterns for TCE obtained using the VCSEL system.

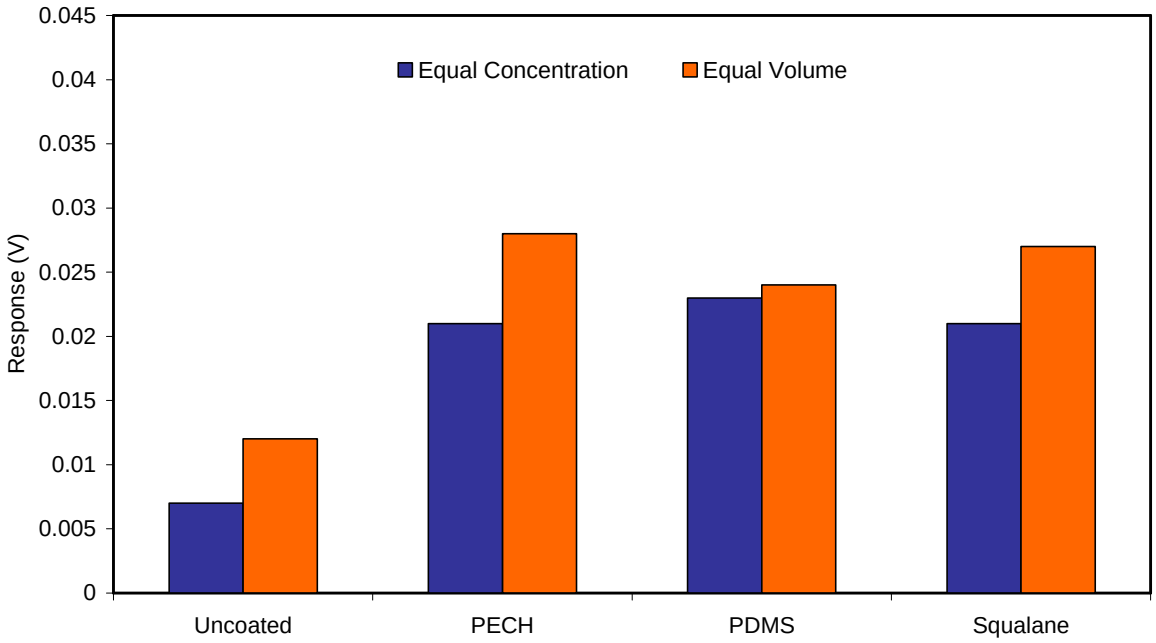

Figure 4.16. Response patterns for an equal concentration and equal volume mixture of TCE and chloroform.

Response patterns were generated over a two-day span, with measurements being made in exactly the same manner both days. In addition, no adjustments were made to the optical setup so that any differences that may arise due to changes in the setup would be avoided. Figure 4.17 shows the response patterns for TCE on two different days. As can be seen from the figure, the two patterns have both different sizes and shapes. Both patterns do however exist in a region of the plot that is relatively unique to TCE when compared to the other two analytes investigated. Figure 4.18 shows the response patterns for chloroform on two different days. As is the case for TCE, the sizes and shapes are different, while the region they exist in is unique to chloroform. The same trends are true for both TrCE and the mixtures studied. Due to the relatively simple but crude method for headspace sampling, some differences in response patterns may be expected due to different samples being utilized. There may also be physical changes in the polymers that occur due to exposure to these organic solvents that limit the responses from being the same over time.

It has been shown that the DDL system is useful for reducing the sources of noise associated with *MC* based measurements. The system also showed some capability to analyze simple mixtures. However, mixtures of higher order could not be measured due to the limited number of sensing elements available. To alleviate this problem, a system based upon VCSELs was used to obtain unique response patterns for individual analytes. The response pattern of a mixture of two analytes was also shown to be characteristic of the two components in the mixture. However, response patterns changed over time, which limits the ability of this system to accurately measure mixtures. Clearly, more

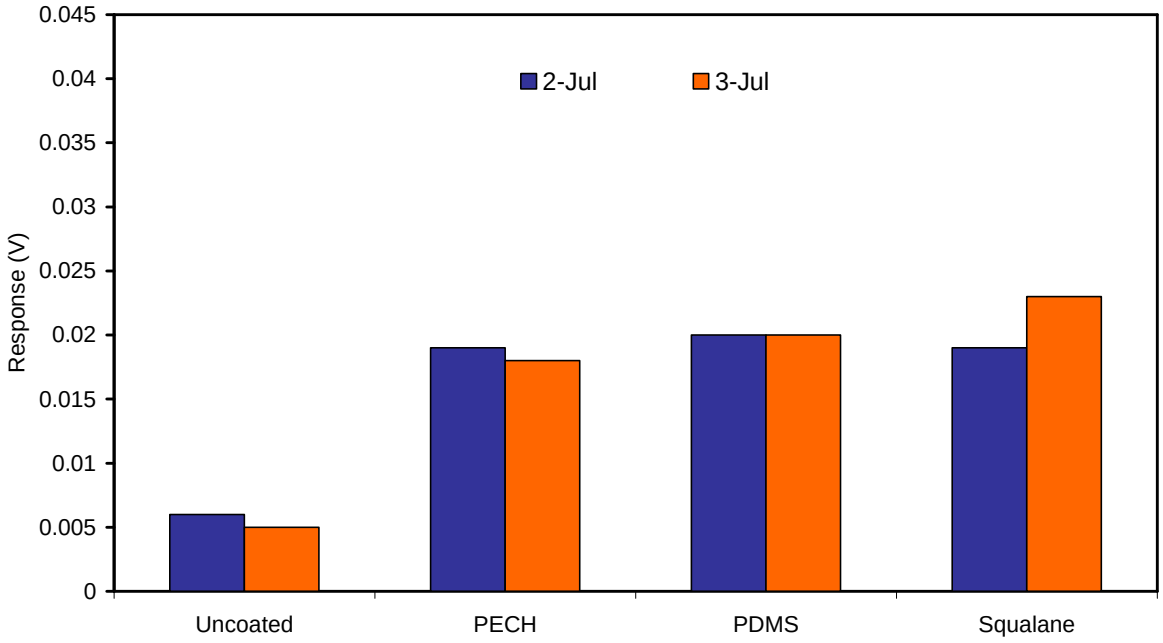

Figure 4.17. Response patterns for TCE obtained on two different days.

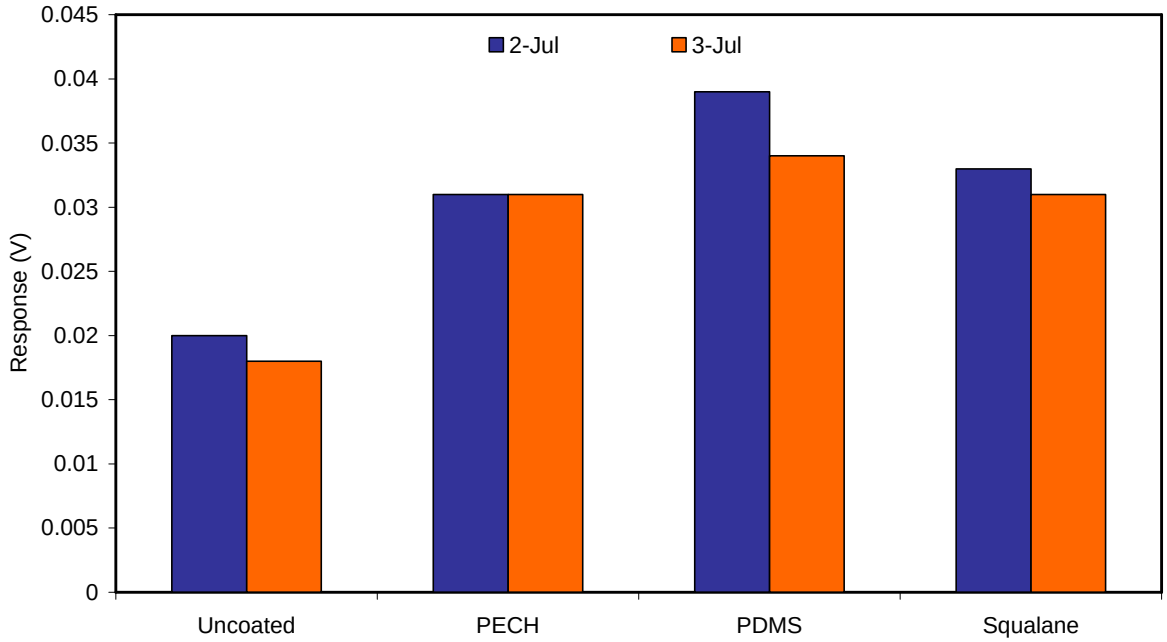

Figure 4.18. Response patterns for chloroform obtained on two different days.

work needs to be done to obtain working arrays that not only exhibit unique response patterns but that also exhibit patterns that are reproducible over time. In addition to this, methods such as physical vapor deposition need to be thoroughly investigated as possible alternatives to the deposition of these polymer films to the surface of the *MC*s.

CHAPTER 5

CONCLUDING REMARKS

Research in the area of chemical sensors based on *MC*s is still in its early stages. It was both exciting and at times extremely frustrating to be a part of *MC* sensor development. There are many hurdles that still need to be conquered in this emerging field. Despite this fact, *MC* based chemical sensors have shown extraordinary promise for the future. These sensors have been used to detect a wide range of analytes, both in the gas and liquid phase. Although conclusions have been drawn at the close of each of the preceding chapters, some overall conclusions, as well as some comments on the future of *MC* based sensors will be provided here.

The application of polymeric phases to *MC*s resulted in sensors that were responsive to a wide range of analytes in the gas phase. These films have been widely used as phases in gas chromatography, which means there exists a large amount of information about their modes of interaction with different classes of analytes. The use of this information aided in the detection of the analytes and in predicting how they would behave on the polymer coated *MC*s. It was also determined that FIB milling of the legs of the *MC* resulted in larger responses. FIB milling also proved useful in removing unwanted material from the surface of *MC*s, aiding in the promotion of the differential surface stress needed for *MC*s to respond.

In moving from the gas to liquid phase, the sensor system became more widely applicable. Along with this came the need to generate larger responses. It was later determined that thicker films applied to the *MC*s caused a larger response, as was

predicted. However, the responses were dependent upon the type of metallic layer on which these films were applied. When applied to a smooth surface, the responses were not very reproducible due to their slipping along the *MC* surface to relieve the stress. By using underlying surfaces with nanostructured features, *MC* responses were increased and made to be more reproducible. Another major development in this research is the development of a new deposition method. The method of physical vapor deposition, routinely used for applying metallic films to surfaces, has been used to deposit organic molecules onto the surface of *MC*s. This method allows for these materials to be deposited onto *MC*s and to readily control the thickness of the deposited material. The combined use of thicker films and nanostructured surfaces resulted in LODs that were up to three orders of magnitude better than those obtained using our early systems.

A change in *MC* design to an array type of device allowed for multiple coatings to be applied to a single chip. This opened the door for differential based sensing, which was used to reduce certain common sources of noise. A system based on dual diode lasers was constructed and used for these differential measurements. Using this system, typical sources of noise in *MC* measurements were reduced on average by a factor of 20. The analysis of a binary mixture, not readily achievable with our normal measurement system, was accomplished using the differential system. Unique response patterns were also obtained for gas phase analytes using an array of diode lasers to interrogate multiple *MC*s simultaneously. A mixture of the analytes also showed a response pattern that appeared to be characteristic of the individual response patterns. However, the response patterns were not reproducible over time. Therefore, more work needs to be done to remedy that problem.

Future studies of *MC* based sensors should focus on the measurement of arrays with a large number of elements. While measurements with a single *MC* can be useful for providing information about new coatings, this type of system is applicable to only a single analyte at a given time. This can be utilized in certain circumstances, such as the detection of airborne chemical warfare agents, for example. However, much information has been garnered over the past several years in regards to different coatings and what classes of analytes they will be most effective for sensing applications. Using information reported herein about these coatings will facilitate the creation of sensors that are able to sense a wider range of analytes. By using an array of *MC*s with these selective coatings, researchers will be able to successfully measure mixtures with several constituents present. The differential technology described above will be applicable in these systems of higher order arrays, as the use of multiple coatings will reduce sources of noise and actually be useful in signal averaging.

Another area that desperately needs attention is that of non-optical interrogation methods. Optical interrogation is somewhat limited as to what sensing medium can be used. For example, measurements on blood samples or inside of waste tanks will be extremely difficult if using optical techniques. Piezoresistance measurements would be well suited for both of these examples. In addition, when very large arrays are employed optical techniques, with the possible exception of interferometric based measurements, will again be limited. Piezoresistive based *MC*s can be fabricated and easily integrated into a total sensing system.

In conclusion, it has been shown that *MC* based sensors hold a great deal of promise. Their use has become more widespread over the past several years and

continues to grow. Further refinement needs to occur for them to take their rightful place in the ever-changing world of chemical sensors.

REFERENCES

(1) Diamond, D., Ed. *Principles of Chemical and Biological Sensors*; John Wiley & Sons: New York, 1998.
(2) Janata, J.; Bezegh, A. *Analytical Chemistry* **1988**, *60*, 62R-74R.
(3) Zemel, J. N. *Review of Scientific Instruments* **1990**, *61*(6), 1579-1606.
(4) Bartlett, P. N.; Guerin, S. *Analytical Chemistry* **2003**, *75*, 126-132.
(5) Issa, T. B.; Singh, P.; Baker, M.; Verma, B. S. *Journal of Applied Electrochemistry* **2001**, *31*(8), 921-924.
(6) Aquino-Binag, C. N.; Kumar, N.; Lamb, R. N.; Pigram, P. J. *Chemistry of Materials* **1996**, *8*(11), 2579-2585.
(7) Reybier, K.; Zairi, S.; Jaffrezic-Renault, N.; Fahys, B. *Talanta* **2002**, *56*(6), 1015-1020.
(8) Josowicz, M.; Janata, J.; Ashley, K.; Pons, S. *Analytical Chemistry* **1987**, *59*(2), 253-258.
(9) Malde, M. K.; Bjorvatn, K.; Julshamn, K. *Food Chemistry* **2001**, *73*(3), 373-379.
(10) Komljenovic, J.; Krka, S.; Radic, N. *Analytical Chemistry* **1986**, *58*(13), 2893-2895.
(11) Gupta, V. K.; Mangla, R.; Agarwal, S. *Electroanalysis* **2002**, *14*(15-16), 1127-1132.
(12) Daunert, S.; Bachas, L. G. *Analytical Chemistry* **1990**, *1990*(62), 14.
(13) Hamalainen, J. P.; Tummavuori, J. L.; Aho, M. J. *Talanta* **1993**, *40*(10), 1575-1581.
(14) Shibata, N. *Analytica Chimica Acta* **1976**, *83*(1), 371-373.
(15) James William Ross, J.; Frant, M. S. *Analytical Chemistry* **1969**, *41*(13), 1900-1902.
(16) R. M. Warner, J.; Grung, B. L. *MOSFET Theory and Design*; Oxford University Press: New York, 1999.
(17) Crawford, R. H. *MOSFET in Circuit Design*; McGraw-Hill Book Company: New York, 1967.
(18) Bergveld, P. *Sensors and Actuators B* **2003**, *88*, 1-20.
(19) Wróblewski, W.; Chudy, M.; Dybko, A.; Brzózka, Z. *Analytica Chimica Acta* **1999**, *401*, 105-110.
(20) Lahav, M.; Kharitonov, A. B.; Katz, O.; Kunitake, T.; Willner, I. *Analytical Chemistry* **2001**, *73*, 720-723.
(21) Mlika, R.; Ouada, H. B.; Hamza, M. A.; Gamoudi, M.; Guillaud, G.; Jaffrezic-Renault, N. *Synthetic Metals* **1997**, *90*, 173-179.
(22) Moschou, E. A.; Chaniotakis, N. A. *Mikrochimica Acta* **2001**, *136*, 205-209.
(23) Reinhoudt, D. N. *Sensors and Actuators B* **1995**, *24-25*, 197-200.
(24) Muñoz, J.; Jimenez, C.; Bratov, A.; Bartrolí, J.; Alegret, S.; Dominguez, C. *Biosensors and Bioelectronics* **1997**, *12*(7), 577-585.
(25) Ali, M. B.; Kalfat, R.; Sfihi, H.; Chovelon, J. M.; Ouada, H. B.; Jaffrezic-Renault, N. *Sensors and Actuators B* **2000**, *62*, 233-237.
(26) Niu, M.-N.; Ding, X.-F.; Tong, Q.-Y. *Sensors and Actuators B* **1996**, *37*, 13-17.
(27) Schroth, P.; Schöning, M. J.; Kordoš, P.; Lüth, H.; Schütz, S.; Weibecker, B.; Hummel, H. E. *Biosensors and Bioelectronics* **1999**, *14*, 303-308.

(28) Osteryoung, J. In *Handbook of Instrumental Techniques for Analytical Chemistry*; Settle, F., Ed.; Prentice Hall: Upper Saddle River, 1997, pp 685-690.
(29) Duda, C. T.; Bruntlett, C. S. In *Handbook of Instrumental Techniques for Analytical Chemistry*; Settle, F., Ed.; Prentice Hall: Upper Saddle River, 1997, pp 691-708.
(30) Pariente, F.; Hernandez, L.; Lorenzo, E. *Analytica Chimica Acta* **1993**, *273*(1-2), 399-407.
(31) Lee, J.-Y.; Park, S.-M. *J. Phys. Chem. B* **1998**, *102*, 9940-9945.
(32) Bard, A. J.; Zoski, C. G. *Analytical Chemistry* **2000**, *72*(9), 346A-352A.
(33) Kounaves, S. P. In *Handbook of Instrumental Techniques for Analytical Chemistry*; Settle, F., Ed.; Prentice Hall: Upper Saddle River, 1997, pp 709-725.
(34) Aoki, H.; Hasegawa, K.; Tohda, K.; Umezawa, Y. *Biosensors and Bioelectronics* **2003**, *18*(2-3), 261-267.
(35) Knake, R.; Guchardi, R.; Hauser, P. C. *Analytica Chimica Acta* **2003**, *475*(1-2), 17-25.
(36) Imato, T.; Morioka, H.; Heineman, W. R. *Sensors and Actuators B* **1993**, *13*(1-3), 68-72.
(37) Cattrall, R. W. *Chemical Sensors*; Oxford University Press: New York, 1997.
(38) Dessy, R. E. *Analytical Chemistry* **1989**, *61*(19), 1079A-1094A.
(39) Sepaniak, M. J.; Tromberg, B. J.; Vo-Dinh, T. *Progress in Analytical Spectroscopy* **1988**, *11*(5), 481-509.
(40) Kulp, T. J.; Camins, I.; Angel, S. M.; Munkholm, C.; Walt, D. R. *Analytical Chemistry* **1987**, *59*(24), 2849-2853.
(41) Arnold, M. A. *Analytical Chemistry* **1985**, *57*(2), 565-566.
(42) Wangsa, J.; Arnold, M. A. *Analytical Chemistry* **1988**, *60*(10), 1080-1082.
(43) Jones, T. P.; Porter, M. D. *Analytical Chemistry* **1988**, *60*(5), 404-406.
(44) Lin, J. *Trends in Analytical Chemistry* **2000**, *19*(9), 541-552.
(45) Arnold, M. A. *Analytical Chemistry* **1992**, *64*(21), 1015A-1025A.
(46) Tromberg, B. J.; Sepaniak, M. J.; Alarie, J. P.; Vo-Dinh, T.; Santella, R. M. *Analytical Chemistry* **1988**, *60*(18), 1901-1908.
(47) Giuliani, J. F. *Journal of Polymer Science Part B: Polymer Physics* **1988**, *26*(10), 2197-2201.
(48) Regan, F.; MacCraith, B. D.; Walsh, J. E.; O'Dwyer, K.; Vos, J. G.; Meaney, M. *Vibrational Spectroscopy* **1997**, *14*, 239-246.
(49) Zhang, Y.; Seitz, W. R.; Grant, C. L.; Sundberg, D. C. *Analytica Chimica Acta* **1989**, *217*, 217-227.
(50) Bright, F. V.; Poirier, G. E.; Hieftje, G. M. *Talanta* **1988**, *35*(2), 113-118.
(51) Headrick, J.; Sepaniak, M.; Alexandratos, S.; Datskos, P. *Analytical Chemistry* **2000**, *72*(9), 1994-2000.
(52) Abanulo, J. C.; Harris, R. D.; Sheridan, A. K.; Wilkinson, J. S.; Bartlett, P. N. *Faraday Discussions* **2002**, *121*, 139-152.
(53) Homola, J.; Yee, S. S.; Gauglitz, G. *Sensors and Actuators B* **1999**, *54*, 3-15.
(54) McDonnell, J. M. *Current Opinion in Chemical Biology* **2001**, *5*, 572-577.
(55) Uznanski, P.; Pecherz, J. *Journal of Applied Polymer Science* **2002**, *86*, 1459-1464.

(56) Kretschmann, E. *Zeitschrift fuer Physik* **1971**, *241*(4), 313-324.
(57) Zhang, H. Q.; Boussaad, S.; Tao, N. J. *Review of Scientific Instruments* **2003**, *74*(1), 150-153.
(58) Kieser, B.; Dieterle, F.; Gauglitz, G. *Analytical Chemistry* **2002**, *74*, 4781-4787.
(59) Yoshida, T.; Sato, M.; Ozawa, T.; Umezawa, Y. *Analytical Chemistry* **2000**, *72*, 6-11.
(60) Dickert, F. L.; Geiger, U.; weber, K. *Fresenius Journal of Analytical Chemistry* **1999**, *364*, 128-132.
(61) Jarrett, M. R.; Finklea, H. O. *Analytical Chemistry* **1999**, *71*, 353-357.
(62) Schneider, T. W.; Buttry, D. A. *Journal of the American Chemical Society* **1993**, *115*(26), 12391-12397.
(63) Bodenhöfer, K.; Hierlemann, A.; Noetzel, G.; Weimar, U.; Göpel, W. *Analytical Chemistry* **1996**, *68*, 2210-2218.
(64) Kobayashi, T.; Murawaki, Y.; Reddy, P. S.; Abe, M.; Fujii, N. *Analytica Chimica Acta* **2001**, *435*, 141-149.
(65) Sun, L.-X.; Okada, T. *Journal of Membrane Science* **2001**, *183*, 213-221.
(66) Ng, S.-C.; Sun, T.; Chan, H. S. O. *Tetrahedron Letters* **2002**, *43*, 2863-2866.
(67) Liao, S.; Shnidman, Y.; Ulman, A. *Journal of the American Chemical Society* **2000**, *122*(15), 3688-3694.
(68) Boschkova, K.; Feiler, A.; Kronberg, B.; Stålgren, J. J. R. *Langmuir* **2002**, *18*(21), 7930-7935.
(69) O'Sullivan, C. K.; Guilbault, G. G. *Biosensors and Bioelectronics* **1999**, *14*, 663-670.
(70) Ali, Z. *Journal of Thermal Analysis and Calorimetry* **1999**, *55*, 397-412.
(71) Cheeke, J. D. N.; Wang, Z. *Sensors and Actuators B* **1999**, *59*, 146-153.
(72) Dorozhkin, L. M.; Rozanov, I. A. *Journal of Analytical Chemistry* **2001**, *56*(5), 399-416.
(73) Amati, D.; Arn, D.; Blom, N.; Ehrat, M.; Saunois, J.; Widmer, H. M. *Sensors and Actuators B* **1992**, *7*, 587-591.
(74) Wagner, J.; Schickfus, M. v. *Sensors and Actuators B* **2001**, *76*, 58-63.
(75) Yang, X.; Du, X.-X.; Shi, J.; Swanson, B. *Talanta* **2001**, *54*, 439-445.
(76) Levit, N.; Pestov, D.; Tepper, G. *Sensors and Actuators B* **2002**, *82*, 241-249.
(77) Thompson, M.; Stone, D. C.; Nisman, R. *Analytica Chimica Acta* **1991**, *248*, 143-153.
(78) Liu, D.; Ge, K.; Chen, K.; Nie, L.; Yao, S. *Analytica Chimica Acta* **1995**, *307*, 61-69.
(79) Groves, W. A.; Zellers, E. T. *Annals of Occupational Hygiene* **2001**, *45*(8), 609-623.
(80) Welsch, W.; Klein, C.; Öksüzoglu, R. M.; Schickfus, M. v.; Hunklinger, S. *Sensors and Actuators A* **1997**, *62*, 562-564.
(81) Josse, F.; Bender, F.; Cernosek, R. W. *Analytical Chemistry* **2001**, *73*, 5937-5944.
(82) Andle, J. C.; Weaver, J. T.; McAllister, D. J.; Josse, F.; Vetelino, J. F. *Sensors and Actuators B* **1993**, *13*(1-3), 437-442.
(83) Welsch, W.; Klein, C.; Schickfus, M. v.; Hunklinger, S. *Analytical Chemistry* **1996**, *68*(13), 2000-2004.

(84) Cai, Q.-Y.; Park, J.; Heldsinger, D.; Hsieh, M.-D.; Zellers, E. T. *Sensors and Actuators B* **2000**, *62*, 121-130.
(85) Cunningham, B.; Weinberg, M.; Pepper, J.; Clapp, C.; Bousquet, R.; Hugh, B.; Kant, R.; Daly, C.; Hauser, E. *Sensors and Actuators B* **2001**, *73*, 112-123.
(86) Pyun, J. C.; Beutel, H.; Meyer, J.-U.; Ruf, H. H. *Biosensors and Bioelectronics* **1998**, *13*, 839-845.
(87) Sepaniak, M. J.; Datskos, P.; Lavrik, N.; Tipple, C. *Analytical Chemistry* **2002**, *74*, 568A-575A.
(88) Battiston, F. M.; Ramseyer, J.-P.; Lang, H. P.; Baller, M. K.; Gerber, C.; Gimzewski, J. K.; Meyer, E.; Güntherodt, H.-J. *Sensors and Actuators B* **2001**, *77*, 122-131.
(89) Lang, H. P.; Baller, M. K.; Berger, R.; Gerber, C.; Gimzewski, J. K.; Battiston, F. M.; Fornaro, P.; Ramseyer, J. P.; Meyer, E.; Güntherodt, H. J. *Analytica Chimica Acta* **1999**, *393*, 59.
(90) Thundat, T.; Warmack, R. J.; Chen, G. Y.; Allison, D. P. *Applied Physics Letters* **1994**, *64*, 2894.
(91) Tamayo, J.; Humphris, A. D. L.; Malloy, A. M.; Miles, M. J. *Ultramicroscopy* **2001**, *86*, 167-173.
(92) Maute, M.; Raible, S.; Prins, F. E.; Kern, D. P.; Weimar, U.; Göpel, W. *Microelectronic Engineering* **1999**, *46*, 439-442.
(93) Maute, M.; Raible, S.; Prins, F. E.; Kern, D. P.; Ulmer, H.; Weimar, U.; Göpel, W. *Sensors and Actuators B* **1999**, *58*, 505-511.
(94) Thundat, T.; Oden, P. I.; Warmack, R. J. *Microscale Thermophysical Engineering* **1997**, *1*, 185-199.
(95) Chen, G. Y.; Thundat, T.; Wachter, E. A.; Warmack, R. J. *Journal of Applied Physics* **1995**, *77*(8), 3618-3622.
(96) Raiteri, R.; Grattarola, M.; Berger, R. *Materials Today* **2002**, 22-29.
(97) Datskos, P. G.; Sauers, I. *Sensors and Actuators B* **1999**, *61*, 75-82.
(98) Ward, M. D.; Buttry, D. A. *Science* **1990**, *249*, 1000-1007.
(99) Stoney, G. G. *Proceedings of the Royal Society of London. Series A, Containing Papers of a Mathematical and Physical Character* **1909**, *82*(553), 172-175.
(100) Raiteri, R.; Grattarola, M.; Butt, H.-J.; Skládal, P. *Sensors and Actuators B* **2001**, *79*, 115-126.
(101) Lavrik, N. V.; Tipple, C. A.; Datskos, P. G.; Sepaniak, M. J. *Biomedical Microdevices* **2001**, *3*(1), 35-44.
(102) Wu, G.; Ji, H.; Thundat, T.; Datar, R.; Cote, R.; Hagan, M.; Chakraborty, A. K.; Majumdar, A. *Proceedings of the National Academy of Sciences* **2001**, *98*, 1560-1564.
(103) Shuttleworth, R. *Proc. Phys. Soc. (London)* **1950**, *63A*, 444-457.
(104) Ibach, H. *Surface Science Reports* **1997**, *29*, 193-263.
(105) Blanc, N.; Brugger, J.; Rooij, N. F. d.; Dürig, U. *Journal of Vacuum Science Technology B* **1996**, *14*(2), 901-905.
(106) Neubauer, G.; Cohen, S. R.; McClelland, G. M.; Horne, D.; Mate, C. M. *Review of Scientific Instruments* **1990**, *61*(9), 2296-2308.

(107) Göddenhenrich, T.; Lemke, H.; Hartmann, U.; Heiden, C. *Journal of Vacuum Science and Technology A* **1989**, *8*(1), 383-387.
(108) Thaysen, J.; Marie, R.; Boisen, A.,14th IEEE International Conference on Micro Electro Mechanical Systems, Interlaken, Switzerland 2001; Institute of Electrical and Electronics Engineers; 401-404.
(109) Luginbuhl, P.; Racine, G.-A.; Lerch, P.; Romanowicz, B.; Brooks, K. G.; Rooij, N. F. d.; Renaud, P.; Setter, N. *Sensors and Actuators A* **1996**, *54*, 530-535.
(110) Thaysen, J.; Yalcinkaya, A. D.; Vettiger, P.; Menon, A. *Journal of Physics D: Applied Physics* **2002**, *35*, 2698-2703.
(111) Kim, Y.-S.; Nam, H.-J.; Cho, S.-M.; Hong, J.-W.; Kim, D.-C.; Bu, J. U. *Sensors and Actuators A* **2003**, *103*, 122-129.
(112) Yi, J. W.; Shih, W. Y.; Shih, W.-H. *Journal of Applied Physics* **2002**, *91*(3), 1680-1686.
(113) Passian, A.; Evans, P. G.; Varma, V. K.; Ferrell, T. L.; Thundat, T. *Review of Scientific Instruments* **2003**, *74*(2), 1031-1035.
(114) Porter, T. L.; Eastman, M. P.; Pace, D. L.; Bradley, M. *Sensors and Actuators A* **2001**, *88*, 47-51.
(115) Fritz, J.; Baller, M. K.; Lang, H. P.; Rothuizen, H.; Vettiger, P.; Meyer, E.; Güntherodt, H.-J.; Gerber, C.; Gimzewski, J. K. *Science* **2000**, *288*, 316-318.
(116) Berger, R.; Delamarche, E.; Lang, H. P.; Gerber, C.; Gimzewski, J. K.; Meyer, E.; Güntherodt, H.-J. *Science* **1997**, *276*, 2021-2024.
(117) Raiteri, R.; Butt, H.-J.; Grattarola, M. *Electrochimica Acta* **2000**, *46*, 157-163.
(118) Xu, X.; Thundat, T. G.; Brown, G. M.; Ji, H.-F. *Analytical Chemistry* **2002**, *74*(15), 3611-3615.
(119) Baselt, D. R.; Fruhberger, B.; Klaassen, E.; Cemalovic, S.; Jr., C. L. B.; Patel, S. V.; Mlsna, T. E.; McCorkle, D.; Warmack, B. *Sensors and Actuators B* **2003**, *88*, 120-131.
(120) Britton, C. L.; Jones, R. L.; Oden, P. I.; Hu, Z.; Warmack, R. J.; Smith, S. F.; Bryan, W. L.; Rochelle, J. M. *Ultramicroscopy* **2000**, *82*, 17-21.
(121) Datskos, P. G.; Rajic, S.; Datskou, I. *Ultramicroscopy* **2000**, *82*, 49.
(122) Stephan, A. C.; Gaulden, T.; Brown, A. D.; Smith, M.; Miller, L. F.; Thundat, T. *Review of Scientific Instruments* **2002**, *73*(1), 36-41.
(123) Ji, H.-F.; Thundat, T.; Dabestani, R.; Brown, G. M.; Britt, P. F.; Bonnesen, P. V. *Analytical Chemistry* **2001**, *73*(7), 1572-1576.
(124) Hansen, K. M.; Ji, H.-F.; Wu, G.; Datar, R.; Cote, R.; Majumdar, A.; Thundat, T. *Analytical Chemistry* **2001**, *73*(7), 1567-1571.
(125) Yang, Y.; Ji, H.-F.; Thundat, T. *Journal of the American Chemical Society* **2003**, *125*, 1124-1125.
(126) Ji, H.-F.; Hansen, K. M.; Hu, Z.; Thundat, T. *Sensors and Actuators B* **2001**, *72*, 233-238.
(127) Lavrik, N. V.; Tipple, C. A.; Sepaniak, M. J.; Datskos, P. G. *Chemical Physics Letters* **2001**, *336*, 371-376.
(128) Ji, H.-F.; Finot, E.; Dabestani, R.; Thundat, T.; Brown, G. M.; Britt, P. F. *Chemical Communications* **2000**(6), 457-458.

(129) Jensenius, H.; Thaysen, J.; Rasmussen, A. A.; Veje, L. H.; Hansen, O.; Boisen, A. *Applied Physics Letters* **2000**, *76*(18), 2615-2617.
(130) Betts, T. A.; Tipple, C. A.; Sepaniak, M. J.; Datskos, P. G. *Analytica Chimica Acta* **2000**, *422*, 89.
(131) Baller, M. K.; Lang, H. P.; Fritz, J.; Gerber, C.; Gimzewski, J. K.; Drechsler, U.; Rothuizen, H.; Despont, M.; Vettiger, P.; Battiston, F. M.; Ramseyer, J.-P.; Fornaro, P.; Meyer, E.; Güntherodt, H.-J. *Ultramicroscopy* **2000**, *82*, 1-9.
(132) Bashir, R.; Hilt, J. Z.; Elibol, O.; Gupta, A.; Peppas, N. A. *Applied Physics Letters* **2002**, *81*(16), 3091-3093.
(133) Kim, B. H.; Prins, F. E.; Kern, D. P.; Raible, S.; Weimar, U. *Sensors and Actuators B* **2001**, *78*, 12-18.
(134) Fagan, B.; Tipple, C. A.; Xue, B.; Datskos, P.; Sepaniak, M. *Talanta* **2000**, *53*, 599.
(135) Moulin, A. M.; Shea, S. J.; Welland, M. E. *Ultramicroscopy* **2000**, *82*, 23.
(136) Wu, G.; Datar, R. H.; Hansen, K. M.; Thundat, T.; Cote, R. J.; Majumdar, A. *Nature Biotechnology* **2001**, *19*, 856-860.
(137) McKendry, R.; Zhang, J.; Arntz, Y.; Strunz, T.; Hegner, M.; Lang, H. P.; Baller, M. K.; Certa, U.; Meyer, E.; Güntherodt, H.-J.; Gerber, C. *Proceedings of the National Academy of Sciences* **2002**, *99*(15), 9783-9788.
(138) Raiteri, R.; Nelles, G.; Butt, H.-J.; Knoll, W.; Skládal, P. *Sensors and Actuators B* **1999**, *61*, 213-217.
(139) Moulin, A. M.; O'Shea, S. J.; Badley, R. A.; Doyle, P.; Welland, M. E. *Langmuir* **1999**, *15*, 8776-8779.
(140) Barnes, J. R.; Stephenson, R. J.; Welland, M. E.; Gerber, C.; Gimzewski, J. K. *Nature* **1994**, *372*, 79.
(141) Datskos, P. G.; Oden, P. I.; Wachter, E. A.; Thundat, T.; Warmack, R. J. *Applied Physics Letters* **1996**, *69*, 2986.
(142) Oden, P. I.; Wachter, E. A.; Datskos, P. G.; Thundat, T.; Warmack, R. J. *Infrared Technol. Appl. XXII. SPIE 2744* **1996**, 345.
(143) Wachter, E. A.; Thundat, T.; Datskos, P. G.; Oden, P. I.; Warmack, R. J.; Sharp, S. L. *Rev. Sci. Instrum.* **1996**, *67*, 3434.
(144) Berger, R.; Gerber, C.; Lang, H. P.; Gimzewski, J. K. *Microelectr. Eng.* **1997**, *35*, 373.
(145) Thundat, T.; Chen, G. Y.; Warmack, R. J.; Allison, D. P.; Wachter, E. A. *Analytical Chemistry* **1995**, *67*, 3662.
(146) Thundat, T.; Wachter, E. A.; Sharp, S. L.; Warmack, R. J. *Applied Physics Letters* **1995**, *66*, 1695.
(147) Thundat, T.; Oden, P. I.; Datskos, P. G.; Chen, G. Y.; Warmack, R. J.: Oak Ridge, TN, 1996.
(148) Grate, J. W.; Martin, S. J.; White, R. M. *Analytical Chemistry* **1993**, *65*, 940A.
(149) Wohltjen, H. *Sensors and Actuators* **1984**, *5*, 307.
(150) Ward, M. D.; Buttry, D. A. *Science* **1990**, *249*, 1000.
(151) Schierbaum, K. D.; Gerlach, A.; Huag, M.; Gopel, W. W. *Sensors and Actuators A* **1992**, *31*, 130.
(152) Scheide, E. P.; Taylor, J. K. *Environ. Sci. Technol.* **1974**, *8*, 1097.

(153) Janata, J. *Principles of Chemical Sensors*; Plenum Press: New York, 1989.
(154) Gomes, M. T.; Duarte, A. C.; Oliveira, J. *Sensors and Actuators B* **1995**, *26*, 191.
(155) Zhong, C. J.; Porter, M. D. *Analytical Chemistry* **1995**, *67*, A709.
(156) O'Toole, R. P.; Burns, S. G.; Bastiaans, G. J.; Porter, M. D. *Analytical Chemistry* **1992**, *64*, 1289.
(157) Preissig, F. J. v. *J. Appl. Phys.* **1989**, *66*, 4262.
(158) Chen, G. Y.; Warmack, R. J.; Thundat, T.; Allison, D. P.; Huang, A. A. *Rev. Sci. Instrum.* **1994**, *65*, 2532.
(159) Sarid, D. *Scanning Force Microscopy with Applications to Electric, Magnetic , and Atomic Forces*; Oxford University Press: New York, 1991.
(160) Tomishenko, S. *Theory of Plates and Shells*; McGraw-Hill, 1940.
(161) Shaver, P. J. *Rev. Sci. Instrum.* **1969**, *40*, 901.
(162) Pintchovski, F.; Price, J. B.; Peavey, P. J.; Kobold, K. *J. Electrochem. Soc.* **1979**, *126*, 1428.
(163) Poole, C. F.; Poole, S. K. *Chromatography Today*; Elsevier: Amsterdam, 1991.
(164) Boisen, A.; Thaysen, J.; Jensenius, H.; Hansen, O. *Ultramicroscopy* **2000**, *82*, 11-16.
(165) Datskos, P. G.; Sepaniak, M. J.; Tipple, C. A.; Lavrik, N. *Sensors and Actuators B* **2001**, *76*(1-3), 393-402.
(166) Israelachvili, J. *Intermolecular and Surface Forces*, 2nd ed.; Academic Press: San Diego, 1991.
(167) Samuel, J.; Brinker, C. J.; Frink, L. J. D.; Swol, F. v. *Langmuir* **1998**, *14*, 2602-2605.
(168) Frink, L. J. D.; Swol, F. v. *Langmuir* **1999**, *15*, 3296-3301.
(169) Hu, Z.; Thundat, T.; Warmack, R. J. *Journal of Applied Physics* **2001**, *90*(1), 427-431.
(170) Rojas, M. T.; Koniger, R.; Stoddart, J. F.; Kaifer, A. E. *Journal of the American Chemical Society* **1995**, *117*, 336.
(171) Takeo, K.; Mitoh, H.; Uemura, K. *Carbohydrate Research* **1989**, *187*, 203-221.
(172) Fox, S. B.; Culha, M.; Sepaniak, M. J. *Journal of Liquid Chromatography and Related Technologies* **2001**, *24*(9), 1209-1228.
(173) Copper, C. L.; Davis, J. B.; Cole, R. O.; Sepaniak, M. J. *Electrophoresis* **1994**, *15*, 785.
(174) Copper, C. L.; Davis, J. B.; Sepaniak, M. J. *Chirality* **1995**, *7*, 401.
(175) Lelièvre, F.; Gareil, P.; Jardy, A. *Analytical Chemistry* **1997**, *69*(3), 385-392.
(176) Culha, M.; Fox, S.; Sepaniak, M. J. *Analytical Chemistry* **2000**, *72*, 88-95.
(177) Weisser, M.; Nelles, G.; Wenz, G.; Mittler-Neher, S. *Sensors and Actuators B* **1997**, *38-39*, 58-67.
(178) Bicchi, C.; Cravotto, G.; D'Amato, A.; Rubiolo, P.; Galli, A.; Galli, M. *Journal of Microcolumn Separations* **1999**, *11*(7), 487-500.
(179) Beck, T.; Liepe, J.-M.; Nandzik, J.; Rohn, S.; Mosandl, A. *J. High Resol. Chromatogr.* **2000**, *23*(10), 569-575.
(180) Winquist, F.; Lundstrom, I.; Wide, P. *Sensors and Actuators, B* **1999**, *58*(1-3), 512-517.

(181) Chadwick, A. V.; Russell, N. V.; Whitham, A. R.; Wilson, A. *Sensors and Actuators B* **1994**, *18*(1-3), 99-102.
(182) Cho, E. J.; Bright, F. V. *Analytica Chimica Acta* **2002**, *470*, 101-110.
(183) Caneiro, A.; Fabry, P.; Khireddine, H.; Siebert, E. *Analytical Chemistry* **1991**, *63*(22), 2550-2557.
(184) Bourgeois, W.; Stuetz, R. M. *Water Research* **2002**, *36*, 4505-4512.
(185) Stella, R.; Barisci, J. N.; Serra, G.; Wallace, G. G.; Rossi, D. D. *Sensors and Actuators B* **2000**, *63*, 1-9.
(186) Hatfield, J. V.; Neaves, P.; Hicks, P. J.; Persaud, K.; Travers, P. *Sensors and Actuators B* **1994**, *18*(1-3), 221-228.
(187) Barkó, G.; Hlavay, J. *Analytica Chimica Acta* **1998**, *367*(1-3), 135-143.
(188) Cygan, M. T.; Collins, G. E.; Dunbar, T. D.; Allara, D. L.; Gibbs, C. G.; Gutsche, C. D. *Analytical Chemistry* **1999**, *71*(1), 142-148.
(189) Mlika, R.; Ouada, H. B.; Hamza, M. A.; Gamoudi, M.; Guillaud, G.; Jaffrezic-Renault, N. *Synthetic Metals* **1997**, *90*, 173-179.
(190) Tipple, C. A.; Lavrik, N. V.; Culha, M.; Headrick, J.; Datskos, P.; Sepaniak, M. J. *Analytical Chemistry* **2002**, *74*(13), 3118-3126.
(191) Dickert, F. L.; Geiger, U.; Weber, K. *Fresenius Journal of Analytical Chemistry* **1999**, *364*, 128-132.
(192) Chueh, H.-T.; Hatfield, J. V. *Sensors and Actuators, B: Chemical* **2002**, *83*(1-3), 262-269.
(193) Yang, Y.-M.; Yang, P.-Y.; Wang, X.-R. *Sensors and Actuators B* **2000**, *66*, 167-170.
(194) Penza, M.; Cassano, G. *Sensors and Actuators B* **2003**, *89*(3), 269-284.
(195) Nguyen, T. A.; Kokot, S.; Ongarato, D. M.; Wallace, G. G. *Electroanalysis* **2000**, *12*(2), 89-95.
(196) Zellers, E. T.; Pan, T.-S.; Patrash, S. J.; Han, M.; Batterman, S. A. *Sensors and Actuators B, Chemical* **1993**, *12*(2), 123-133.
(197) Suah, F. B. M.; Ahmad, M.; Taib, M. N. *Sensors and Actuators B* **2003**, *90*(1-3), 182-188.
(198) Henkel, K.; Schmeisser, D. *Analytical and Bioanalytical Chemistry* **2002**, *374*(2), 329-337.
(199) Corcoran, P.; Lowery, P.; Anglesea, J. *Sensors and Actuators B* **1998**, *48*(1-3), 448-455.
(200) Rebiere, D.; Bordieu, C.; Pistre, J. *Sensors and Actuators B* **1995**, *25*(1-3), 777-780.

VITA

Christopher Alan Tipple was born in Orlando, Florida on February 7, 1973. He attended schools in the Orange County Public School system in Orlando and graduated from Edgewater High School in June of 1991. He entered the University of Central Florida to pursue a degree in Aeronautical Engineering, but changed his major to Chemistry in 1993. In May of 1998 he received his Bachelor of Science in Chemistry. He entered the doctorate program in chemistry at the University of Tennessee, Knoxville in August of 1998 pursuing research in analytical chemistry. In January of 1999, he got married to his wife Jessica. He earned his Ph.D. in August of 2003 and will be pursuing post-doctoral research at the Naval Research Laboratory in Washington, D.C. His research will involve the detection of chemical warfare agents using a variety of techniques.